

2 アイソトープ Supply of Radioisotopes

2.1 アイソトープの供給量 Amounts of Radioisotopes Supplied

2.1.1 おもな非密封アイソトープの供給量の推移(核種別, 年度別)

Amounts of Major Unsealed Radioisotopes[§] Supplied in Fiscal 2012-2016

(単位Unit: MBq)

核種 Nuclide	年度 Year	2012	2013	2014	2015	2016
³ H Total		230,198	262,603	148,831	210,084	415,415
(標識化合物 ³ H-Labeled compound)		230,197	188,601	148,829	210,081	415,413
¹⁴ C Total		77,391	86,604	129,476	67,834	37,840
(標識化合物 ¹⁴ C-Labeled compound)		77,391	86,604	118,355	67,832	37,839
¹⁸ F		29,970	41,070	37,555	50,750	38,170
²² Na		122	171	74	122	818
³² P Total		113,024	96,418	73,030	68,456	52,664
(標識化合物 ³² P-Labeled compound)		69,264	62,632	54,296	42,583	52,647
³³ P Total		12,230	11,188	9,166	8,155	3,435
(標識化合物 ³³ P-Labeled compound)		4,220	3,602	4,763	5,250	3,435
³⁵ S Total		56,649	51,670	38,915	38,522	28,965
(標識化合物 ³⁵ S-Labeled compound)		53,134	49,561	36,658	36,154	28,964
⁴⁵ Ca		1,222	815	963	815	561
⁵¹ Cr		31,943	32,737	23,562	20,787	24,236
⁵⁴ Mn		108	71	75	56	37
⁵⁵ Fe		335	777	296	222	296
⁵⁷ Co		168	371	249	235	149
⁵⁹ Fe		298	538	463	186	166
⁶⁰ Co		7	32	9	6	8
⁶³ Ni		28	37	9	0	2
⁶⁵ Zn		66	104	108	23	54
⁶⁷ Ga		518	703	1,083	1,130	999
⁶⁸ Ge		3,488	4,255	2,447	3,330	2,072
⁷⁵ Se		226	7	44	11	4
⁸⁵ Kr		211,650	214,260	226,508	4,840	70,892
⁸⁵ Sr		420	364	212	268	134
⁸⁶ Rb		592	148	121	74	148
⁸⁹ Sr		458	160	149	141	1
⁹⁰ Sr		6	13	32	21	9
⁹⁰ Y		20,572	7,363	4,403	6,505	3,885
⁹⁹ Mo		148,000	175,750	236,874	155,400	156,325
^{99m} Tc		99,561	78,494	63,399	64,870	42,290
¹⁰⁹ Cd		10	6	21	3	12
¹¹¹ In		10,915	12,765	11,396	13,886	11,259
¹²³ I		16,440	12,710	24,919	56,410	77,004
¹²⁵ I Total		77,832	71,950	61,978	65,890	46,132
(標識化合物 ¹²⁵ I-Labeled compound)		4,236	4,007	3,892	4,184	46,126
¹³¹ I		17,432	20,397	15,355	15,591	21,519
¹³⁴ Cs		41	9	5	26	8
¹³⁷ Cs		251	246	248	159	141
¹⁷⁷ Lu		370	370	-	-	-
²⁰¹ Tl		666	353	333	639	1,036
その他 Others		76	69	119	71	194
合計 Total		1,163,283	1,185,598	1,112,427	855,518	1,036,880
供給先事業所数 Number of users		503	488	428	417	391

§ Radionuclide/Labeled Compounds, Radiopharmaceuticals for research purpose

2.1.2 おもな非密封アイソトープの供給量(核種別, 機関別) 2016年度

Amounts of Major Unsealed Radioisotopes[§] Supplied in Fiscal 2016 (by Organization)

(単位Unit: MBq)

核種 Nuclide	Organization 機関	総数 Total	医療機関 Hospital and Clinic	教育機関 Educational Institution	研究機関 Research Institute	民間企業 Private Company	その他の機関 Others
³ H		415,415	19,086	305,054	62,057	29,218	0
¹⁴ C		37,840	0	1,234	34,522	2,084	-
¹⁸ F		38,170	925	6,105	12,580	18,005	555
²² Na		818	-	89	729	-	-
³² P		52,664	351	26,206	21,242	4,643	222
³³ P		3,435	-	794	2,641	-	-
³⁵ S		28,965	-	21,687	6,975	303	-
⁴⁵ Ca		561	-	518	43	-	-
⁵¹ Cr		24,236	259	9,259	6,744	7,900	74
⁵⁴ Mn		37	-	37	-	-	0
⁵⁵ Fe		296	-	259	37	-	-
⁵⁷ Co		149	-	130	19	-	-
⁵⁹ Fe		166	-	55	92	-	19
⁶⁰ Co		8	-	-	3	1	4
⁶³ Ni		2	-	-	2	-	-
⁶⁵ Zn		54	-	43	11	-	-
⁶⁷ Ga		999	148	851	-	-	-
⁶⁸ Ge		2,072	925	-	-	1,147	-
⁷⁵ Se		4	-	-	4	-	-
⁸⁵ Kr		70,892	-	-	-	70,892	-
⁸⁵ Sr		134	-	59	75	-	-
⁸⁶ Rb		148	-	74	74	-	-
⁸⁹ Sr		1	-	-	0	1	0
⁹⁰ Sr		9	-	1	7	1	0
⁹⁰ Y		3,885	-	2,405	1,480	-	-
⁹⁹ Mo		156,325	5,550	115,625	24,050	9,250	1,850
^{99m} Tc		42,290	-	24,790	16,650	110	740
¹⁰⁹ Cd		12	-	10	2	-	-
¹¹¹ In		11,259	148	5,661	5,106	-	344
¹²³ I		77,004	62,789	12,069	2,035	111	-
¹²⁵ I		46,132	269	10,961	15,172	19,730	-
¹³¹ I		21,519	-	3,108	3,971	14,070	370
¹³⁴ Cs		8	-	1	7	-	-
¹³⁷ Cs		141	-	43	98	0	0
²⁰¹ Tl		1,036	148	666	-	222	-
その他 Others		194	-	19	175	0	0
合計 Total		1,036,880	90,598	547,813	216,603	177,688	4,178

§ Radionuclide/Labeled Compounds, Radiopharmaceuticals for research purpose

TABLE I
RADIONUCLIDES ARRANGED IN ORDER OF THEIR MOST RESTRICTIVE
(MPC)_a VALUE

HIGH TOXICITY

Pa²³¹, Cf²⁴⁹, Th-Nat, Pu²³⁹, Pu²⁴⁰, Pu²⁴², Th²³², Pu²³⁸, Ac²²⁷, Th²³⁰, Np²³⁷, Th²²⁸, Am²⁴¹, Am²⁴³, Cm²⁴³, Cm²⁴⁵, Cm²⁴⁶, Cf²⁵⁰, Cf²⁵², Cm²⁴⁴, U²³², Ra²²⁶, Ra²²⁸, Sm¹⁴⁷, U-Nat, Nd¹⁴⁴, U²³⁸, Pu²⁴¹, Pb²¹⁰, U²³⁰, U²³³, U²³⁴, U²³⁵, U²³⁶, Cm²⁴², Th²²⁷, Po²¹⁰, Ra²²³, Sr⁹⁰,

MEDIUM TOXICITY

Upper Sub-Group A

Ra²²⁴, Pa²³⁰, Bk²⁴⁹, I¹²⁹, Eu¹⁵⁴, Ru¹⁰⁶, Ce¹⁴⁴, Bi²¹⁰, At²¹¹, Na²², Co⁶⁰, Ag^{110m}, I¹²⁶, I¹³¹, Cs¹³⁴, Eu^{152(13yr)}, Cs¹³⁷, Bi²⁰⁷, Pb²¹², Ac²²⁸, In^{114m}, Sb¹²⁴, Ta¹⁸², Cl³⁶, Sc⁴⁶, Sb¹²⁵, Ir¹⁹², Tl²⁰⁴, Ca⁴⁵, Mn⁵⁴, Y⁹¹, Zr⁹⁵, Sr⁸⁹, Cd^{115m}, In¹¹⁵, Te^{127m}, Te^{129m}, I¹³³, Ba¹⁴⁰, Tb¹⁶⁰, Tm¹⁷⁰, Hf¹⁸¹, Th²³⁴,

Lower Sub-Group B

P³², Y⁴⁸, Fe⁵⁹, Co⁵⁸, Ni⁶³, Zn⁶⁵, Rb⁸⁶, Rb⁸⁷, Tc⁹⁹, Cd¹⁰⁹, Sn¹¹³, Pm¹⁴⁷, Sm¹⁵¹, Os¹⁸⁵, Hg²⁰³, As⁷⁶, Y⁹⁰, Zr⁹⁷, Nb⁹⁵, Ru¹⁰³, Ag¹⁰⁵, Sn¹²⁵, Cs¹³⁵, Eu¹⁵⁵, Gd¹⁵³, Bi²¹², K⁴², As⁷⁴, Se⁷⁵, Sr⁸⁵, Nb^{93m}, Zr⁹³, Te^{125m}, Te¹³², I¹³⁵, La¹⁴⁰, Tm¹⁷¹, W¹⁸¹, W¹⁸⁵, Na²⁴, Sc⁴⁸, Mn⁵², Y⁹³, Tc^{97m}, Sb¹²², Ce¹⁴¹, Pt¹⁴², Re¹⁸³, Ir¹⁹⁴, Bi²⁰⁶, Ca⁴⁷, Co⁵⁷, Ga⁷², Br⁸², Cd¹¹⁵, Te^{131m}, Cs¹³⁶, Pt¹⁴³, Ho¹⁶⁶, Re¹⁸⁸, Pa²³³, Mo⁹⁹, Ce¹⁴³, Dy¹⁶⁶, Tc⁹⁶, Ag¹¹¹, I¹³², Nd¹⁴⁷, Pm¹⁴⁹, Re¹⁸⁶, Au¹⁹⁸, Tl²⁰², S³⁵, Sr⁹¹, Os¹⁴³, Zn^{69m}, As⁷³, As⁷⁷, Sr⁹², Y⁹², Tc⁹⁷, Pd¹⁰⁹, Ba¹³¹, Sm¹⁵³, Eu^{152(4.2h)}, Gd¹⁵⁹, Er¹⁶⁹, W¹⁸⁷, Os¹⁹¹, Ir¹⁹⁰, Pt¹⁹³, Rn²²⁰, Rn²²², * Sc⁴⁷, Mn⁵⁶, Ni⁵⁹, Ni⁶⁵, Kr⁸⁷, Ru¹⁰⁵, Rh¹⁰⁵, I¹³⁴, Er¹⁷¹, Yb¹⁷⁵, Lu¹⁷⁷, Re¹⁸⁷, Pt¹⁹¹, Pt¹⁹⁷, Au¹⁹⁶, Np²³⁹, Si³¹, Fe⁵⁵, Pd¹⁰³, Te¹²⁷, Au¹⁹⁹, Hg^{197m}, Tl²⁰⁰, Tl²⁰¹, Be⁷, A⁴¹, Cu⁶⁴, Hg¹⁹⁷, Th²³¹, Nd¹⁴⁹, Ru⁹⁷, In^{115m}, Pb²⁰³, Cl³⁸, Dy¹⁶⁵, Cr⁵¹, F¹⁸, C¹⁴, Kr^{85m}, Te¹²⁹, Xe¹³⁵, Cs¹³¹,

LOW TOXICITY

H³, Zn⁶⁹, Ge⁷¹, Nb⁹⁷, In^{113m}, Cs^{134m}, Pt^{193m}, Pt^{197m}, Tc^{99m}, Co^{58m}, Kr⁸⁵, Xe¹³³, Os^{191m}, Xe^{131m}, Y^{91m}, Sr^{85m}, Tc^{96m}, Rh^{103m}, A³⁷.

* The figure used for this isotope is the same as that given in Basic Safety Standards for Radiation Protection [3].

Alpha Emitters for Radiotherapy: Basic Radiochemistry to Clinical Studies – Part 2

Running title: Alpha Emitters for Radiotherapy

Sophie Poty¹, Lynn C. Francesconi^{2,3}, Michael R. McDevitt^{1,4}, Michael J. Morris⁵,

Jason S. Lewis^{1,6}

¹*Department of Radiology and the Program in Molecular Pharmacology, Memorial Sloan Kettering Cancer Center, New York, NY, USA*

²*Department of Chemistry, Hunter College, New York, NY, USA*

³*The Graduate Center of the City University of New York, New York, NY, USA*

⁴*Department of Radiology, Weill Cornell Medical College, New York, NY, USA*

⁵*Department of Medicine, Memorial Sloan Kettering Cancer Center, New York, NY, USA*

⁶*Departments of Radiology and Pharmacology, Weill Cornell Medical College, New York, NY, USA*

Correspondence: Jason S. Lewis, PhD, 1275 York Avenue, New York, NY 10065, USA. Phone: 646-888-3038, FAX: 646-422-0408, Email: lewisj2@mskcc.org

First author: Sophie Poty, PhD, 1275 York Avenue, New York, NY 10065, USA. Phone: 646-888-3080, FAX: 646-422-0408, Email: potys@mskcc.org

Word count: 5845

Disclaimer: The authors have nothing to disclose.

Financial support: The authors gratefully acknowledge the Radiochemistry and Molecular Imaging Probe core, which was supported in part by the NIH/NCI Cancer Center Support Grant P30 CA008748. We gratefully acknowledge Mr. William H. and Mrs. Alice Goodwin and the Commonwealth Foundation for Cancer Research and The Center for Experimental Therapeutics of Memorial Sloan Kettering Cancer Center (JSL) and the fellowship from the François Wallace Monahan Fellowship from the JLM Benevolent Fund (SP).

Key words: Radiotherapy, Alpha Emitters, Radiochemistry, Clinical Trials

Learning Objectives: On successful completion of this activity, participants should be able to (1) match α -emitters to potential vectors or targets of interest; (2) highlight the potential of α -emitters in preclinical work; and (3) identify the current clinical uses of α -emitters and the importance of clinical trial design for broader application of α -therapy.

Abstract: The use of radioactive sources to deliver cytotoxic ionizing radiation to disease sites dates back to the early 20th century, with the discovery of radium and its physiological effects. Alpha-emitters are of particular interest in the field of clinical oncology for radiotherapy applications. The first part of this review explored α -emitting radionuclides' basic radiochemistry, high cell-killing potency, and availability, together with hurdles such as radiolabeling methods and daughter redistribution. The second part of this review will give an overview of the most promising and current uses of α -emitters in preclinical and clinical studies.

The short particle range and high linear energy transfer of alpha-emitting radionuclides complement the large particle range and low energy transfer of β -particles. These physical characteristics allow α -particles to deposit the great majority of their energy in the area surrounding the desired targeted tumor cells ($< 100 \mu\text{m}$), enabling them to kill isolated tumor cells. Alpha-emitting radionuclides are therefore of particular interest for the treatment of systemic disease such as leukemia or lymphoma but also minimal disseminated disease composed of small clusters or isolated tumor cells. The past few years have also seen the preclinical and/or clinical use of alpha-emitters for the treatment of solid primary and metastatic disease such as glioblastoma or castration-resistant prostate cancer (CRPC) (1,2). Six α -emitters are currently under investigation in preclinical and clinical studies using either their intrinsic targeting properties or targeted alpha-therapy (TAT) strategies. Antibodies, peptides, and small molecules have been successfully conjugated to α -particle emitters; however, few of these α -conjugates have been translated to the clinic for evaluation.

For basic physical characteristics of the described alpha-emitters, the authors would like to refer the readers to Part 1 of this review.

PRECLINICAL EVALUATION (PUBLISHED OVER THE LAST 10 YEARS)

The design of preclinical studies plays an important role in the success and translation of α -therapy to the clinical stage (Fig. 1). The following section presents a selection of preclinical studies with strong translational potential.

Systemic cancers: Lymphoma and leukemia

CD20 is a well-known target for the treatment of B-cell lymphoma. Despite its intermediate half-life, ^{211}At has been conjugated to an anti-CD20 monoclonal antibody and evaluated in two lymphoma models: a subcutaneous tumor xenograft and a disseminated model (3). High total doses (1.78 MBq) of ^{211}At -anti-CD20 radioimmunotherapy (RIT) demonstrated moderate attenuation in tumor growth in a subcutaneous xenograft model. In contrast, a 0.55 MBq total dose resulted in complete disease eradication in 70% of the animals with the disseminated lymphoma model (Fig. 2A) (3). Following the 0.55 MBq total dose, universally lethal toxicity was observed within five days with severe weight loss and petechiae. This study highlights the different potential of α -therapy depending on tumor cell accessibility.

The longer-lived α -emitting radioisotope, ^{227}Th , was originally conjugated to antibodies such as trastuzumab and anti-CD20 mAb (rituximab), demonstrating significant tumor growth delay and prolonged survival in breast, ovarian, and lymphoma models (4,5). Long-term toxicity (up to 1 year) was assessed in mice with human lymphoma Raji xenografts (6). A 1000 kBq/kg dosage for [^{227}Th]Th-rituximab resulted in significant body weight decrease with temporary white blood cell and platelet count drops (6). The MTD was determined to be between 600-1000 kBq/kg with a maximum absorbed dose to the bone marrow between 2.1-3.5 Gy (6).

Reducing non-specific toxicity and hematotoxicity using the pretargeting method was investigated. Pretargeted α -RIT using an anti-CD20 single-chain variable region (scFv)-streptavidin construct and a [^{213}Bi]Bi-DOTA-biotin was reported by Park *et al.* to treat non-Hodgkin lymphoma (7). A favorable biodistribution profile was obtained using the pretargeting method with specific tumor uptake of $16.5\% \pm 7.0\%$ injected dose per gram at 90 minutes post-injection (Fig. 2B) (7). A therapy study with injections of up to 29.6 MBq (total dose) of [^{213}Bi]Bi-DOTA-Biotin exhibited dose-dependent tumor response (7). Three

mice out of 10 achieved complete remission with the highest dose and only one showed signs of early toxicity, losing approximately 10% of its body weight. The median survival for the 22.2 MBq [²¹³Bi]Bi-DOTA-Biotin total dose group was 90 days compared to 19 days for untreated mice (7).

The anti-CD33 antibody, lintuzumab (HuM195), has a long history of TAT applications for the treatment of acute myeloid leukemia (AML) and the clinical use of this agent will be discussed later in this review. Preclinically, it was first conjugated to ²¹³Bi and ²²⁵Ac, and more recently conjugated to ²²⁷Th (8). In this study, complete tumor regression up to 20 days was observed in an AML xenograft model with a dose of 700 kBq/kg of ²²⁷Th-RIT (8).

Metastatic prostate cancer

The external domain of prostate-specific membrane antigen (PSMA) is a major target of interest for TAT. McDevitt et al. successfully conjugated ²¹³Bi to J591, an anti-PSMA monoclonal antibody, and demonstrated the ability of the developed α -RIT to improve median tumor-free survival together with reduction of prostate specific antigen (PSA) levels in mice with intramuscular LNCaP xenografts (9). The past decade has also seen the development of numerous small molecule PSMA inhibitors to diagnose and treat prostate cancer. The actinium-225 conjugate will be described later in the clinical section of this review. An ²¹¹At-labeled small PSMA inhibitor conjugate was recently evaluated in PSMA-positive mice models, showing significant tumor growth delay and improved survival (10). Long-term toxicity (up to 12 months) revealed nephropathy to be the dose-limiting effect, and the maximum tolerated dose (MTD) was set to be 37 kBq total dose in immunocompetent CD1 mice (10).

Radium-223 is a particularly interesting radionuclide due to its bone-seeking properties and its antitumor effects were demonstrated in animal models (11). Validation of this radionuclide in both preclinical and clinical studies is extensive, leading to the commercialization and use of this radioisotope in men with metastatic prostate cancer. We will, therefore, focus our interest on the clinical studies performed with this α -emitter in the clinical section below.

Disseminated intraperitoneal disease

Lead-212 (β -emitter), the decay daughter of ^{224}Ra and parent of ^{212}Bi (α -emitter), is widely exploited as an α -particle nanogenerator. ^{212}Pb was first validated preclinically when conjugated to trastuzumab to treat disseminated human epidermal growth factor receptor 2 (HER-2) positive peritoneal disease; its clinical application will be discussed in the next section (12). The contribution of internalization in HER-2 TAT in terms of efficacy was compared to a non-internalizing ^{212}Pb -labeled anti-carcinoembryonic antigen 35A7 antibody (13). A-431 intraperitoneal xenografted mice that express both HER-2 (low level) and carcinoembryonic antigen (high level) were injected with the same activity of both radioimmunoconjugates. Absorbed dose calculations revealed higher dose to the tumor in the case of the non-internalizing antibody [^{212}Pb]Pb-35A7 (35.5 Gy) compared to the internalizing [^{212}Pb]Pb-trastuzumab (27.6 Gy) (13). However, the trastuzumab conjugate led to an unexpected longer mean survival (> 130 days) (13). This study demonstrates the advantage of internalizing antibodies for therapy of small-volume xenograft tumors but also highlights the need for microdosimetry studies. With ^{212}Pb α -therapy of disseminated intraperitoneal disease well established, the Brechbiel group developed α -therapy targeting HER-1 (also referred to as epidermal growth factor receptor) to provide another possibility or treatment combination for patients with residual tumor tissue following debulking

surgery, micrometastatic disease, or disseminated peritoneal disease. Cetuximab was therefore radiolabeled with ^{212}Pb and total doses of 370-740 MBq were well tolerated by mice with minimal toxicity (14).

Emerging targets of interest – targeting the tumor microenvironment

CD70 belongs to the tumor necrosis factor superfamily and together with CD27L, plays an important role in T-cell signaling. It is overexpressed on T and B-cell lymphomas as well as on several types of solid tumors (i.e., renal cell carcinoma, ovarian and pancreatic adenocarcinoma, breast and colon cancer). CD-70 is notably a promising target for immunotherapy and was also investigated by Hagemann *et al.* for ^{227}Th -TAT (15). Mice bearing human renal cell carcinoma 789-O subcutaneous xenografts experienced complete growth inhibition with doses as low as 50 kBq/kg (15). Decreased circulating neutrophils, lymphocytes, and total white blood cells as compared to the control group indicated myelosuppression in the treated mice (Fig. 2C). However, this toxicity was transient and mice recovered by day 114 (15).

Targeting the tumor microenvironment such as the tumor vasculature and the neovascular endothelium are interesting targets for α -therapy. ^{225}Ac -E4G10 antibody-conjugate, which targets monomeric vascular endothelial cadherin, recently demonstrated inhibition of tumor growth and improved survival in a high-grade glioblastoma mouse model (1). Mechanistic studies highlighted the tumor blood-brain barrier microenvironment remodeling by dual depletion of endothelial and perivascular cells (16). Even though more than 20% of injected dose per gram of tissue of ^{225}Ac -E4G10 was observed in the liver after 10 days post-treatment, no liver toxicity was reported (1).

Integrins play an important role in tumor angiogenesis and their blockade can result in inhibition of tumor growth or metastasis. Among them, $\alpha_v\beta_3$ antagonists demonstrate

strong potential for the treatment of cancer. A DOTA-(RGDyK) peptide conjugate radiolabeled with ^{225}Ac displays high affinity for $\alpha_v\beta_3$ integrin (17). Cerenkov imaging performed in U87mg xenografted mice upon injection of 1.9 MBq (total dose) of the radiolabeled peptide, showed tumor, liver, and kidneys uptake. *Ex vivo* imaging confirmed the biodistribution (Fig. 2D) (17). Cerenkov radiation is observed with a wide range of medical isotopes, including ^{225}Ac (18). Since α -particles travel with low velocity, ^{225}Ac Cerenkov emissions are postulated to result from the β -decay of ^{213}Bi , ^{209}Tl , and ^{209}Pb . A therapy study using three different doses based on [^{225}Ac]Ac-DOTA-(RGDyK) MTD (0.04 MBq; 1 MTD, 0.5 MTD, and 0.25 MTD) showed high blood urea nitrogen retention in all cohorts, suggesting kidney impairment (17).

ALPHA VS. BETA STUDIES

The following studies compare the efficacy of α -particle therapy to β -particle therapy. ^{225}Ac -labeled anti-rat HER-2/neu mAb (7.16.4) efficacy was compared to ^{213}Bi and ^{90}Y conjugates to treat breast cancer lung metastasis (Fig. 3A) (19). Injection of the MTD resulted in improved median survivals: 50 days for the [^{90}Y]Y-7.16.4 group and 61 days for the [^{213}Bi]Bi-7.16.4 group. Of a total 12 mice, 8 achieved long-term survival (up to one year) in the [^{225}Ac]Ac-7.16.4-treated group (19). Alpha-therapy superiority compared to beta-therapy was attributed to the local α -radiation dose delivery vs. the β -particle energy that was mostly deposited outside of the metastasis. Due to the pharmacokinetics of the antibody-radioconjugates, >90% of the ^{213}Bi -conjugate decay occurred before reaching its target. The longer physical half-life of ^{225}Ac together with the emission of 4 net α -particles per decay therefore resulted in higher absorbed doses, which explains the longer survival of the ^{225}Ac -treated mice. Slow but significant release of ^{225}Ac daughters resulted in long-term renal toxicity (Fig. 3B) (19).

Peptide receptor radionuclide therapy using the somatostatin analog DOTATOC radiolabeled with ^{225}Ac and ^{177}Lu also compared α to β therapeutic potential (20). Equitoxic doses of the α - and β -emitter radiopharmaceuticals were determined using comparative cytotoxicity assessment and a factor of approximately 700 was applied between the ^{225}Ac - and ^{177}Lu -conjugates. The degree of DNA double-strand breaks was determined using quantification of γH2AX levels. The overall percentage of cells with γH2AX foci was significantly higher in tumors treated with 48 kBq (total dose) of [^{225}Ac]Ac-DOTATOC (35%) than those treated with 30 MBq (total dose) of [^{177}Lu]Lu-DOTATOC (21%) (Fig. 3C) (20). This observation was consistent with a delayed exponential tumor growth of 25 days with [^{225}Ac]Ac-DOTATOC vs. 21 days with [^{177}Lu]Lu-DOTATOC (Fig. 3D) (20).

Alpha-particle emitters have substantial therapeutic potential due to their ability to generate higher levels of double-DNA strand breaks compared to β -particle. However, alpha versus beta studies can be biased by the use of α -emitters with long half-lives and numerous alpha-emitting progeny that increase the tumor-absorbed dose. Dosimetric considerations, even though challenging with α -emitters, should be a parameter of choice for the determination of the administered activity in such comparative studies. Moreover, parameters such as the tumor size, hypoxia or the intratumoral radiopharmaceutical distribution should be considered.

In the clinic, the choice between α - or β -therapy is currently dependent on the patient tumor burden and previous response to β -therapy. Alpha-therapy is currently only offered at late disease stage and the efficacy of this therapy is still unknown at earlier disease stages (21). Comparison of the therapeutic potentials of alpha vs. beta therapy for clinical applications would therefore be premature at this moment. Further evaluation of α -therapy

is required at early stage disease but also in combination with current standard of care or new therapeutic approaches such as inhibition of DNA repair pathways (e.g. PARP inhibitors) (21). Cocktail approaches of α - and β -therapy should also be evaluated due to the complementary nature of their particle range.

CLINICAL EVALUATION

To our knowledge, 62 clinical trials were registered on clinicaltrials.gov using alpha emitters; among them, 52 involved [^{223}Ra]Ra-dichloride (Table 1) utilizing the bone-seeking properties of radium. This last section will focus on clinical achievement and evolution of the most notable clinical studies performed with α -emitting radionuclides.

Advanced myeloid leukemia: from [^{213}Bi]Bi-Lintuzumab to [^{225}Ac]Ac-Lintuzumab

In a phase I dose escalation trial, a humanized anti-CD33 mAb, HuM195 (lintuzumab) that targets myeloid leukemia cells was radiolabeled with ^{213}Bi (22). The choice of an α -emitting radionuclide was justified by the significant toxicities, particularly prolonged myelosuppression, observed in previous studies using β -particle emitters. Eighteen patients with primary refractory or relapsed advanced myeloid leukemia (AML) were treated with 10.4-37.0 MBq/kg (22). Although all patients developed transient myelosuppression (recovery time of 22 days), no extramedullary toxicity was observed. Of the evaluable patients, 93% showed a reduction in peripheral blood leukemia cells and 78% showed a reduction in bone marrow blasts. However, no patient achieved complete remission (22), likely because of the patients' large tumor burden (up to 10^{12} cells). Partial cytoreduction of the tumor burden prior to the ^{213}Bi treatment was evaluated in a phase I/II trial with sequential treatment with cytarabine (200 mg/m²/d) and [^{213}Bi]Bi-HuM195

(18.5-46.3 MBq/kg) (23). A decrease in marrow blasts was reported for all dose levels and a ^{213}Bi dose-response relationship with remission was observed for doses ≥ 37 MBq/kg (23).

Actinium-225 was next considered as an alternative therapeutic radioisotope to ^{213}Bi in order to take advantage of the greater cytotoxic potential and significantly longer half-life of ^{225}Ac . [^{225}Ac]Ac-HuM195 was subsequently evaluated in a Phase I study with relapsed or refractory patients AML (24). Doses between 18.5-148 kBq/kg were administered. Redistribution of daughters in the kidneys was anticipated, but no evidence of radiation-induced nephrotoxicity was seen. Peripheral blasts were eliminated in 63% of the patients but only at doses of 37 kBq/kg or higher. Bone marrow blast reduction was observed in 67% of patients (24). A phase I/II study in AML patients currently evaluates the MTD and efficacy of the combination of low-dose cytarabine and [^{225}Ac]Ac-HuM195. Preliminary results recommend a 74 kBq/kg/fraction dose for the phase II study in order to limit prolonged myelosuppression (25). Patients receiving [^{225}Ac]Ac-HuM195 have also been administered furosemide and spironolactone in order to prevent potential radiation-induced renal toxicity (25,26). Furosemide has since been discontinued as it was causing dehydration in some patients. However, without furosemide, there has been no renal toxicity observed in patients receiving [^{225}Ac]Ac-HuM195.

Neuroendocrine tumors: [^{213}Bi]Bi-DOTATOC for β -radiation-refractory tumors

Kratochwil and colleagues performed a first-in-human study using a somatostatin analogue TAT, [^{213}Bi]Bi-DOTATOC, as a therapeutic option for patients with refractory neuroendocrine tumors that were pretreated with β -emitting [^{90}Y]Y/[^{177}Lu]Lu-DOTATOC (27). Patients with progressive advanced neuroendocrine tumors with liver metastasis were treated with intraarterial infusions, and one patient with bone carcinosis was treated with a systemic infusion (Fig. 4A). [^{213}Bi]Bi-DOTATOC was administered in cycles with

increasing activities (1.0-4.0 GBq, total dose) every two months. All patients showed long-lasting anti-tumor responses, highlighting the ability of [²¹³Bi]Bi-DOTATOC to overcome β-radiation resistance. Renal toxicity was minimized due to a protocol developed with the β-emitting particle radiopeptide therapy, including lysine, arginine, and Gelofusine administration (27).

HER2-expressing ovarian carcinoma: [²¹²Pb]Pb-TCMC-Trastuzumab

The biodistribution, pharmacokinetics, and safety of [²¹²Pb]Pb-TCMC-trastuzumab in patients with HER2-expressing ovarian cancer with malignancies mainly confined to the peritoneal cavity that progressed after multiple therapies were assessed in a first-in-human study by Meredith et al (28). A single intraperitoneal injection of [²¹²Pb]Pb-TCMC-trastuzumab (7.4 MBq/m²) following a 4 mg/kg intravenous injection of trastuzumab (28) was first evaluated followed by a dose escalation study (7.4-21.1 MBq/m²) (29). Furosemide and spiro lactone were administered as renal protective agents. Minimal radiopharmaceutical redistribution out of the peritoneal cavity and no significant myelosuppression was observed (28). However, no patient met criteria for a partial response (29).

Metastatic castration-resistant prostate cancer: from [²²³Ra]Ra-dichloride to [²²⁵Ac]Ac-DOTA-PSMA

With 52 clinical trials registered on clinicaltrial.gov, the use of [²²³Ra]Ra-dichloride (Alpharadin or Xofigo®) has impacted the therapeutic landscape of α-radiation therapy. Approximately 80% of the clinical trials involve prostate cancer and 35% employ a combination of drugs and [²²³Ra]Ra-dichloride. First clinical experiments with [²²³Ra]Ra-dichloride (46-250 kBq/kg) performed on prostate and breast cancer patients reported

pain relief and reduction in alkaline phosphatase (30). ALSYMPCA, a phase III, randomized, double-blind, placebo-controlled trial aimed to evaluate the efficacy and safety of [²²³Ra]Ra-dichloride (50 kBq/kg every 4 weeks for a total of 6 cycles) vs. placebo plus standard of care in symptomatic CRPC patients (31). Overall survival was significantly longer with [²²³Ra]Ra-dichloride: 14.9 months compared to 11.3 months with the placebo (Fig. 4B) (31). These primary results led to the FDA approval of [²²³Ra]Ra-dichloride to treat CRPC in May 2013. Prolonged time to increase total alkaline phosphatase and prostate-specific antigen (PSA) was also observed (32). [²²³Ra]Ra-dichloride is well tolerated, minimally toxic and patients reported significant improvement in quality of life (32); however, it does not target soft tissue disease or the circulating component of the disease (late manifestations).

Another promising α -therapeutic option for metastatic CRPC employs a small urea-based PSMA inhibitor (2) already used in the clinic for prostate cancer positron emission tomography (PET) imaging (33) and β -therapy (34). While promising, this β -therapy is ineffective in about 30% of patients and contraindicated for patients with diffuse red marrow infiltration. ²²⁵Ac was considered to overcome β -resistance and reduce hematologic toxicity. Two metastatic CRPC patients in challenging clinical situations first received [²²⁵Ac]Ac-PSMA-617 (100 kBq/kg, bimonthly) as salvage therapy after the validation of PSMA-positive tumor phenotype by [⁶⁸Ga]Ga-PSMA-11 PET/CT scans (2). Both patients showed complete response (Fig. 4C) with a drop of PSA levels below the measurable level. Xerostomia was reported in the two patients (2). A larger study with 14 mCRPC patients identified the best compromise between toxicity and antitumor response (35). A treatment activity of 100 kBq/kg was determined to be tolerable with significant antitumor activity (35). Though, a solution to preserve the salivary glands should be investigated. [²²⁵Ac]Ac-PSMA-617 offers the major advantage of targeting metastases in any tissue and could

therefore be used as a complementary option to [²²³Ra]Ra-dichloride therapy. Shortage of ²²⁵Ac, however, remains a challenge and limits the evaluation of ²²⁵Ac-TAT in large studies.

INTEGRATING ALPHA-THERAPY INTO CURRENT AND FUTURE CLINICAL PARADIGMS:

The future of alpha-therapy lies in the resolution of hurdles mentioned in Part 1 of this review, that is to say availability, production concerns and issues associated with daughter redistribution. Solutions to these issues are currently being investigated and should facilitate the broader development of α -emitter radiotherapy with larger, randomized, prospective clinical studies that would ultimately result in more meaningful efficacy and toxicity evaluation.

The future of alpha-therapy also lies in the proper design of clinical trials and the incorporation of this mode of therapy into current standard of care or in combination with new therapeutic approaches. An irony of the current status of [²²³Ra]Ra-dichloride is that despite the completion of early-phase studies and ALSYMPCA, the optimal dose and duration of therapy is still not known. Currently, a randomized phase II trial (NCT02023697) examines men with mCRPC with two or more skeletal metastases under three separate treatment arms; standard [²²³Ra]Ra-dichloride regimen (55 kBq/kg, FDA approved), a high-dose regimen (88 kBq/kg, every month for six months), and an extended duration regimen (55 kBq/kg injections, every month for 12 months). This study will complement a completed smaller single-arm study (NCT01934790) in which patients who had received a six-month course of [²²³Ra]Ra-dichloride underwent another six months of the drug at standard doses (55 kBq/kg per month). Preliminary data on 44 patients reveals that 66% of patients completed re-treatment with an excellent safety profile (36). The clinical impact of additional treatments still needs to be defined.

The optimization of [²²³Ra]Ra-dichloride treatment is also explored in combination with tumor-targeting therapy such as androgen receptor (AR) axis-directed therapy. A randomized phase III trial (NCT02043678) compares the androgen biosynthesis inhibitor abiraterone acetate and prednisone with abiraterone, prednisone and [²²³Ra]Ra-dichloride in men with mCRPC who had not received cytotoxic chemotherapy. The Independent Data Monitoring Committee recommended that this trial be unblinded when it observed an imbalance in fractures and deaths, favoring treatment with abiraterone/prednisone alone (37). At this time, the details of these data are pending, but for now clinicians are increasingly cautious about treating men with early mCRPC with the combination of abiraterone, prednisone, and [²²³Ra]Ra-dichloride.

The combination of [²²³Ra]Ra-dichloride with chemotherapy is also being explored in men with mCRPC. [²²³Ra]Ra-dichloride has been tested in a phase Ib/IIa study (NCT01106352) in combination with docetaxel (step-down dose 60 mg/m²). Patients were randomized to either the combination arm or to docetaxel on a 2:1 basis. PSA declines of over 50% occurred in 61% of patients in the combination arm and 54% in the docetaxel arm. Sustained suppression was also apparent in the Kaplan-Meier analysis, with a significantly longer time to PSA progression in favor of the combination (6.6 vs 4.8 months; P=.0198) (38). A number of newer trials are exploring [²²³Ra]Ra-dichloride as an adjunct to boost other treatment effects, such as PARP inhibitor (i.e., olaparib (39) or niraparib (NCT03076203)), or as an immune adjuvant leveraging the abscopal effect to enhance the impact of immunotherapy ([²²³Ra]Ra-dichloride in combination with PD-L1 inhibitor atezolizumab (NCT02814669)). Combinations of tumor and bone targeting offer a promise of amplifying the effects of treatment beyond the host compartment of bone and would allow patients with visceral metastases to receive [²²³Ra]Ra-dichloride, which at the present time, is not permissible in the US. Dual tumor and bone targeting is also possible with

tumor-directed α -emitters ($[^{225}\text{Ac}]\text{Ac-PSMA-617}$), although formal dose-finding prospective studies for these agents are still needed, in which the optimal dose and treatment intervals are defined, and toxicity mitigation strategies (in particular for xerostomia) are developed.

CONCLUSION

Studies described in this review demonstrate that α -emitting radionuclides have the potential to be excellent therapeutic candidates and, along with β -particle therapy, can expand the options for therapy. Alpha-emitting radionuclides are currently considered at late disease stages as an alternative choice when resistance to β -therapy is observed or when the patient presents with extended bone marrow disease; however, applications in earlier disease stages should be evaluated. Together Part 1 and Part 2 of this review give a broad overview of α -emitters from basic radiochemistry to clinical use. The future of α -radiotherapy is dependent on numerous factors; Part 1 highlights hurdles and new approaches for a wider use of α -emitting radionuclides, and Part 2 highlights the importance of clinical trials design for a proper determination of α -therapy optimal dose and incorporation into standard of care protocols.

References

1. Behling K, Maguire WF, Lopez Puebla JC, et al. Vascular targeted radioimmunotherapy for the treatment of glioblastoma. *J Nucl Med.* 2016;57:1576-1582.
2. Kratochwil C, Bruchertseifer F, Giesel FL, et al. ^{225}Ac -PSMA-617 for PSMA-targeted a-radiation therapy of metastatic castration-resistant prostate cancer. *J Nucl Med.* 2016;57:1941-1944.
3. Green DJ, Shadman M, Jones JC, et al. Astatine-211 conjugated to an anti-CD20 monoclonal antibody eradicates disseminated B-cell lymphoma in a mouse model. *Blood.* 2015;125:2111-2119.
4. Dahle J, Bruland OS, Larsen RH. Relative biologic effects of low-dose-rate alpha-emitting ^{227}Th -rituximab and beta-emitting ^{90}Y -tiuxetan-ibritumomab versus external beam X-radiation. *Int J Radiat Oncol.* 2008;72:186-192.
5. Heyerdahl H, Krogh C, Borrebaek J, Larsen A, Dahle J. Treatment of HER2-expressing breast cancer and ovarian cancer cells with alpha particle-emitting ^{227}Th -trastuzumab. *Int J Radiat Oncol.* 2011;79:563-570.
6. Dahle J, Jonasdottir TJ, Heyerdahl H, et al. Assessment of long-term radiotoxicity after treatment with the low-dose-rate alpha-particle-emitting radioimmunoconjugate ^{227}Th -rituximab. *Eur J Nucl Med Mol Imaging.* 2010;37:93-102.
7. Park SI, Shenoi J, Pagel JM, et al. Conventional and pretargeted radioimmunotherapy using bismuth-213 to target and treat non-Hodgkin lymphomas expressing CD20: a preclinical model toward optimal consolidation therapy to eradicate minimal residual disease. *Blood.* 2010;116:4231-4239.
8. Hagemann UB, Wickstroem K, Wang E, et al. In vitro and in vivo efficacy of a novel CD33-targeted Thorium-227 conjugate for the treatment of acute myeloid leukemia. *Mol Cancer Ther.* 2016;15:2422-2431.

9. McDevitt MR, Barendswaard E, Ma D, et al. An alpha-particle emitting antibody (^{213}Bi) for radioimmunotherapy of prostate cancer. *Cancer Res.* 2000;60:6095-6100.
10. Kiess A, Minn IL, Vaidyanathan G, et al. (2S)-2-(3-(1-Carboxy-5-(4- ^{211}At astatobenzamido)pentyl)ureido)-pentanedioic acid for PSMA-targeted alpha-particle radiopharmaceutical therapy. *J Nucl Med.* 2016;57:1569-1575.
11. Larsen RH, Saxtorph H, Skydsgaard M, et al. Radiotoxicity of the alpha-emitting bone-seeker ^{223}Ra injected intravenously into mice: histology, clinical chemistry and hematology. *In vivo.* 2006;20:325-331.
12. Milenic DE, Garmestani K, Brady ED, et al. Alpha-particle radioimmunotherapy of disseminated peritoneal disease using a ^{212}Pb -labeled radioimmunoconjugate targeting HER2. *Cancer Biother Radio.* 2005;20:557-568.
13. Boudousq V, Bobyk L, Busson M, et al. Comparison between internalizing anti-HER2 mAbs and non-internalizing anti-CEA mAbs in alpha-radioimmunotherapy of small volume peritoneal carcinomatosis using ^{212}Pb . *PLoS One.* 2013;8:e69613.
14. Milenic DE, Baidoo KE, Kim YS, Brechbiel MW. Evaluation of cetuximab as a candidate for targeted alpha-particle radiation therapy of HER1-positive disseminated intraperitoneal disease. *mAbs.* 2015;7:255-264.
15. Hagemann UB, Mihaylova D, Uran SR, et al. Targeted alpha therapy using a novel CD70 targeted thorium-227 conjugate in in vitro and in vivo models of renal cell carcinoma. *Oncotarget.* 2017;8:56311-56326.
16. Behling K, DiGialleonardo V, Maguire WF, et al. Remodelling the vascular microenvironment of glioblastoma with alpha-particles. *J Nucl Med.* 2016;57:1771-1777.
17. Pandya DN, Hantgan R, Budzevich MM, et al. Preliminary therapy evaluation of ^{225}Ac -DOTA-c(RGDyK) demonstrates that cerenkov radiation derived from ^{225}Ac daughter

decay can be detected by optical imaging for in vivo tumor visualization. *Theranostics*. 2016;6:698-709.

18. Ruggiero A, Holland JP, Lewis JS, Grimm J. Cerenkov luminescence imaging of medical isotopes. *J Nucl Med*. 2010;51:1123-1130.

19. Song H, Hobbs RF, Vajravelu R, et al. Radioimmunotherapy of breast cancer metastases with alpha-particle emitter ^{225}Ac : comparing efficacy with ^{213}Bi and ^{90}Y . *Cancer Res*. 2009;69:8941-8948.

20. Graf F, Fahrner J, Maus S, et al. DNA double strand breaks as predictor of efficacy of the alpha-particle emitter Ac-225 and the electron emitter Lu-177 for somatostatin receptor targeted radiotherapy. *PLoS One*. 2014;9:e88239.

21. Fendler WP, Cutler C. More alpha than beta for prostate cancer? *J Nucl Med*. 2017;58:1709-1710.

22. Jurcic JG, Larson SM, Sgouros G, et al. Targeted alpha particle immunotherapy for myeloid leukemia. *Blood*. 2002;100:1233-1239.

23. Rosenblat TL, McDevitt MR, Mulford DA, et al. Sequential cytarabine and alpha-particle immunotherapy with bismuth-213-lintuzumab (HuM195) for acute myeloid leukemia. *Clin Cancer Res*. 2010;16:5303-5311.

24. Jurcic JG, Rosenblat TL. Targeted alpha-particle immunotherapy for acute myeloid leukemia. *Am Soc Clin Oncol Educ Book*. 2014:e126-131.

25. Jurcic JG, Levy MY, Park JH, et al. Phase I Trial of Targeted alpha-particle therapy with Actinium-225 (Ac-225)-Lintuzumab and low-dose cytarabine (LDAC) in patients age 60 or older with untreated acute myeloid leukemia (AML). *Blood*. 2016;128:4050.

26. Jaggi JS, Seshan SV, McDevitt MR, Sgouros G, Hyjek E, Scheinberg DA. Mitigation of radiation nephropathy after internal alpha-particle irradiation of kidneys. *Int J Radiat Oncol Biol Phys*. 2006;64:1503-1512.

27. Kratochwil C, Giesel FL, Bruchertseifer F, et al. ^{213}Bi -DOTATOC receptor-targeted alpha-radionuclide therapy induces remission in neuroendocrine tumours refractory to beta radiation: a first-in-human experience. *Eur J Nucl Med Mol Imaging*. 2014;41:2106-2119.
28. Meredith RF, Torgue J, Azure MT, et al. Pharmacokinetics and imaging of ^{212}Pb -TCMC-trastuzumab after intraperitoneal administration in ovarian cancer patients. *Cancer Biother Radio*. 2014;29:12-17.
29. Meredith R, Torgue J, Shen S, et al. Dose escalation and dosimetry of first-in-human alpha radioimmunotherapy with ^{212}Pb -TCMC-trastuzumab. *J Nucl Med*. 2014;55:1636-1642.
30. Nilsson S, Larsen RH, Fossa SD, et al. First clinical experience with alpha-emitting radium-223 in the treatment of skeletal metastases. *Clin cancer Res*. 2005;11:4451-4459.
31. Parker C, Nilsson S, Heinrich D, et al. Alpha emitter radium-223 and survival in metastatic prostate cancer. *N Engl J Med*. 2013;369:213-223.
32. Sartor O, Coleman R, Nilsson S, et al. Effect of radium-223 dichloride on symptomatic skeletal events in patients with castration-resistant prostate cancer and bone metastases: results from a phase 3, double-blind, randomised trial. *Lancet Oncol*. 2014;15:738-746.
33. Afshar-Oromieh A, Holland-Letz T, Giesel FL, et al. Diagnostic performance of ^{68}Ga -PSMA-11 (HBED-CC) PET/CT in patients with recurrent prostate cancer: evaluation in 1007 patients. *Eur J Nucl Med Mol Imaging*. 2017;44:1258-1268.
34. Brauer A, Grubert LS, Roll W, et al. ^{177}Lu -PSMA-617 radioligand therapy and outcome in patients with metastasized castration-resistant prostate cancer. *Eur J Nucl Med Mol Imaging*. 2017;44:1663-1670.

35. Kratochwil C, Bruchertseifer F, Rathke H, et al. Targeted alpha-therapy of metastatic castration-resistant prostate cancer with ^{225}Ac -PSMA-617: dosimetry estimate and empiric dose finding. *J Nucl Med.* 2017;58:1624-1631.
36. Sartor O, Heinrich D, Mariados N, et al. Re-treatment with radium-223: first experience from an international, open-label, phase I/II study in patients with castration-resistant prostate cancer and bone metastases. *Ann. Oncol.* 2017;28:2464-2471.
37. <http://www.prnewswire.com/news-releases/phase-iii-trial-of-radium-ra-223-dichloride-in-combination-with-abiraterone-acetate-and-prednisoneprednisolone-for-patients-with-metastatic-castration-resistant-prostate-cancer-unblinded-early-300564844.html>.
38. Morris MJ, Lortol Y, Fizazi K, et al. Effects of radium-223 (Ra-223) with docetaxel versus docetaxel alone on bone biomarkers in patients with bone-metastatic castration-resistant prostate cancer (CRPC): A phase I/IIa clinical trial. *J Clin Oncol.* 2017;35(suppl 6S; abstract 154).
39. Mateo J, Carreira S, Sandhu S, et al. DNA-repair defects and olaparib in metastatic prostate cancer. *N Engl J Med.* 2015;373:1697-1708.
40. Zalutsky MR, Reardon DA, Akabani G, et al. Clinical experience with alpha-particle emitting ^{211}At : treatment of recurrent brain tumor patients with ^{211}At -labeled chimeric antitenascin monoclonal antibody 81C6. *J Nucl Med.* 2008;49:30-38.
41. Andersson H, Cederkrantz E, Back T, et al. Intraperitoneal alpha-particle radioimmunotherapy of ovarian cancer patients: pharmacokinetics and dosimetry of ^{211}At -MX35 F(ab')₂--a phase I study. *J Nucl Med.* 2009;50:1153-1160.
42. Cederkrantz E, Andersson H, Bernhardt P, et al. Absorbed doses and risk estimates of ^{211}At -MX35 F(ab')₂ in intraperitoneal therapy of ovarian cancer patients. *Int J Radiat Oncol.* 2015;93:569-576.

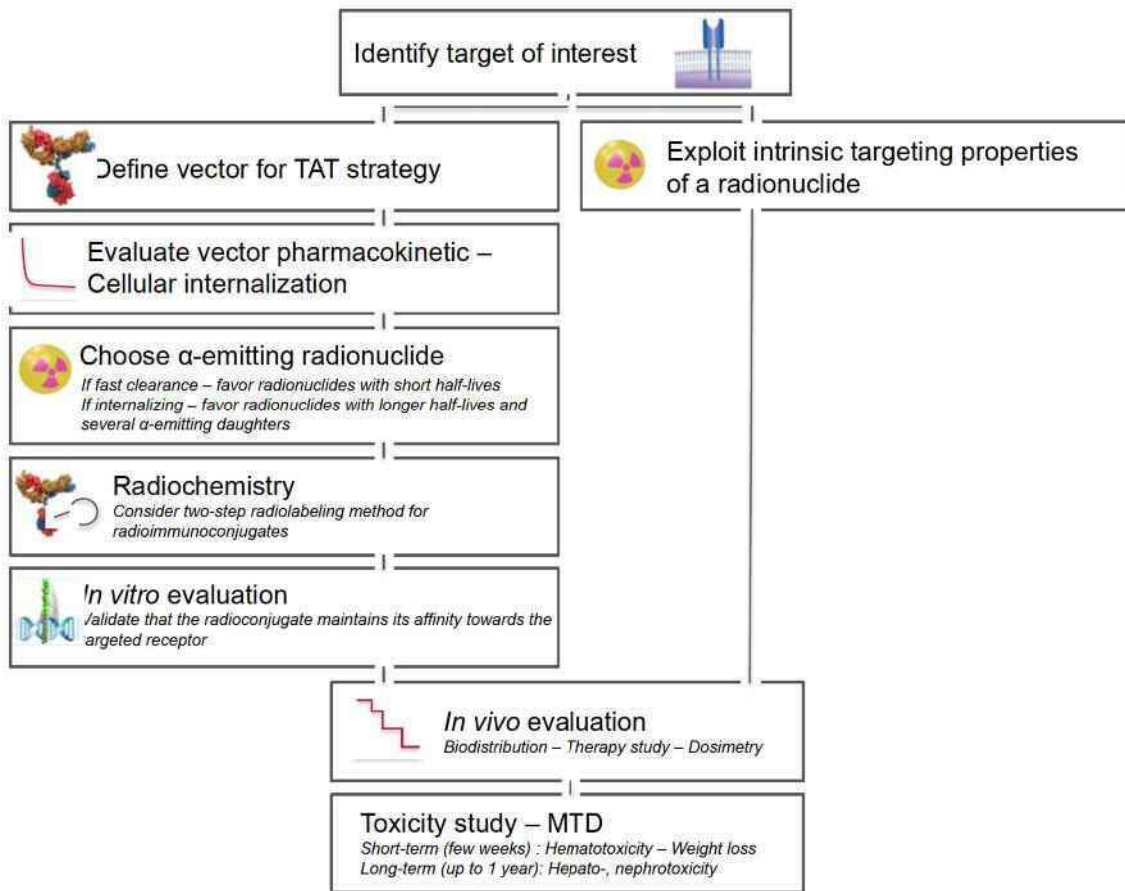


Figure 1. Preclinical study design flow chart. MTD: Maximum Tolerated Dose; TAT: Targeted α-therapy.

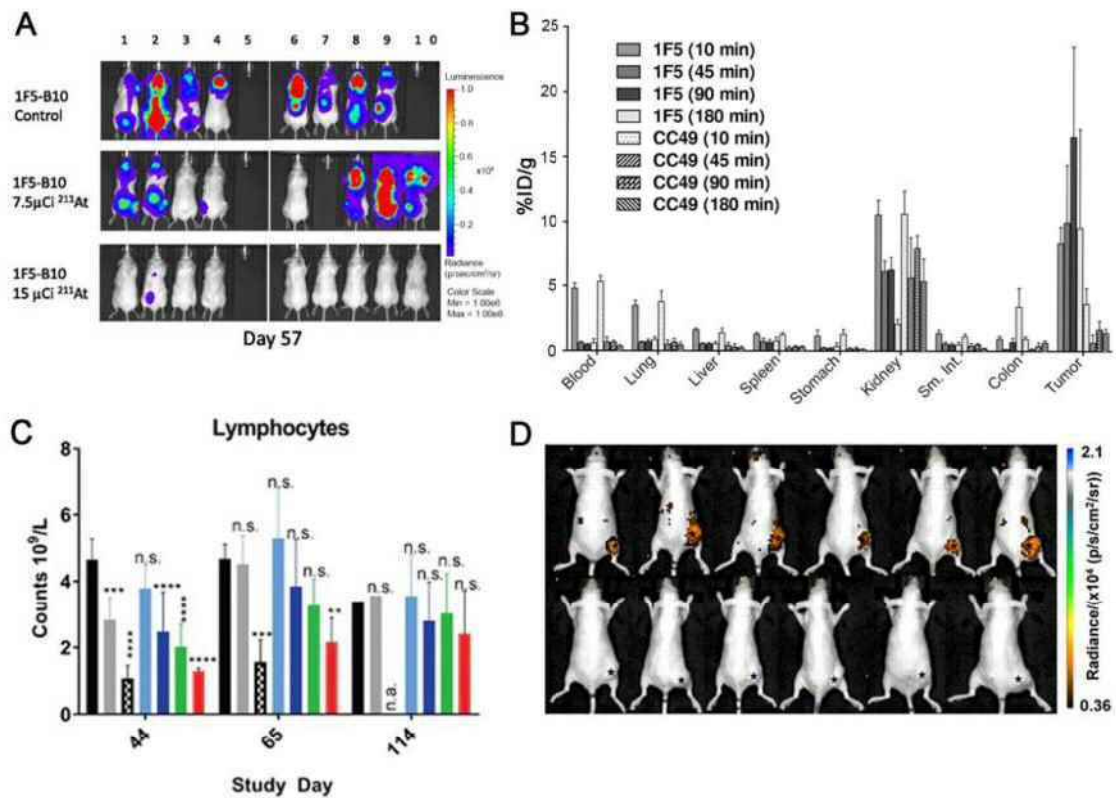


Figure 2. Preclinical studies, potency, imaging, and pitfalls of α -therapy. A) Bioluminescence imaging of [^{211}At]At-B10-1F5 (anti-CD20) RIT in Granta-519^{Luc}, a minimal residual disease model of lymphoma. Animals were treated on day 6 with 278 kBq (7.5 μCi) or 555 kBq (15 μCi) and received 1×10^7 bone marrow cells intravenously from syngeneic donors two days after treatment (3). B) Biodistribution of [^{213}Bi]Bi-DOTA-biotin after pretargeting RIT with 1F5(scFv)4-streptavidin (anti-CD20) and CC49(scFv)4-streptavidin (negative control) (7). C) Transient lymphocytes decrease after CD70-targeted ^{227}Th -conjugate (TTC) therapy indicative of myelosuppression (15). D) Cerenkov imaging acquired 24 h post-injection of [^{225}Ac]Ac-DOTA-c(RGDyK) in U87MG tumor-bearing mice. Top images show efficient tumor accumulation; bottom images show reduced tumor uptake upon blockage and demonstrate the specificity of the radiotherapy for $\alpha_v\beta_3$ integrin (17). Reprinted with permission.

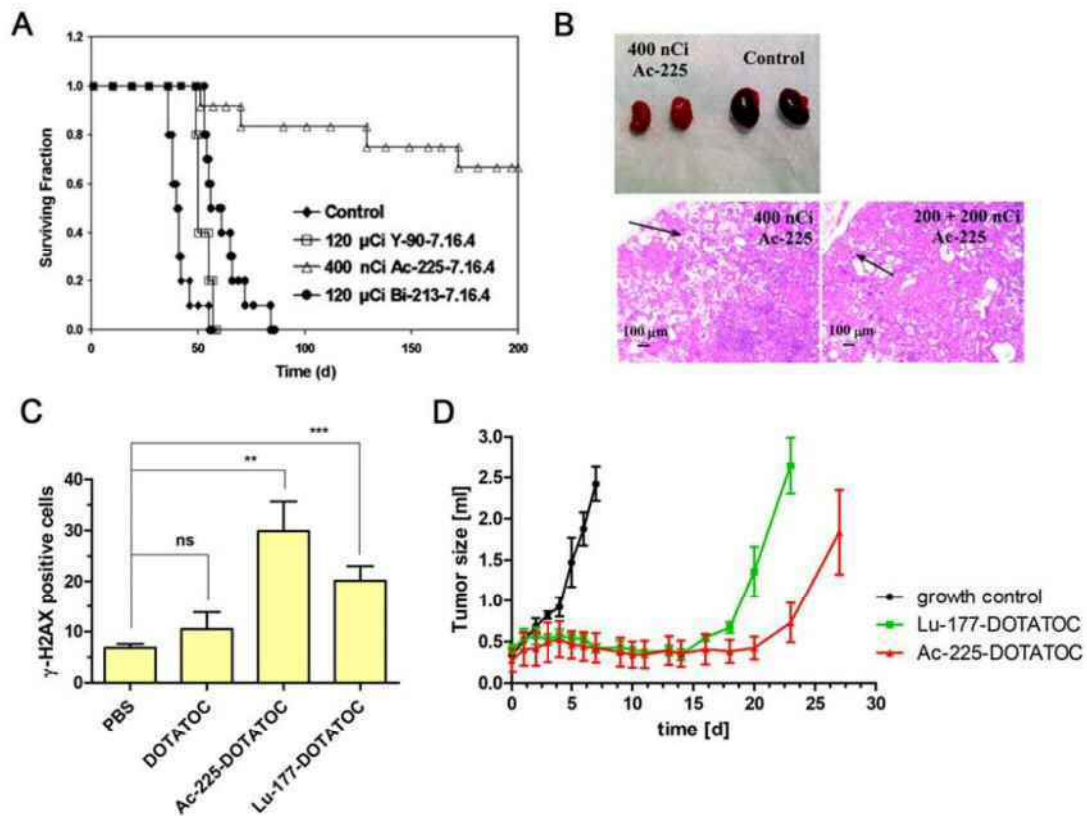


Figure 3. Preclinical alpha vs. beta studies. A) Kaplan-Meier survival curves of *neu-N* transgenic mice treated with 14.8 kBq (400 nCi) of ^{225}Ac -7.16.4, 4.4 MBq (120 μCi) of ^{213}Bi Bi-7.16.4, and 4.4 MBq (120 μCi) of ^{90}Y Y-7.16.4, three days after intravenous injection of 1×10^5 NT2.5 cells (19). B) *Top*, Photographs of kidneys from a *neu-N* mouse surviving one year after treatment with 14.8 kBq (400 nCi) of ^{225}Ac Ac-7.16.4 compared to a healthy *neu-N* mouse. *Bottom*, H&E staining of kidneys from *neu-N* mice surviving one year after treatment with 14.8 kBq (400 nCi) (*middle*) and 7.4 + 7.4 kBq (200 + 200 nCi) of ^{225}Ac Ac-7.16.4 (*right*). Arrows indicate collapse of cortical tissue due to loss of tubular epithelium in the kidney cortex (19). C) Quantification of γH2AX -positive cells after immunofluorescent staining of DNA DSBs in AR42J tumors following treatment with 47 kBq of ^{225}Ac Ac-DOTATOC, 30 MBq of ^{177}Lu Lu-DOTATOC, 1 μg of DOTATOC (unlabelled), or PBS(20). D) Tumor size measurement showing growth delay after treatment with equitoxic doses of ^{225}Ac Ac-DOTATOC (44 kBq) and ^{177}Lu Lu-DOTATOC (34 MBq) (20). Reprinted with permission.

Radiopharma-ceutical and dosage	Target and study population	Features and outcome	Dose-limiting observations and toxicity	Ref.
[²¹¹At]At-ch81C6 71-347 MBq	Tenascin 18 patients with primary or metastatic brain tumor	Phase I and II: Feasibility, safety, and efficacy Overall survival of 54.1 weeks vs. 23 weeks for glioblastoma patients	No grade 3 or higher toxicity	(40)
[²¹¹At]At-MX35 F(ab')₂ 22.4-101 MBq/L	Sodium-dependent phosphate transport protein 2b Women with complete clinical remission after second-line chemotherapy of recurrent ovarian cancer	Phase I: Pharmacokinetic and dosimetry Estimated absorbed dose to peritoneal 15.6 ± 1.0 mGy/(MBq/L)	With 200 MBq/mL, effective dose of 2.6 Sv (lifelong lethal cancer risk of 10%)	(41,42)
[²¹³Bi]Bi-DOTATOC 1.0-4.0 GBq	Somatostatin receptors Patients with progressive neuroendocrine tumors	First-in-human Long-lasting tumor response. Remission of tumors refractory to β-radiation.	Moderate acute hematologic and chronic kidney toxicities	(27)
[²¹³Bi]Bi-HuM195 10.36-37.0 MBq/kg	CD-33 Primary refractory or relapsed AML	Phase I: Dose escalation Reduction in peripheral blood leukemia cells and bone marrow blasts	Transient myelosuppression	(22)
[²²⁵Ac]Ac-HuM195 18.5-148 kBq/kg	CD-33 Patients with AML	Phase I: Dose escalation MTD of 111 kBq/mL bone marrow and peripheral blast reduction	Myelosuppression	(24)
[²²⁵Ac]Ac-PSMA-617 100 kBq/kg	PSMA 2 patients with metastatic CRPC	First-in-human Complete response on PET imaging and PSA level below measurable levels	Xerostomia	(2)
[²²⁷Th]Th-epratuzumab BAY1862864 Starting dose: 1.4 MBq	CD-22 Patients with relapsed or refractory CD-22 positive non-Hodgkin's lymphoma	Phase I: Dose escalation, determination of MTD Currently recruiting: NCT02581878		
[²²³Ra]Ra-dichloride 50 kBq/kg	Intrinsic bone-seeking properties Symptomatic CRPC	Phase III: ALSYMPCA Overall survival and time to disease progression Overall survival of 14.9 months vs. 11.3 months		(31,32)
[²¹²Pb]Pb-trastuzumab 7.4-21.1 MBq/m ²	HER2 Progressive ovarian carcinoma after multiple therapy	Phase I: Safety and tolerability Few tumor volume decreases		(29)

Table 1. Examples of clinical evaluation of α-therapy.

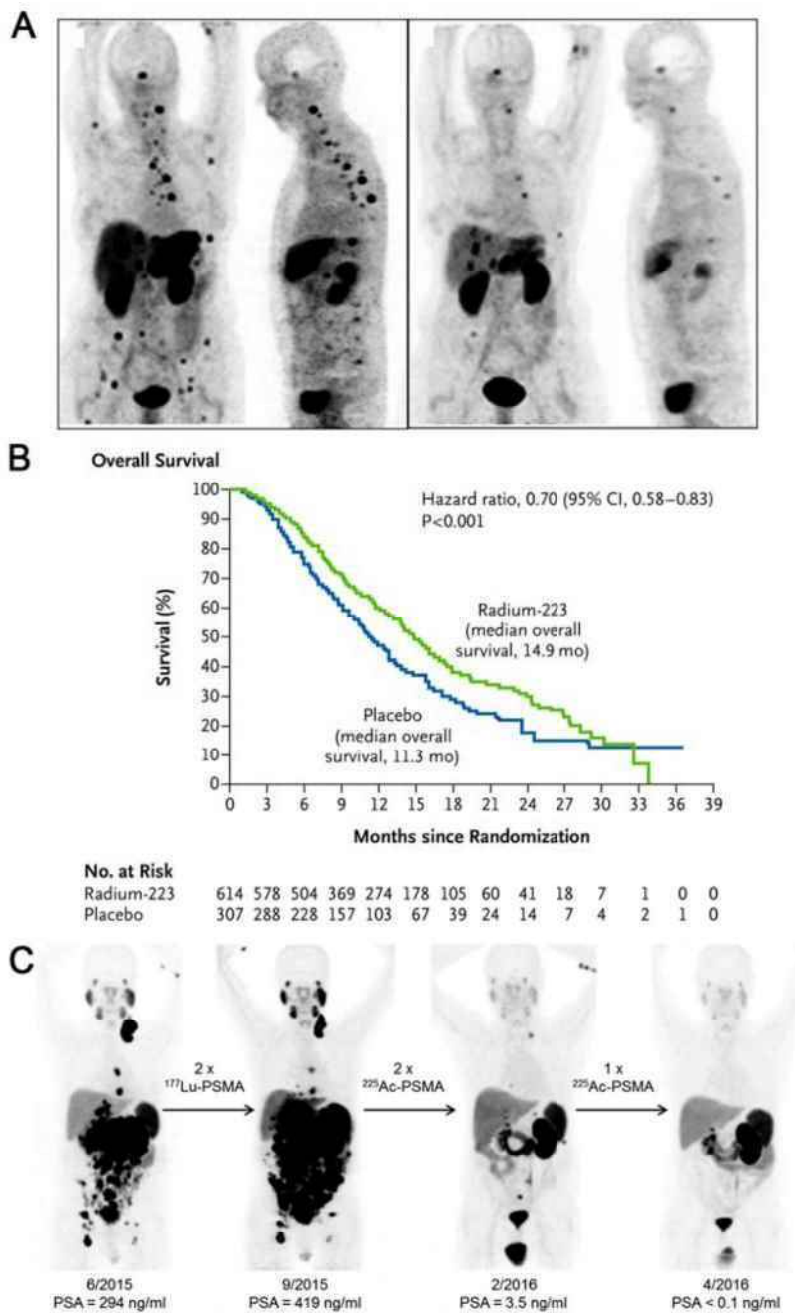


Figure 4. Clinical application of α -radiotherapy. A) *Left*, [^{68}Ga]Ga-DOTATOC PET maximum intensity projection of a neuroendocrine tumor patient showing an extensive tumor burden in the liver as well as disseminated bone marrow metastases. *Right*, significant reduction of the liver metastases after administration of 10.5 GBq of [^{213}Bi]Bi-DOTATOC into the common hepatic artery (27). B) Kaplan-Meier estimates of overall survival of patients with symptomatic CRPC following treatment with ^{223}Ra -dichloride as compared to the placebo group (31). C) Evolution of [^{68}Ga]Ga-PSMA-11 PET/CT scans of a patient with metastatic CRPC showing extended peritoneal carcinomatosis and liver metastases. After two cycles of [^{177}Lu]Lu-PSMA-617, the patient showed disease progression and was offered [^{225}Ac]Ac-PSMA-617. After three cycles of ^{225}Ac -TAT, PET/CT indicated complete response and PSA level dropped to immeasurable levels (2). Reprinted with permission.



The Journal of
NUCLEAR MEDICINE

Alpha Emitters for Radiotherapy: Basic Radiochemistry to Clinical Studies – Part 2

Sophie Poty, Lynn C Francesconi, Michael Robert McDevitt, Michael J. Morris and Jason S. Lewis

J Nucl Med.

Published online: March 1, 2018.

Doi: 10.2967/jnumed.117.204651

This article and updated information are available at:

<http://jnm.snmjournals.org/content/early/2018/02/28/jnumed.117.204651>

Information about reproducing figures, tables, or other portions of this article can be found online at:

<http://jnm.snmjournals.org/site/misc/permission.xhtml>

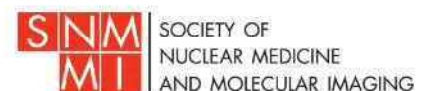
Information about subscriptions to JNM can be found at:

<http://jnm.snmjournals.org/site/subscriptions/online.xhtml>

JNM ahead of print articles have been peer reviewed and accepted for publication in *JNM*. They have not been copyedited, nor have they appeared in a print or online issue of the journal. Once the accepted manuscripts appear in the *JNM* ahead of print area, they will be prepared for print and online publication, which includes copyediting, typesetting, proofreading, and author review. This process may lead to differences between the accepted version of the manuscript and the final, published version.

The Journal of Nuclear Medicine is published monthly.
SNMMI | Society of Nuclear Medicine and Molecular Imaging
1850 Samuel Morse Drive, Reston, VA 20190.
(Print ISSN: 0161-5505, Online ISSN: 2159-662X)

© Copyright 2018 SNMMI; all rights reserved.



MIRD Pamphlet No. 22 (Abridged): Radiobiology and Dosimetry of α -Particle Emitters for Targeted Radionuclide Therapy*

George Sgouros¹, John C. Roeske², Michael R. McDevitt³, Stig Palm⁴, Barry J. Allen⁵, Darrell R. Fisher⁶,
A. Bertrand Brill⁷, Hong Song¹, Roger W. Howell⁸, and Gamal Akabani⁹

In collaboration with the SNM MIRD Committee: Wesley E. Bolch, A. Bertrand Brill, Darrell R. Fisher,
Roger W. Howell, Ruby F. Meredith, George Sgouros (Chair), Barry W. Wessels, and Pat B. Zanzonico

¹Department of Radiology and Radiological Science, Johns Hopkins University, Baltimore, Maryland; ²Department of Radiation Oncology, Loyola University Medical Center, Maywood, Illinois; ³Departments of Medicine and Radiology, Memorial Sloan-Kettering Cancer Center, New York, New York; ⁴Dosimetry and Medical Radiation Physics Section, International Atomic Energy Agency, Vienna, Austria; ⁵Centre for Experimental Radiation Oncology, St. George Cancer Centre, Kogarah, Australia; ⁶Radioisotopes Program, Pacific Northwest National Laboratory, Richland, Washington; ⁷Department of Radiology, Vanderbilt University, Nashville, Tennessee; ⁸Division of Radiation Research, Department of Radiology, New Jersey Medical School Cancer Center, University of Medicine and Dentistry of New Jersey, Newark, New Jersey; and ⁹Department of Nuclear Engineering, Texas A&M University, College Station, Texas

The potential of α -particle emitters to treat cancer has been recognized since the early 1900s. Advances in the targeted delivery of radionuclides and radionuclide conjugation chemistry, and the increased availability of α -emitters appropriate for clinical use, have recently led to patient trials of radiopharmaceuticals labeled with α -particle emitters. Although α -emitters have been studied for many decades, their current use in humans for targeted therapy is an important milestone. The objective of this work is to review those aspects of the field that are pertinent to targeted α -particle emitter therapy and to provide guidance and recommendations for human α -particle emitter dosimetry.

Key Words: α -particle emitters; human α -particle emitter dosimetry; targeted α -particle emitter therapy

J Nucl Med 2010; 51:311–328

DOI: 10.2967/jnumed.108.058651

Several reviews have been published on the topic of α -particle-emitting radionuclides, which have been the subject of considerable investigation as cancer therapeutics (1–8). In the context of targeted therapy, α -particle emitters have the advantages of high potency and specificity. These advantages arise from the densely ionizing track and short path length of the emitted positively charged helium nucleus in tissue. The practical implication of these features, as well as the distinction between α -particles and the more widely

used β -particle emitters for targeted radionuclide therapy, is that it is possible to sterilize individual tumor cells solely from self-irradiation with α -particle emitters. This is generally not possible with β -particle emitters given achievable antibody specific activity, tumor-cell antigen expression levels, and the need to avoid prohibitive toxicity (5). These attributes combine to provide the fundamental strength and rationale for using α -particle-emitting radionuclides for cancer therapy. Current approaches to cancer treatment are largely ineffective once the tumor has metastasized and tumor cells are disseminated throughout the body. There is also increasing evidence that not all tumor cells are relevant targets for effective tumor eradication and that sterilization of a putative subpopulation of a small number of tumor stem cells may be critical to treatment efficacy (9). The eradication of such disseminated tumor cells, or of a subpopulation of tumor stem cells, requires a systemic targeted therapy that is minimally susceptible to chemo- or radioresistance, is potent enough to sterilize individual tumor cells and microscopic tumor cell clusters (even at a low dose-rate and low oxygen tension), and exhibits an acceptable toxicity profile (10). α -Particle-emitting radionuclides address this critical need. To accomplish these goals, a reliable, cost-effective source of α -particle emitters is needed for research and development and for routine use in clinical practice. Improved chemical labeling and stability will be needed to achieve the desired biodistribution and associated dose distribution necessary for successful therapy with acceptable acute and long-term toxicities. These limitations have slowed the development and clinical use of α -emitter targeted therapy relative to the use of β - and Auger-electron-emitting radionuclides.

Received Sep. 29, 2008; revision accepted Jun. 29, 2009.

For correspondence or reprints contact: George Sgouros, Department of Radiology and Radiological Science, CRB II 4M61/1550 Orleans St., School of Medicine, Johns Hopkins University, Baltimore, MD 21231.

E-mail: gsgouros@jhmi.edu

*Unabridged version of this document is available at: <http://interactive.snm.org/index.cfm?PageID=1110&RPID=2199&FileID=144234>.

COPYRIGHT © 2010 by the Society of Nuclear Medicine, Inc.

The first clinical trial of an α -particle emitter in radio-labeled antibody therapy used ^{213}Bi conjugated to the antileukemia antibody HuM195 and was reported in 1997 (11,12), 4 years after ^{213}Bi was first suggested for therapeutic use (13). This trial was followed by a human trial of the antitenascin antibody 81C6 labeled with the α -emitter ^{211}At in patients with recurrent malignant glioma (14). In addition to these 2 antibody-based trials, a clinical trial of unconjugated ^{223}Ra against skeletal metastases in patients with breast and prostate cancer was recently completed (15). More recently, a patient trial of ^{211}At targeting ovarian carcinoma has been initiated (16). Future trials of α -emitters are anticipated using antibodies labeled with ^{211}At or ^{213}Bi and directed against tumor neovasculature (17–19). A conjugation methodology for ^{225}Ac was recently described

(20), and a phase I trial of this radionuclide with the antileukemia antibody HuM195 in leukemia patients has recently been initiated (21). Table 1 summarizes clinical trials involving α -particle-emitting radiopharmaceuticals.

This report focuses on α -emitter dosimetry as it relates to human use in targeted therapy. A review of α -particle radiobiologic studies is provided with a focus on the radiobiology of α -emitters that are relevant to targeted therapy in humans. Closely related to the radiobiology of α -emitters is the concept of relative biological effectiveness (RBE), which is also reviewed. The dosimetry of α -emitters has been addressed in a large number of publications. The criteria for microdosimetry, the different approaches for performing such calculations, and selected studies in which such calculations have been performed are briefly described.

TABLE 1. Summary of Recently Reported Clinical Trials Using α -Particle Emitters

Radionuclide	Delivery vehicle	Type of cancer	Comments	Reference
^{211}At	Antitenascin IgG	Glioblastoma multiforme	Ongoing phase I trial using surgical cavity injection of labeled antitenascin IgG; median survival of 60 wk; 2 patients with recurrent glioblastoma multiforme survived nearly 3 y	14
	MX35 F(ab') ₂	Ovarian carcinoma	Ongoing phase I trial using MX35 F(ab') ₂ ; bone marrow and peritoneal absorbed doses of 0.08 and 8 mGy/MBq, respectively	16
^{213}Bi	Anti-CD33 IgG	Myelogenous leukemia (acute or chronic)	Phase I completed with no toxicity, substantial reduction in circulating and bone marrow blasts; phase I/II in cytoreduced patients, 4 of 23 patients at very high risk showed lasting complete response (up to 12 mo)	11,21
	Antineurokinin receptor peptide	Glioblastoma	Two patients treated with ^{213}Bi ; 1 with oligodendroglioma treated by distillation in resection cavity alive more than 67 mo	148
	Anti-CD20 IgG (rituximab)	Relapsed or refractory non-Hodgkin lymphoma	Phase I study with 9 patients treated to date	149
	9.2.27 IgG	Melanoma	Sixteen patients; intralesional administration led to massive tumor cell kill and resolution of lesions; significant decline in serum marker melanoma-inhibitory-activity protein at 2 wk after treatment	150
^{223}Ra	RaCl ₂	Skeletal breast and prostate cancer metastases	Phase IA dose-escalation studies completed involving single-dose infusion of 46–250 kBq/kg in 25 patients with no dose-limiting hematologic toxicity; phase IB study in 6 patients to evaluate repeated injections (2 or 5 fractions) totaling up to 250 kBq/kg; phase II randomized trial in 33 patients with metastatic breast or prostate cancer treated with external beam plus saline or 4 times 50 kBq/kg dose of ^{223}Ra at 4-wk intervals; shows significant (–66%) decrease in bone alkaline phosphatase compared with placebo and 15 of 31 patients with prostate-specific antigen decrease > 50% from baseline vs. 5 of 28 in control group	151,152
^{225}Ac	Anti-CD33 IgG	Acute myelogenous leukemia	Phase I trial, ongoing, at first dose-level of 18.5 kBq/kg (0.5 $\mu\text{Ci}/\text{kg}$); 1 of 2 patients had elimination of peripheral blasts and reduction in marrow blasts	21

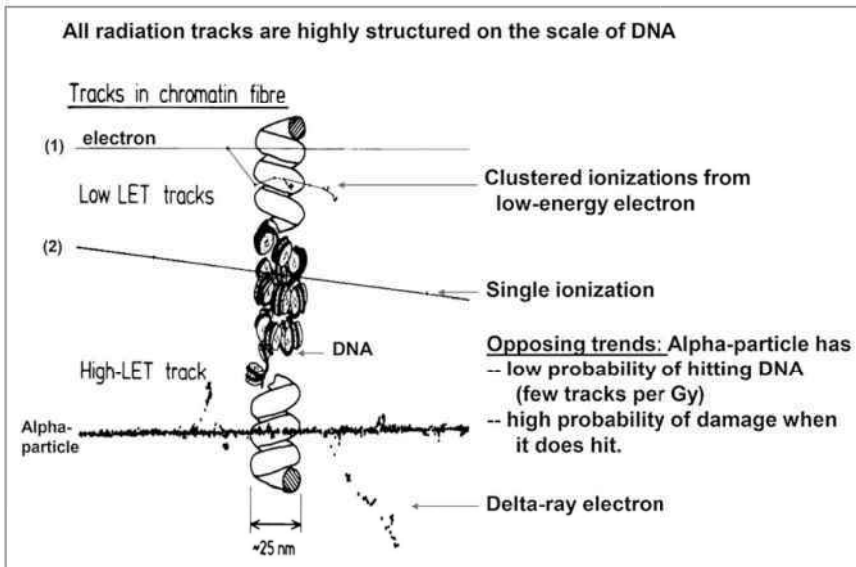


FIGURE 1. Illustration of difference in ionization density between low- and high-LET tracks. (Reprinted with permission of (153).)

Therapeutic nuclear medicine is already a highly multidisciplinary field. Therapy with α -particle emitters is easily one of the more multidisciplinary endeavors within this enterprise. This review is intended to provide the necessary background including the physics and dosimetry perspective to aid in the design, conduct, and analysis of clinical trials using α -emitting radiotherapeutics.

α -PARTICLE RADIOBIOLOGY

Interest in α -particle-emitting radionuclides for cancer therapy is driven by the physical and radiobiologic properties of α -particles as compared with those of photons and electrons (Fig. 1). The energy deposited along the path of an α -particle per unit path length is shown in Figure 2. As shown in the figure, the energy deposition along the path, or

linear energy transfer (LET), of an α -particle can be 2 or 3 orders of magnitude greater than the LET of β -particles emitted by radionuclides such as ^{131}I and ^{90}Y .

One of the first studies demonstrating the biologic effects of heavy charged particles was by Raymond Zirkle in 1932 (22). He examined the effect of polonium α -particles on cell division in fern spores and showed a much greater biologic effect when the spore nucleus was placed in the Bragg peak of the α -particle track, compared with the plateau region of the track (23). Much of the subsequent radiobiology of α -particles was established in a series of seminal studies performed by Barendsen et al. in the 1960s (24–32). These studies first demonstrated the now familiar and accepted features of α -particle irradiation. A subsequent series of studies on the mutation and inactivation

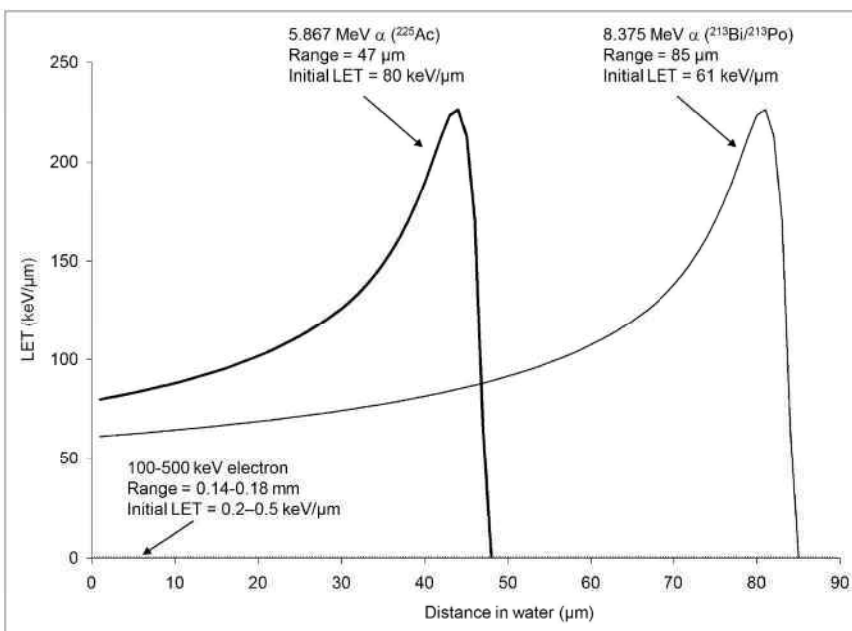


FIGURE 2. LET vs. distance traveled in tissue for α -particles with 2 different initial kinetic energies. α -Particles emitted with lower initial energy are closer to their Bragg peak and, therefore, start out with higher LET. LET of electrons with initial energy of 100–500 keV is also shown at bottom of plot for comparison. (Plot generated using data from (108).)

of 3 different mammalian cell types exposed to helium, boron, or nitrogen ions spanning LET values in the range of 20–470 keV· μm^{-1} was key in evaluating the various biophysical models that had been posited to explain low-versus high-LET effects (33–36). The work was also instrumental in providing both the experimental results and the biophysical analysis to help understand the RBE-versus-LET relationship established by Barendsen. The biophysical analysis in the last paper of the series (33) provided compelling theoretic support for the concept of 2 types of radiation-induced cellular inactivation. The first type is that due to the accumulation of multiple events that can be repaired at low doses (i.e., sublethal damage) but that saturate the cellular repair mechanisms at higher doses. This type of inactivation yields the characteristic linear-quadratic dose–response curve for low-LET radiation, corresponding to a small number, approximately 3–9 (i.e., ~100–300 eV) ionizations in a distance of about 3 nm associated with a low probability of producing lethal lesions. The second type of inactivation arises from a single lethal event for high-LET radiation. In this case, a larger number of ionizations, more than 10, over the 3-nm distance depositing more than 300 eV produces lethal lesions with a high probability. It is important, however, to remember that these studies were performed using external beams of α -particles in which the incident α -particles were generally orthogonal to an α -permeable surface on which the cells were cultured as a monolayer of adherent cells.

As initially demonstrated experimentally by Fisher et al. (37), and then theoretically by Humm et al. (38), and most recently by Kvinnsland et al. (39), the spatial distribution of α -particle emitters has an important impact on the absorbed dose distribution and, correspondingly, on the slope of the cell-survival curve. Neti and Howell recently provided experimental evidence of a lognormal cellular uptake of ^{210}Po citrate among a cell population uniformly exposed to the radiochemical and showed that this distribution can substantially alter the cell survival curve (40). Although many of the results obtained from the external-beam studies (summarized in Table 2) are generally applicable regardless of the α -particle distribution, specific parameters such as the average number of α -particle traversals to induce a lethal event or the D_0 value (i.e., the absorbed dose required to reduce cell survival to 0.37) are highly sensitive to experimental factors such as the geometry of the cells, the thickness or diameter of the cell nucleus, the distribution of DNA within the nucleus (i.e., the phase of the cell cycle), and the number and spatial distribution of the α -particle sources relative to the target nuclei.

The distinction between DNA double-strand breaks (DSBs) caused by a single high-LET track versus DNA damage caused by multiple low-LET tracks is illustrated in Figure 3. This basic observation underpins almost all the radiobiology of α -particles.

TABLE 2. α -Particle Beam Findings That Are Also Applicable to Internally Administered α -Particle Emitters

No.	Finding
1	RBE > 1 for cell sterilization, chromosomal damage/cancer induction relative to low-LET radiation
2	Reduced susceptibility to modulation by radiosensitizers and radioprotectors
3	Reduced capacity to repair sublethal damage
4	Higher induction of DNA DSBs at low total absorbed doses
5	Monoexponential surviving fraction curve after uniform irradiation (absence of a shoulder)

Traversals Required for Cell Kill

The average number of α -particle nuclear traversals required to kill a cell, as measured by loss of the subsequent ability to form a colony, ranges from as low as 1 (41) to as high as 20 (42). If bystander effects are included, the lower end of the range would include 0. The variability in this value when bystander effects are not considered arises because of the high sensitivity of this determination to the geometry of the cell and the nucleus during irradiation and also the LET of the incident α -particles and the LET distribution within the nucleus.

Quoting from a publication of Raju et al. (43), “The notion that a cell will be inactivated by the passage of a single α particle through a cell nucleus prevailed until Lloyd and her associates (42) demonstrated that 10 to 20 5.6 MeV α particles were required to induce one lethal lesion in flattened C3H 10T1/2 cells. Studies by Bird, et al. (44) showed that approximately four ^3He ions were required to pass through the cell nucleus to induce one lethal lesion in V79 cells at the G_1/S -phase border, cells in late S phase required five to eight ^3He ions. Todd, et al. (45) investigated the effect of 3.5 MeV α particles on synchronized T-1 cells, and observed that approximately one α particle out of four to five traversing a cell nucleus is effective in inducing one lethal lesion. Roberts and Goodhead (46) estimated that one out of six 3.2 MeV α -particle traversals through a C3H 10T1/2 cell nucleus is lethal. Barendsen (47) concluded that the probability of inactivation per unit track length of high-LET α particles is approximately 0.08 μm^{-1} for both T-1 and C3H 10T1/2 cells consistent with the results of Roberts and Goodhead for C3H10T1/2 cells (46).” In a study comparing high-LET effects of Auger versus α -particle emitters, Howell et al. found that about 9 decays of ^{210}Po were required to reduce cell survival to 37% (D_0) when it was distributed between the cytoplasm and nucleus of V79 cells; the energy deposited in the cell nucleus corresponds to about 2 complete (maximum chord length) traversals of the cell nucleus (48). In a murine lymphoma cell line, approximately 25 cell-bound α -particle-emitting ^{212}B immunoconjugates were required to reduce clonogenic

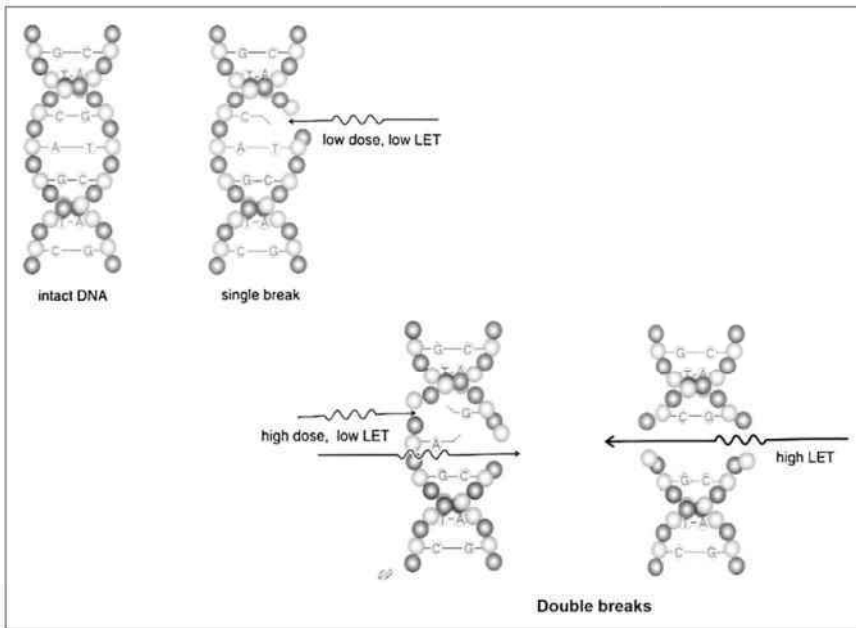


FIGURE 3. Single high-LET track has high probability of yielding DNA DSB, whereas probability of DSB induction with low-LET tracks becomes comparable only at higher absorbed doses. (Reprinted with permission of (154).)

survival by 90% (49). The theoretic efficiency of DSB production when an α -particle passes through DNA was examined by Charlton et al. (50) and was found to be surprisingly low; approximately one eighth of 10-MeV α -particles passing through a 54-nucleotide section of DNA produce a DSB. One passage in 4 of 1.2-MeV α -particles produces a DSB.

Barendsen's estimate of the inactivation probability per unit track length and Goodhead et al.'s determination of the number of lethal lesions per micrometer track through the nucleus (33) suggest another approach for estimating inactivation probability. Along these lines, Charlton and Turner introduced the total α -particle path length (or chord length) through the nucleus as a useful parameter (51). This was used to derive λ , the mean free path between lethal events for α -particles traveling through nuclei. Drawing from an extensive compilation of experimental data, the investigators found that this parameter ranged from 1.5 to 64.4 μm . As expected, λ was found to be dependent on the LET (Fig. 4). An inactivation probability per unit track length through the nucleus has also been used in a model describing radiation-induced cellular inactivation and transformation. By incorporating aspects of a state vector model for carcinogenesis (52) into the inactivation/transformation model, Crawford-Brown and Hofmann (53) have described a model that successfully predicts both cell survival and transformation after irradiation by α -particles of different LETs at absorbed doses below 1 Gy. This model was used to examine the impact on model predictions of including a correlation between initiation of cellular transformation and cellular inactivation. At absorbed doses greater than 1 Gy, a significant difference was observed in the predicted probability that a cell is transformed and survives.

Cell Survival Curve

Cell survival curves (i.e., surviving fraction, SF, vs. absorbed dose, D) for low-LET radiation such as x-rays exhibit an initial "shoulder" that is thought to reflect the repair of radiation damage. This type of cell survival curve can be represented by the linear-quadratic equation

$$SF = e^{-\alpha D - \beta D^2}, \quad \text{Eq. 1}$$

The parameters α and β are, respectively, sensitivity per unit dose (D) and per unit dose squared (D^2). As the absorbed dose exceeds a certain threshold level, presumably

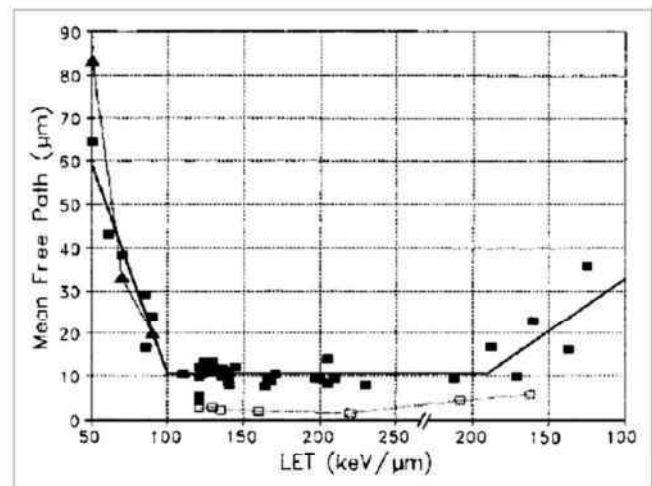
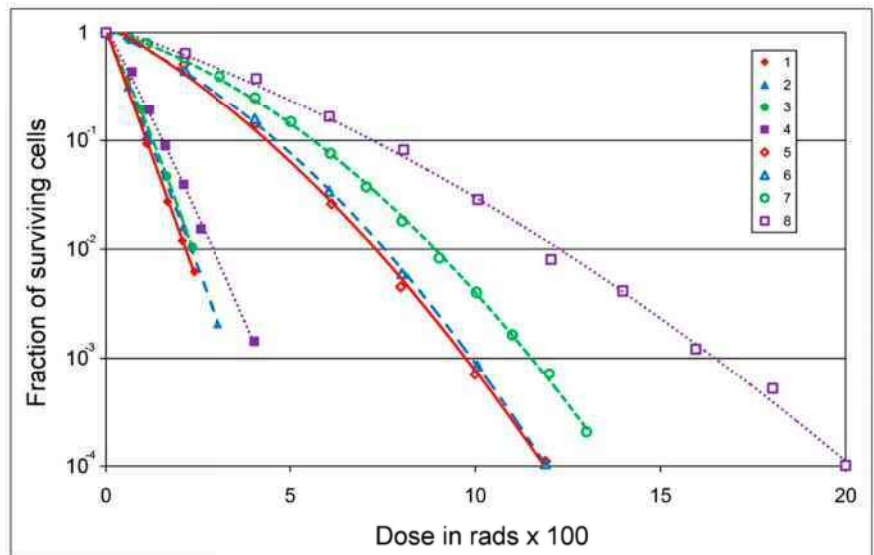


FIGURE 4. Dependence of mean free path on LET. LET is plotted (e.g., from 200 to 100 keV/ μm after 250 keV/ μm) so that stopping powers on low-energy side of Bragg peak can be identified. (Reprinted with permission of (51).)

FIGURE 5. Survival curves obtained with ^{210}Po α -particles (1–4) or 250-kVp x-rays (5–8) and with different cell lines: R₁ cells derived from rhabdomyosarcoma of rat (1 and 8), subline of human kidney cell line T₁ with mean chromosome number of 121 (2 and 5), subline of T₁ with 62 chromosomes (3 and 6), and subline of T₁ with 63 chromosomes (4 and 7). (Adapted from (155).)



the dose at which the radiation damage repair rate is reduced relative to the rate of induced damage, the relationship between surviving fraction and absorbed dose approaches log-linearity. As shown in Figure 5, the cell survival curve for α -particle radiation is log-linear at low as well as high absorbed doses; that is, it does not exhibit a shoulder region, reflecting the reduced capability of cells to repair α -particle damage. The equation describing this is

$$\text{SF} = e^{-D/D_0}, \quad \text{Eq. 2}$$

with the parameter D_0 equal to the absorbed dose required to yield a surviving fraction of 37%. The log-linear aspect of cell survival curves after α -particle irradiation reflects a reduced repair capacity, not the absence of repair. That α -particle damage is repaired has been demonstrated by several studies, as described in the “Radiomodulation” section. Repair of damage is not inconsistent with single-event lethality and a log-linear survival curve. The key distinction is whether death is a result of accumulated damage or of a single event. Cell survival curves that exhibit an initial shoulder reflect cell death that results from the accumulation of damage, whereas log-linear cell survival curves reflect cell death arising from a single event, without the need to accumulate damage. In both situations, repair is possible.

Oxygen Effect

In addition to dose rate, the influence of oxygen concentration has long been recognized as an important factor in the response of cells to radiation (54,55). Figure 6 demonstrates that this effect is strongly influenced by the LET of the radiation. The oxygen enhancement ratio (OER), or relative radiosensitivity of cells to oxygen concentration, is 1 for charged particles with an LET greater than 140 $\text{keV}/\mu\text{m}$ (24). The initial LET of 4- to 8-MeV α -particles typical of the α -emitters of interest in

targeted α -emitter therapy ranges from 110 to 61 $\text{keV}/\mu\text{m}$. The OER values in this LET range are 1.3 to 2.1. Because the LET of the emitted α -particles increases well beyond the 140 $\text{keV}/\mu\text{m}$ threshold for OER = 1 as the Bragg peak is approached, the ability of α -particles to overcome radioresistance due to hypoxia will depend on the spatial distribution of the α -emitters relative to the hypoxic region. The ability to overcome hypoxia, noted above, is strictly radiobiologic. There are studies suggesting that hypoxia may alter the phenotype of the cell via cell signaling pathways associated with increased concentrations of hypoxia-inducible factor 1 α , leading to a cell phenotype that is inherently more resistant to radiation and other cytotoxic agents, including chemotherapeutics (56). The classic OER effect has been explained as a free radical-mediated effect in which the presence of oxygen “fixes” free radical-induced damage, thereby making repair of the damage more difficult (57). In this case, the reduced OER effect with α -particle radiation may be explained by the

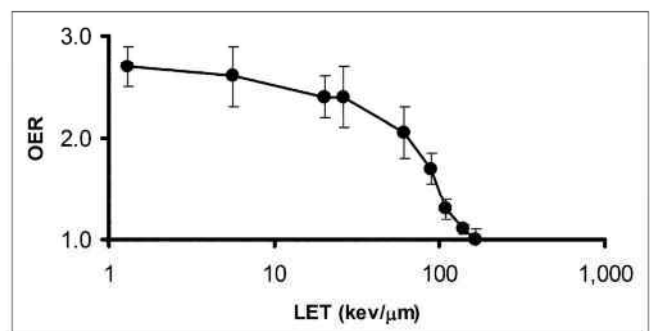


FIGURE 6. OER as function of LET. OER was measured using cultured human kidney-derived cells incubated in air or nitrogen. α -Particles of different energies generated by cyclotron or 250-kVp x-rays (average LET \approx 1.3 $\text{keV}/\mu\text{m}$) were used. (Data replotted from (24).)

preponderance of oxygen-independent direct DNA damage (vs. oxygen-dependent indirect, i.e., free radical-mediated, DNA damage) characteristic of α -particles.

Dose Rate

The influence of absorbed dose rate on cell survival for low-LET emissions is well established. As the dose rate is lowered and the exposure time extended, the biologic effect of a given dose is generally reduced (58). The primary explanation for this effect is that lower dose rates provide a greater time interval for DNA damage repair. Because high-LET damage is not easily repaired, dose rate or even dose fractionation should not impact cellular survival. Barendsen examined changes in survival after α -particle irradiation over a dose-rate range of 0.5–100 rad/min, and no dose-rate effect was observed (26).

Oncogenesis

Although not of prime concern in cancer therapy, a much higher incidence of cancer induction is associated with α -particle irradiation (59). Accordingly, the radiation weighting factor for α -particles is 20, meaning that a committee review of the relevant experimental and human data has determined that per unit absorbed dose, α -particles are associated with a 20-fold greater risk of cancer induction than is a similar absorbed dose of photons or β -particles (60). A review of human and animal data related to cancer risk estimates has called the value of 20 into question for bone cancer and leukemia risk, particularly at low absorbed doses (61). Consideration of dose to target cells on bone surfaces as opposed to the average bone dose gives an RBE for bone cancer risk of 3–12. The authors (61) noted that these estimates may also change since there is evidence that bone cancer risk may be best assessed by calculating dose to a 50- μm layer of marrow adjacent to the endosteal bone surface as opposed to a single 10- μm layer as currently assumed. Likewise, a factor of 2 to 3 is more consistent with the experimental data for leukemia induction. All these estimates are based on α -particle emitters not projected for use in targeted α -emitter therapy. The few studies that have been performed to examine carcinogenesis of the short-lived α -emitters of interest in targeted α -emitter therapy have used ^{211}At . Neoplastic changes, predominately papillary carcinomas in various organs, were seen in a few animals but not more than what was expected for untreated mice. Brown and Mitchell (62) reported a 13% incidence of plasmacytoma in tumor-bearing mice of the same strain 13–21 mo after treatment with 200–750 kBq of $6\text{-}^{211}\text{At}$ -astato-2-methyl-1,4-naphthoquinol bis(diphosphate salt). The frequency of low-grade B-cell non-Hodgkin lymphoma was high but similar to that of the control population. A high incidence of pituitary adenomas and mammary tumors has been seen in rats treated with ^{211}At (63,64). These tumors, however, were partially attributed to secondary effects associated with a hormonal imbalance resulting from thyroid or ovarian tissue compromise.

Fractionation

The fundamental rationale for fractionation in external-beam radiotherapy is based on the differential repair capacity of most normal organs compared with most tumors. This is expressed in terms of early versus late responding tissues, corresponding to high versus low α/β ratios (65). Fractionation tends to spare normal organs without a reduced efficacy against tumors. As shown in Figure 7, this is not the case with high-LET radiation (26). Cultured cells derived from human kidneys showed the same surviving fraction for a single total absorbed dose of α -particle radiation or the same total dose delivered in 2 equal fractions, separated by 12 h. For the same cell line, similar results have been observed when the total dose was delivered in 3 equal fractions at 4, 8, and 12 h after cell plating (25). Extension of the biologically effective dose formalism to account for RBE effects has also demonstrated that fractionation is theoretically not likely to confer a normal tissue-sparing effect for high-LET radiation (66). Similar conclusions may be drawn for the chronic, exponentially decreasing dose rates delivered by internally administered α -particle emitters.

Radiomodulation

Few examples of agents that can modulate α -particle radiation-induced damage have been reported. In the early 1960s, Barendsen et al. compared the radioprotective effects of cysteamine and glycerol (25). The surviving fraction of T_1 (human kidney-derived) cells increased by a factor of 3.7 for 250-kVp x-irradiation and only 1.2 for

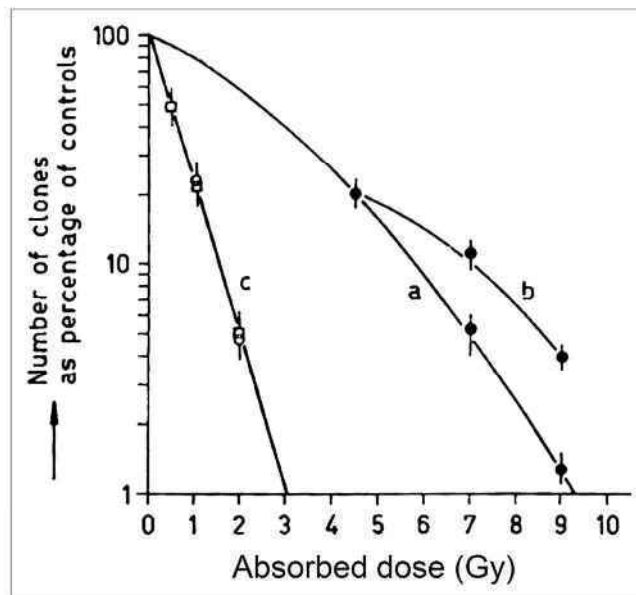


FIGURE 7. Effect of fractionation on cell survival: cell survival curve obtained with single doses of 200-kV x-rays (a), curve obtained when 200-kV x-ray doses are separated by 12 h (4.5 Gy, then 2.5 or 4.5 Gy) (b), and curve obtained with 3.4-MeV α -particles (c). In (c), circles correspond to single exposure, and squares to 2 equal exposures separated by 12 h. (Adapted from (26).)

^{210}Po α -particle radiation. Similar results were observed with glycerol; cell survival was increased by 2.0 and 1.2 for 250-kVp x-rays and ^{210}Po α -particles, respectively. Qualitatively consistent but quantitatively different results have been obtained with the radiosensitizer Wortmannin. This irreversible and potent inhibitor of DNA-dependent protein kinase is involved in the nonhomologous end-joining DNA repair pathway invoked in the repair of DNA DSBs (67). In V79 Chinese hamster cells, Wortmannin led to a 3- to 4-fold increase in genotoxic damage, as measured by the induction of micronuclei. High-LET irradiation, as delivered by a boron neutron-capture reaction, leading to the release of α -particles with an average energy of 2.3 MeV, yielded an increase in micronucleus induction of approximately 2-fold. This finding suggests that the more complex double-strand damage induced by high-LET radiation is a substrate of the nonhomologous end-joining pathway (68,69). In vivo studies in mouse testes have shown that soybean oil, *S*-(2-aminoethyl)isothiuronium bromide hydrobromide, and cysteamine afford some protection against the cytotoxic effects of 5.3-MeV α -particles emitted by ^{210}Po (70-73). When spermatogonial cell survival was used as the biologic endpoint, dose modification factors of 2.2, 2.4, and 2.6, respectively, were obtained. No modification of the spermatogonial response to α -particles was observed when dimethyl sulfoxide or vitamin C was used (74,75).

That DNA damage and its repair are at the core of α -emitter radiobiologic effects is supported by many years of experimental and theoretic work. It is important, however, to keep in mind that all the foundation work regarding the radiobiology of α -emitters was performed well before modern molecular biology came into existence. In light of the remarkable and far-reaching gains in our understanding of the molecular mechanisms involved in cancer genesis, the cellular response to radiation, and DNA single and DSB repair, a reexamination of α -particle radiobiology using modern tools is warranted.

RBE

The biologic effect of ionizing radiation is influenced by the absorbed dose, the dose rate, and the quality of radiation. Radiation quality is characterized by the spatial distribution of the energy imparted and by the density of ionizations per unit path length, referred to as the LET or stopping power of a charged particle (22,60). Depending on the effect considered, greater ionization density along a track will increase the probability of inducing a biologic effect. Compared with electrons and β -particles, α -particles exhibit a high density of ionization events along their track (76). Electrons and β -particles that are emitted by radionuclides generally range in energy from several megaelectron volts to as low as several kiloelectron volts, with corresponding LET values ranging from about 0.1 to 1 keV/ μm (β -particles actually are characterized by a spectrum of energies; the bottom end of the spectrum is zero). The exception to these is Auger electrons, which have energies

as low as several electron volts and corresponding LET values as high as 25 keV/ μm . α -Particles emitted by radionuclides range in energy from 2 to 10 MeV, with initial LET values ranging from 60 to 110 keV/ μm . A given tissue-absorbed dose resulting from α -particles, therefore, is likely to yield considerably greater biologic effects (again depending on the effect being considered) than the same absorbed dose delivered by typical electrons or β -particles. To account for differences in energy deposition pattern exhibited by different quality radiations, the concept of RBE has been established. An authoritative review of this concept, its derivation, and appropriate application has been published by the International Commission on Radiological Protection (ICRP) (60,77), and the reader is encouraged to consult this source for additional information. In radiobiology, RBE equals the ratio of absorbed doses of 2 types of radiation that produce the same specified biologic effect.

RBE Defined

RBE is calculated as the absorbed dose of a reference radiation (e.g., x-rays, γ -rays, β -particles), $D_r(x)$, required to produce a biologic effect, x , divided by the absorbed dose of the test radiation, $D_t(x)$, required to produce the same biologic effect:

$$\text{RBE}(x) = \frac{D_r(x)}{D_t(x)} \quad \text{Eq. 3}$$

RBE is thus an experimentally determined value defined for a particular biologic effect and therefore for a particular biologic system.

The experimentally determined value can be influenced by the variability of the biologic system across different laboratories. This issue has been examined for studies in vitro (78). The methodology used for calculating the absorbed dose of the 2 radiation types will also impact the result. Ideally, this should not be the case. The methodology used should provide the true absorbed dose value or specific energy distribution ("Case for Microdosimetry" section) to the relevant biologic target for both the test and the reference radiations. In practice, however, this is a challenge even for studies in vitro (79). In the setting of human α -particle emitter dosimetry, consistency and reproducibility will be as important as accuracy. This issue is discussed in greater detail in "Recommendations for Dosimetry of Deterministic Effects" section.

The fact that the RBE is related to the pattern of ionizing energy deposition along a particle track leads to a third factor that will impact the results. The RBE for a particular radiation type will also depend on the initial emission energy of the particle (i.e., how close the particle is to the end of its track [the Bragg peak]). This factor has been examined by Charlton et al. (80) and Howell et al. (81). In the studies by Howell et al., a uniform distribution of decays was assumed to calculate the D_0 for 7 α -emitting

isotopes covering a wide range of initial energies. Using the D_0 obtained for x-rays for the cell line used in the α -emitter calculations, a linear relationship between RBE and initial α -particle energy was obtained over an initial α -energy ranging from 5 to 8.5 MeV. The straight line was given by $RBE = 2.9 - 0.167E_i$, where E_i is the initial α -particle energy in megaelectron volts. This is an approximate scaling of the equation derived from in vivo experimental data by Howell et al. (81). In addition to effects related to the Bragg peak, nonuniform biodistribution of the α -emitters also leads to microdosimetric effects that impact RBE and the slope of the cell-survival curve (37–39).

If the reference radiation yields a dose–response relationship that is not log-linear for the biologic system examined, the RBE value will depend on the specific biologic quantitative endpoint selected (e.g., D_{50} , D_{37} (= D_0), D_{10} , etc., which determines whether the comparison falls in the shoulder or in the log-linear region of a dose–response or survival curve). The type of biologic endpoint (e.g., survival, mutation) and the dose rates of the test and reference radiations will also influence the RBE value. Strictly speaking, the test radiation should be delivered in a manner identical to that of the reference radiation (e.g., chronic or acute). However, acute externally administered x- and γ -rays are often used as the reference radiation when RBE values are determined for internally administered radionuclides. Given the often-sizeable difference in biologic responses to acute-versus-chronic low-LET radiation, the dose rate at which the reference radiation is delivered can impact the resulting RBE (48). The dose-rate pattern delivered by radiopharmaceuticals is generally well represented by multicomponent exponential functions. Howell et al. have delivered such patterns with external beams of ^{137}Cs γ -rays (82). This approach was used to study the bone marrow response to exponentially decreasing dose rates of ^{137}Cs γ -rays (83). The response of granulocyte–macrophage colony-forming cells in the marrow to decreasing dose rates with half-times ranging from 62 h to ∞ (i.e., constant dose rate) were studied and compared with the response to acute exposures. Mean lethal doses for chronic irradiation were up to 40% higher than those for acute exposures. Thus, care must be taken when comparing RBE values based on different reference radiations.

Based on a review of experimental literature, an RBE value of between 3 and 5 was recommended for cell killing by a panel convened by the Department of Energy in 1996 (84). Because human studies using α -particle emitters have yet to be analyzed for deterministic effects, an RBE of 5 was recommended for projecting the possible deterministic biologic effects associated with an estimated α -particle absorbed dose.

RBE, Q, and w_R

The discussion thus far has focused on RBE. RBE is occasionally confused with quality factors, Q , and radiation

weighting factors, w_R . This confusion reflects the historical evolution of RBE which was originally defined as relative biological efficiency and intended to apply to both radiobiology (deterministic effects) and protection (stochastic effects). As currently recommended by the ICRP, however, RBE is not to be used directly in radiation protection but only as a starting quantity to derive the radiation weighting factor w_R , which replaced the quality factor Q in the most recent ICRP recommendations (85,86). The RBE values used to arrive at w_R relate to stochastic endpoints such as cancer induction, rather than deterministic endpoints such as normal-tissue toxicity and tumor cell sterilization in cancer therapy patients. The ICRP radiation weighting factor for α -particles is 20. This value, intended only for stochastic effects caused by α -particle irradiation, is based on animal experiments and from analysis of historical α -emitter exposures. In contrast to RBE values, weighting factors are not directly measured values but rather are consensus recommendations of the ICRP (60).

The radiation weighting factor w_R is a unitless factor that converts average absorbed dose (in units of grays) to equivalent dose in an organ or tissue. The SI unit for equivalent dose is referred to by the special name *sievert*. The sievert is not a unit in the conventional sense but is intended to indicate that the absorbed dose value has been adjusted to reflect a biologic risk that is associated with stochastic effects. Although the sievert is often used in the context of deterministic effects, this use is not strictly correct because the ICRP has stipulated that the sievert should be used only to designate the risk of incurring stochastic biologic effects such as cancer. The ICRP has reported on RBE for deterministic effects (RBE_M), but no special name has been chosen by the ICRP for the product of absorbed dose and a factor such as RBE that specifically reflects similar scaling for a deterministic effect (77).

α -PARTICLE DOSIMETRY

Radiation dosimetry offers a means for standardizing and comparing the efficacy of different radiation-based treatments. It provides a logical basis for understanding the effects that various radiation qualities have on biologic matter. For α -particle emitters, accurate dosimetry calculations require knowledge of the activity distribution as a function of time at the cellular and subcellular levels (87). Furthermore, an accurate representation of the geometry at this level is also required. For in vitro experiments (i.e., cell survival studies), the activity distribution is straightforward, consisting of uptake on the surface or within the cell, along with a known fraction in the surrounding solution. In these experiments, the cell and nucleus can be approximated as concentric spheres, the dimensions of which can easily be measured. However, for clinical applications, these idealizations give way to complex activity and tissue geometries. In these cases, modeling the 3-dimensional geometry of a spheroid (88,89) or using microscopic data from tissue biopsy samples (90) can provide information on the target

geometry. Determining the activity distribution, however, remains difficult. Autoradiography (91) may provide a snapshot of the activity distribution at a single instance in time. However, the determination of the activity as a function of time may require mathematic modeling (92–94) of the carrier molecules as they diffuse through tissue and bind to markers on cell surfaces. Ideally, such modeling should be validated using animal model measurements in vivo.

Case for Microdosimetry

There are 2 methods for calculating the energy deposited by individual α -particles. One method uses the MIRD formalism to calculate the average dose to the target (cell nucleus) for a variety of source compartments (cell surface, cytoplasm, and nucleus). Extensive tables have been produced for various combinations of α -particle-emitting radionuclides and cellular geometries (95,96). The basis for using mean absorbed dose is related to the biologic properties of low-LET radiations such that a large number, often several thousands, of statistically independent radiation deposition events in a single cell nucleus is required to induce a demonstrable biologic effect. In such a case, the statistical variation of the energy imparted to different cell nuclei is minimal. In contrast, for high-LET irradiation, such as α -particles, the effect of even a single event in the cell nucleus is so great that the mean absorbed dose can be a misleading index of biologic effect. This is due to several reasons. Foremost is that the number of α -particles that traverse a cell nucleus is often few, and therefore stochastic variations become important. In addition, the path of the α -particle through the cell nucleus is also critical. An α -particle that crosses directly through a cell nucleus will deposit a large amount of energy, whereas one that merely grazes the surface will deposit little or no energy. Thus, a second method for α -particle dosimetry—microdosimetry—takes into account the stochastic nature of energy deposited in small targets. The fundamental quantities in classic microdosimetry are specific energy (energy per unit mass) and lineal energy (energy per unit path length through the target) (97). Microdosimetry was originally proposed by Rossi (98) to explain the stochastic nature of energy deposited in matter by external ionizing radiation. It has subsequently been adapted to the case of internally deposited α -particle emitters (99–101).

Microdosimetric Techniques

Microdosimetric spectra may be calculated using either analytic or Monte Carlo methods (102). Analytic methods use convolutions (via Fourier transforms) of the single-event spectrum to calculate multievent distributions (98). The single-event spectrum represents the pattern of specific energy depositions for exactly 1 α -particle hit. Kellerer developed a method to efficiently determine the multiple-event spectrum through the use of Fourier transforms (103). Although analytic codes are computationally efficient, they are often limited to simple source–target geometries be-

cause the single-event spectrum must be known for each source–target configuration. Monte Carlo codes offer greater flexibility than analytic methods and can simulate a wide variety of geometries and source configurations. Idealizations are often made to simplify the coding and reduce calculation time. In nearly all Monte Carlo codes, α -particles are assumed to travel in straight lines. This approximation is valid for α -particles having energies less than 10 MeV (97). In addition, the range of δ -rays (energetic electrons originating from the α -particle track that cause secondary ionizations in the vicinity of the track) and the width of the α -particle track (~ 100 nm) are often ignored because the targets that are studied (i.e., cell nucleus) are much larger than these dimensions (104). The rate of α -particle energy loss is characterized by the stopping power. These data for a variety of media can be obtained from the literature (105–108). Inherent in the stopping-power formulation is the continuous slowing-down approximation. As the name implies, this approximation assumes that α -particles lose energy continuously as they traverse matter. Thus, the calculated specific energy imparted depends on the choice of stopping powers used.

Criterion for Adopting Microdosimetry

The rationale for microdosimetry was outlined by Kellerer and Chmelevsky (109). They suggested that the stochastic variations of energy deposited within the target must be considered when the relative deviation of the local dose exceeds 20%. For example, a small cell nucleus with a diameter of 5 μm irradiated by α -particles would require an average dose of at least 100 Gy for the relative deviations to be less than the 20% threshold. Thus, the necessity for microdosimetric methods will depend on the source distribution, the target size and shape, and the expected mean dose. For small average doses (such as those expected by nontargeted tissues) microdosimetry may be important in characterizing the pattern of energy deposition and in understanding how this pattern relates to clinical outcomes. However, in tumor, where the mean dose may be large, a microdosimetric treatment may not be necessary.

Microdosimetry Implementation Techniques

Although microdosimetry has increased our understanding of stochastic patterns of energy deposition by α -particles in both simple and complex geometries and has made it possible to explain in vitro observations, application to clinical practice has been limited because time-dependent activity distributions at the subcellular level are complex and not well characterized in vivo. Roeske and Stinchcomb (110) described a technique for determining dosimetric parameters that are important in α -particle dosimetry. These parameters consist of the average dose, SD of specific energy, and the fraction of cells receiving zero hits. The individual values are determined using tables of the “S” value (111), and the first and second moments of the single-event spectra. The average dose is determined by

multiplying the S value by the cumulated activity within the source compartment. Dividing the average dose by the first moment of the single-event spectrum yields the average number of hits. Subsequently, the fraction of cells receiving zero hits (or any number of hits) can be determined using the average number of hits and the Poisson distribution. The SD is the product of the average number of hits and the second moment of the single-event spectrum. Individual moments may be determined using either analytic methods or Monte Carlo calculations. Stinchcomb and Roeske (112) have produced tables of the S value and the individual moments for several geometries and source configurations appropriate for α -particle therapy. These tables were also used in the analysis of cell survival after α -particle irradiation (112).

Applications of Microdosimetry

Early applications of microdosimetry were performed to assess the probability of cancer induction after exposure to α -emitters. These exposures were generally not intended for therapeutic purposes, and carcinogenesis was of concern. In one such application, the specific energy distributions for plutonium oxide in dog lung were calculated. The calculations accounted for the size distribution of the inhaled aerosol and the associated deposition probabilities in the lung for various particle sizes. The distribution of target sites; the probability of an α -particle intersecting a target site; and the range, energy loss, straggling characteristics, and δ -ray production of α -particle tracks were also considered. The analysis provided an improved understanding of the relationship between dose, as described by microdosimetric specific energy spectra, and response, as measured by the incidence of lung tumors in beagle dogs (113).

In radioimmunotherapy, microdosimetry has been used in several α -particle applications. These applications can be broadly characterized as theoretic studies of simple cellular geometries, experimental analysis of cell survival after α -particle irradiation, and the microdosimetry of realistic geometries such as multicellular spheroids and bone marrow. The work in each of these categories will be discussed separately.

Roesch (99) described an approach for calculating microdosimetric spectra. Fisher et al. (37) subsequently applied this approach to several geometries that have therapeutic application, including sources distributed on and within individual cells, sources distributed within spheric clusters of cells, and sources located in cylinders (i.e., blood vessels) that deposited energy within spheric cell nuclei a short distance away. These calculations showed the number of α -particle emissions originating from cell surfaces that would be needed to inactivate cancer cells with high efficiency. The basic geometries that described the spatial distribution of α -emitters relative to the spatial distribution of target spheres have served as the basis of those used in several theoretic studies. In one such study, Humm (114) used a Monte Carlo method with

a model of cell survival to estimate the surviving fraction of cells located outside a capillary and cells located within a tumor with uniformly distributed ^{211}At . Although the mean dose was similar for these 2 types of geometries, there was a significant variation in the expected cell survival due to the differences in the specific energy spectra. In particular, the fraction of cells receiving no α -particle hits increased with distance from the capillary (due to the short range of the α -particles). The surviving fraction versus mean specific energy was biexponential. That is, for low doses, the slope of this curve was similar to that of a uniformly irradiated tumor. However, with increasing doses, the curve was less steep and asymptotically approached a value corresponding to the fraction of nonhit cells. Building on the previous analysis, Humm and Chin (38) analyzed how specific energy spectra are affected by cell nucleus size, binding fraction, cell volume fraction, and nonuniform binding. Their results indicated that nonuniform distributions of α -particle emitters can result in expected survival curves that deviate significantly from the classic monoexponential curves produced by a uniform, external source of α -particles. In these studies, although the inherent cell sensitivity (z_0) was held constant, the slope of the cell survival curve as a function of absorbed dose to the medium was highly dependent on the source configuration. Furthermore, simulations in which cells were more uniformly irradiated resulted in steeper cell survival curves than those in which the distribution of α -emitters was highly heterogeneous. The effects of cell size and shape on expected cell survival were further studied by Stinchcomb and Roeske (115). In their analysis, the cell and nucleus were assigned various shapes ranging from spheres to ellipsoids where the ratio of the major-to-minor axis was varied from 1 to 5 while the volume of the nucleus was held constant. Separately, the dimensions of the nucleus were varied while the shape was held constant. Calculations of specific energy spectra and resulting cell survival demonstrated that the expected surviving fraction was not a strong function of the target shape, provided the volume was fixed. However, significant variations in cell survival were observed as the volume of the nucleus was varied. More recently, Aubineau-Laniece et al. developed a Monte Carlo code to simulate cylindrical geometries as a model for bronchial airway bifurcations (116). In a series of reports on α -particles from radon progeny, Fakir et al. (117–119) demonstrated that for uniform surface emissions, there were significant variations in cellular energy deposition. Larger variations in the hit frequencies and energy deposited were observed when a nonuniform distribution of activity was also considered. Palm et al. (120) examined the microdosimetric effects of daughter products from ^{211}At . Separate simulations were performed assuming the daughter products decayed at the site of ^{211}At emission or that they diffused away from the site. Based on an analysis of experimental data, the ^{210}Po daughter product seemed to diffuse from the decay site, decreasing the energy deposited

in the cell nucleus by a factor of 2. All these studies illustrate the need to accurately model the source–target geometry. Moreover, approximations, such as using mean values, may impact both the specific-energy spectrum and subsequent calculation of cell survival (39).

Application to Cellular Clusters

Single-cell survival analyses after α -particle irradiation has also been extended to multicellular clusters. Charlton (89) described a multicellular spheroid model and simulated α -particle energy deposition events within individual cell nuclei. A cell survival model that takes into account the effects of varying LET (51) was combined with the distribution of α -particle tracks throughout cells within the spheroid. Simulating a uniform source distribution (average 1 decay per cell, 50% cell packing), this analysis demonstrated that cell survival decreased significantly (from 57% to 37%) as the spheroid diameter increased from 75 to 225 μm . The number of hits per cell also increased in larger spheroids when longer-ranged α -particle emitters were considered. Cell survival subsequently decreased from 46% to 26% in 200- μm -diameter spheroids as the packing fraction was increased from 40% to 70% (also with 1 decay per cell). The decrease in cell survival was due to the increased crossfire dose as the packing fraction was increased. In a separate simulation, the total number of decays per spheroid was kept constant while a small fraction of cells (20%) was assumed not to take up any activity. This process simulated the effects of cells that lacked a specific targeting moiety. It is interesting to note that the unlabeled fraction did not significantly alter the expected cell survival. In these studies, the specific energy distribution is highly nonuniform and varies with depth below the spheroid surface. Thus, a single dose or specific-energy distribution is not representative of that through the entire tumor. By combining the specific-energy distribution with cell survival models, it is possible to gain insight into those factors that will influence the therapeutic efficacy of a particular targeting approach. However, most of these cell survival models do not take into account second-order processes such as the bystander effect that may play an important role in modeling cellular clusters and micrometastases. Refinement of these models is currently an active area of research (121,122).

Application to Bone Marrow

Bone marrow is often the dose-limiting organ in radioimmunotherapy. The dosimetry of bone marrow is difficult because of its complex geometry and the presence of tissue inhomogeneities. Thus, idealized models, as have been used in the previous studies, must be replaced by more realistic geometries. The work to date on estimating specific energy spectra for bone marrow has focused largely on using histologic samples obtained from humans or animal models. Akabani and Zalutsky (90) obtained histologic samples of beagle bone marrow and manually measured chord length distributions. Using a Monte Carlo

program, they calculated the single-event specific energy distribution for sources both in the extracellular fluid and on the surface of red marrow cells. These single-event distributions were combined with a model of cell survival. This analysis demonstrated that activity concentrated on the cell surface resulted in significantly greater cell killing than did activity in the extracellular fluid. The effect of LET on the survival of human hematopoietic stem cells in various geometries was studied by Charlton et al. (80). These geometries were determined from human marrow samples obtained from cadavers. Microdosimetric spectra and cell survival were calculated for 3 different source–target geometries; isolated cells labeled on their surfaces, a nontargeted distribution of decays in an extended volume, and nontargeted decays in marrow with 36% of the marrow volume occupied by fat. Two different radionuclides, ^{149}Tb and ^{211}At , were considered. These simulations indicated that for targeted decays ^{149}Tb was 5 times more effective than ^{211}At when compared on a hit-by-hit basis. This enhancement was due to the lower energy of ^{149}Tb resulting in a higher LET of the incident α -particles. Those authors also concluded that cell survival was a function of the position of the decay relative to the cell nucleus. Using a model similar to that of Charlton et al. (80), Utteridge et al. (123) considered the risk of the development of secondary malignancies (i.e., leukemia) from α -particles. This risk may be important in evaluating the future therapeutic application of α -particles in patients who have an excellent prognosis. Three α -emitting radionuclides were considered on the basis of the relative range (short, medium, and long) of the particle. In this analysis, the authors calculated the fraction of cells that are hit and would survive (as these would potentially cause secondary malignancies). They determined that the lowest fraction occurred for low energies and the highest fraction occurred for the highest-energy α -particle emitter.

RECOMMENDATIONS FOR DOSIMETRY OF DETERMINISTIC EFFECTS

Beyond providing a rational basis for a starting administered activity value for a phase I study, dosimetry has an important role in guiding clinical trial design to help maximize the likelihood of a successful, minimally toxic implementation. This is particularly important because α -emitter targeted therapy has the potential to be both highly effective and also quite toxic. Which of these 2 aspects emerges in a therapeutic trial will depend on having an understanding of the physical and biologic factors that impact response and toxicity. It is essential that clinical trials investigating targeted α -particle therapy be rationally designed; otherwise, there is the risk that α -emitters may be abandoned before they have been properly tested in the clinic.

This increased importance of dosimetric analysis is coupled with a greater difficulty in obtaining the human data necessary to perform dosimetry. In contrast to most

targeted therapy trials to date, collection of biodistribution data for dosimetry from pretreatment imaging studies will not be possible for most α -particle-emitting radionuclides with therapeutic potential. This places a greater emphasis on preclinical studies and extrapolation of results obtained from such studies to the human. Several of the α -emitting radiotherapeutics decay to α -emitting daughters whose distribution may not be that of the carrier. Aside from understanding the biodistribution and dosimetry of the α -emitter-labeled carrier, therefore, the biodistribution and dosimetry of the daughter must also be considered (124–131).

In this section, the focus of the discussion and the recommendations that are made are specific to deterministic effects.

Recommendations

After stability and radiochemical purity of the radiopharmaceutical have been established and an appropriate target identified, the following progression of studies is proposed. Elements of these recommendations have also been described elsewhere (132–134).

1. Determine cellular targeting kinetics and properties.
 - A. Determine number of sites per cell and fraction of cells expressing target.
 - B. Determine distribution of binding sites per cell among the targeted cells.
 - C. Determine binding and dissociation constants for cell targeting (e.g., antibody affinity).
 - D. Determine internalization rate and fraction internalized.
 - E. Determine fate of internalized radionuclide.
 - F. Determine median lethal dose in targeted versus nontargeted cells.
 - G. Determine cell-level dosimetry for targeted and nontargeted cells.
2. Perform animal (xenograft or transgenic) model studies.
 - A. Evaluate maximum tolerated administered activity.
 - B. Identify likely dose-limiting organs.
 - C. Collect macroscopic (whole-organ) pharmacokinetics.
 - D. Collect microscopic (e.g., by autoradiography or optical imaging) biodistribution in dose-limiting organs.
 - E. Evaluate stability of the radiopharmaceutical in vivo.
 - F. Evaluate efficacy at maximum tolerated administered activity.
 - G. Perform cell- and organ-level dosimetry for the animal model.
3. Extrapolate data obtained in steps 1 and 2 to the human to arrive at initial activity for a phase I study.
 - A. Develop and fit a pharmacokinetic model to data obtained in steps 1 and 2.
 - B. Replace model parameter values with estimated human values; simulate biodistribution in humans.
 - C. Use model-derived biodistribution to estimate absorbed dose to dose-limiting organs identified in step 2B.
4. Assess radiopharmaceutical distribution during the phase I study.

- A. Image (if possible).
- B. Collect and count blood samples.
- C. Collect, count, and autoradiograph biopsy samples (if practical).

If there are concerns (not addressed by animal studies) about possible renal, urinary bladder wall, or gastrointestinal toxicity related to the localization of activity in luminal contents versus the organ wall:

- D. Collect and count urine samples.
- E. Collect and count fecal samples.

Steps 1–3 are general guidelines. The primary objective is to collect adequate preclinical data so as to have an understanding of the α -emitters' likely biodistribution and kinetics in humans. This objective is particularly important because pretherapy patient imaging will not be possible. It is essential that this approach not be seen as mandatory for moving α -emitter-labeled radiopharmaceuticals to the clinic; in particular, step 3 may be replaced by a projected conservative (worst-case) scenario analysis or by a direct translation of small-animal pharmacokinetics to the human using standard methods to adjust for differences in body size and organ mass (135). The autoradiography proposed in steps 2D and 4C will clearly be subject to the practical constraint of α -emitter half-life. For short-lived α -emitters, microscopic imaging of fluorescently tagged agents may be a viable alternative to autoradiography in animal models.

Conventional Versus Cell-Level Dosimetry. In most cases, a microdosimetric analysis will not be necessary for targeted therapy applications because the activity level administered and mean absorbed doses to targeted cells are larger than in the cases described here and the resulting stochastic deviation is expected to be substantially less than 20%. In such cases, standard dosimetry methods may be applied (111,136). The standard approach to dosimetry calculations has been described by the MIRD Committee (111). In this formalism, the absorbed dose to a target volume from a source region is given as the total number of disintegrations in the source region multiplied by a factor (the S value) that provides the absorbed dose to a target volume per disintegration in the source region. The sum of these products across all source regions gives the total absorbed dose to the target. MIRD cellular S values have been published for cell level dosimetry calculations for situations in which the number of disintegrations in different cellular compartments can be measured or modeled (95). With these S values, the absorbed dose to the nucleus may be calculated from α -particle emissions uniformly distributed on the cell surface, in the cytoplasm, or in the nucleus.

Conventional Dosimetry for Organs and Tumors. Estimation of the average absorbed dose to a particular normal organ or tumor volume is based on the assumption that the radioactivity is uniformly distributed in the organ and that

the energy deposited by the emitted α -particles is also distributed uniformly within the organ. With some exceptions (137–141), the cross-organ dose from α -particle and electron emissions can be assumed negligible for human organ and tumor dosimetry. Care is required in applying S values for α -emitters because α -emitters may have multiple decay pathways and multiple radioactive daughters that should be considered. For example, S values for ^{213}Bi will not include the emissions from the ^{213}Po daughter, which has a 4- μs half-life and contributes 98% of the α -particles emitted by ^{213}Bi decay (the remaining 2% come from decay of ^{213}Bi itself). This consideration and also the importance of separately accounting for absorbed dose due to electron and photon emissions from that due to α -particles requires that the dosimetry calculations be based on absorbed fraction calculations rather than on S values. The methodology is described by the following equations (presented using the recently published updated MIRD schema) (142):

$$D_{\alpha}(r_T, T_D) = \bar{A}(r_S, T_D) \cdot \frac{\sum_i \Delta_i^{\alpha} \phi(r_T \leftarrow r_S; E_i^{\alpha})}{M(r_T)}, \quad \text{Eq. 4}$$

$$D_e(r_T, T_D) = \bar{A}(r_S, T_D) \cdot \frac{\sum_i \Delta_i^e \phi(r_T \leftarrow r_S; E_i^e)}{M(r_T)}, \quad \text{Eq. 5}$$

$$D_{ph}(r_T, T_D) = \frac{\sum_{r_S} \left(\bar{A}(r_S, T_D) \cdot \sum_i \Delta_i^{ph} \phi(r_T \leftarrow r_S; E_i^{ph}) \right)}{M(r_T)}, \quad \text{Eq. 6}$$

$$D_{RBE}(r_T, T_D) = RBE_{\alpha} \cdot D_{\alpha}(r_T, T_D) + RBE_e \cdot D_e(r_T, T_D) + RBE_{ph} \cdot D_{ph}(r_T, T_D), \quad \text{Eq. 7}$$

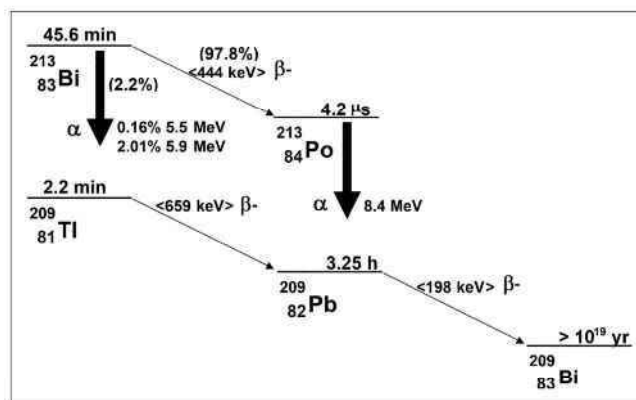


FIGURE 8. Decay scheme for ^{213}Bi .

where $D_x(r_T, T_D)$ is absorbed dose to the target region, r_T , from emission type x , over the dose integration period, T_D ; $D_{RBE}(r_T, T_D)$ is RBE-weighted dose to the target region, r_T ; r_T and r_S are the target and source region (or tissue), respectively; $\bar{A}(r_T, T_D)$ is time-integrated activity or total number of nuclear transitions in the target region, r_T ; $M(r_T)$ is the mass of the target region; Δ_i^x is mean energy emitted per nuclear transition for the i th emission of particle type x (alpha, electron, or photon); $\phi(r_T \leftarrow r_S; E_i^x)$ is the fraction of energy emitted per nuclear transition in the source region, r_S , that is absorbed in the target region, r_T , by the i th emission of particle type x that is emitted with initial energy E ; and RBE_{α} , RBE_e , and RBE_{ph} are RBEs for α -particles (α), electrons (e), and photons (ph), respectively ($RBE_e = RBE_{ph} = 1$).

The total number of nuclear transitions in a particular tissue or region is typically obtained by longitudinal imaging, or counting tissue samples for radioactivity. Values for the Δ_i 's are obtained from decay-scheme tabulations published for each radionuclide (143). The absorbed fraction for each decay type, ϕ , must be calculated from tabulations of absorbed fractions for the particular tissue geometry. In almost all cases, non-cell-level dose calculations, the absorbed fractions for α -particles,

TABLE 3. Electron Emissions Considered in Absorbed Dose Calculations

Isotope	Electrons					
	Energy (keV)	Isotope % per disintegration	Effective % per disintegration	Mean energy (keV/disintegration)	Δ^e (Gy·kg/Bq·s)	Electron range (mm)
^{213}Bi	200	0.20	0.20	0.40	6.41E-17	0.5
^{213}Bi	347	2.55	2.55	8.85	1.42E-5	1.4
^{213}Bi	423	0.40	0.40	1.69	2.71E-16	1.9
^{213}Bi (β)	444	97.80	97.80	434.23	6.96E-14	2.1
^{209}Tl (β)	659	100.00	2.20	14.50	2.32E-15	4.2
^{209}Pb (β)	198	100.00	100.00	198.00	3.17E-14	0.5
Sum				657.67	1.05E-13	

Mean energy and range values are listed for β -emissions. Dominant contributors to electron absorbed dose are shown in bold.

TABLE 4. α -Particle Emissions Considered in Absorbed Dose Calculations

Isotope	α -Particles					
	Energy (keV)	Isotope % per disintegration	Effective % per disintegration	Mean energy (keV/disintegration)	Δ^{α} (Gy·kg/Bq·s)	α -range (μm)
^{213}Bi	5,549	0.16	0.16	8.88	$1.42\text{E}-15$	42.0
^{213}Bi	5,869	2.01	2.01	117.97	$1.89\text{E}-14$	45.5
^{213}Po	7,614	0.003	0.003	0.22	$3.58\text{E}-17$	66.0
^{213}Po	8,375	100.00	97.80	8,190.75	$1.31\text{E}-12$	75.6
Sum				8,317.82	$1.33\text{E}-12$	

can be assumed equal to 1; the absorbed fractions for electrons are likewise usually assumed equal to 1. A description of the methods used to calculate these values is beyond the scope of this review but are provided in the references (141,144,145), one of which (141), in particular, describes absorbed fractions that are tabulated by α -particle energy for bone marrow trabeculae. For α -emitters that decay via a branched decay scheme, as in ^{213}Bi , for example (Fig. 8), it is important to account for the relative yield of each branch in determining the total energy emitted by each type of emission (i.e., the Δ_i 's). In the case of ^{213}Bi , Tables 3 and 4 summarize the electron and α -particle emissions. The tables illustrate how to tally the total electron and α -particle energy. As shown, 2.2% of ^{213}Bi decays results in ^{209}Tl with the emission of an α -particle; the initial energy of the emitted α -particle is either 5.5 or 5.8 MeV, with the probability of each given by the yields shown in Table 2. In the remaining 97.8% of decays, ^{213}Bi decays to ^{213}Po with the emission of a β -particle. ^{213}Po itself decays rapidly via the emission of an 8.4-MeV α -particle to ^{209}Pb , which in turn decays to ^{209}Bi with the emission of a 198-keV β -particle. The exercise illustrates that a careful accounting of emissions is required in tallying the energy emitted per disintegration of the administered α -emitter, even when the decay scheme is relatively simple as for ^{213}Bi . Although outside the scope of this review, the photon S values (Table 5) can be calculated on the basis of tabulations of photon absorbed fractions to different source-target organ combinations and photon energies (146).

Units

The issue of identifying the most appropriate dosimetry quantities and units is particularly important for α -emitters because, as noted earlier, there can be confusion regarding the calculation of dosimetry quantities that relate to stochastic versus deterministic effects. It is incorrect to assign the unit sievert to the quantity defined by Equation 7. The sievert is not a unit in the conventional sense but, rather, is intended to indicate that the absorbed dose value has been scaled to reflect a biologic risk that is associated with stochastic effects. Although the product of deterministic RBEs and absorbed dose in grays has been referred to as a sievert, this is not strictly correct because sievert should be used only to designate the risk of incurring stochastic

biologic effects such as cancer. No special named unit has been widely adopted to reflect a dose value that has been multiplied by an RBE and that specifically reflects the magnitude of deterministic effects. The MIRD Committee has proposed that the barendsen (Bd) be defined as the special named unit for the product of deterministic RBE and absorbed dose and has published a commentary to this effect (147). To avoid confusion during the transition period, the MIRD Committee recommends that the 3 absorbed dose values, for α -, electron, and photon emissions, be provided separately and reported in the absorbed dose unit, gray. This removes any ambiguity as to interpretation of reported absorbed doses for α -emitter therapy applications.

Daughters

The example provided above is for an α -emitter with a relatively simple decay scheme. Each disintegration of the parent ^{213}Bi leads to a single α -particle emission; there are no long-lived α -emitting daughters. This is not the case for the longer-lived α -emitters ^{223}Ra , ^{225}Ac , and ^{227}Th , which decay via α -emitting daughters. Because emission of an α -particle by the parent atom leads to a 50- to 100-nm recoil of the resulting daughter, daughter atoms may not remain conjugated to the molecular carrier. In the most complex scenario, the biologic distribution of the daughter will depend on the site of parent decay (124). In practice, the biologic distribution of long-lived daughters tends to be dominated by the chemical fate of the daughter atom. For example, ^{213}Bi , the longest-lived daughter of ^{225}Ac , concentrates in the kidneys. Likewise, ^{223}Ra , the daughter of ^{227}Th , localizes to bone. Dosimetry calculations for such radionuclides must, therefore, account for the biodistribution of both the parent and all daughters.

TABLE 5. Individual Photon S Factors and Summed Photon S Factor Used for ^{213}Bi Photon Dosimetry (25)

Isotope	Photon energy (keV)	S factor (Gy/MBq·s)
^{213}Bi	440	$5.78\text{E}-11$
^{213}Bi	79	$9.84\text{E}-13$
^{209}Tl	117	$1.60\text{E}-12$
^{209}Tl	467	$6.71\text{E}-12$
^{209}Tl	1,566	$2.37\text{E}-11$
Sum = S_{WB-WB}		$9.08\text{E}-11$

ACKNOWLEDGMENT

We thank David E. Charlton for providing guidance, vigorous discussions, and for his critical reading of the manuscript.

REFERENCES

1. Bloomer WD, McLaughlin WH, Lambrecht RM, et al. ^{211}At radiocolloid therapy: further observations and comparison with radiocolloids of ^{32}P , ^{165}Dy , and ^{90}Y . *Int J Radiat Oncol Biol Phys*. 1984;10:341–348.
2. Macklis RM, Kinsey BM, Kassis AI, et al. Radioimmunotherapy with alpha-particle emitting immunoconjugates. *Science*. 1988;240:1024–1026.
3. Zalutsky MR, Vaidyanathan G. Astatine-211-labeled radiotherapeutics: an emerging approach to targeted alpha-particle radiotherapy. *Curr Pharm Des*. 2000;6:1433–1455.
4. McDevitt MR, Ma D, Lai LT, et al. Tumor therapy with targeted atomic nanogenerators. *Science*. 2001;294:1537–1540.
5. McDevitt MR, Sgouros G, Finn RD, et al. Radioimmunotherapy with alpha-emitting nuclides. *Eur J Nucl Med*. 1998;25:1341–1351.
6. Mulford DA, Scheinberg DA, Jurcic JG. The promise of targeted α -particle therapy. *J Nucl Med*. 2005;46(suppl 1):199S–204S.
7. Jurcic JG. Antibody therapy for residual disease in acute myelogenous leukemia. *Crit Rev Oncol Hematol*. 2001;38:37–45.
8. Wilbur DS. Potential use of alpha-emitting radionuclides in the treatment of cancer. *Antibody Immunocjugates Radiopharm*. 1990;4:85–97.
9. Wicha MS. Cancer stem cells and metastasis: lethal seeds [commentary]. *Clin Cancer Res*. 2006;12:5606–5607.
10. Sgouros G, Song H. Cancer stem cell targeting using the alpha-particle emitter, ^{213}Bi : mathematical modeling and feasibility analysis. *Cancer Biother Radiopharm*. 2008;23:74–81.
11. Jurcic JG, Larson SM, Sgouros G, et al. Targeted alpha particle immunotherapy for myeloid leukemia. *Blood*. 2002;100:1233–1239.
12. Jurcic JG, McDevitt MR, Sgouros G, et al. Targeted alpha-particle therapy for myeloid leukemias: a phase I trial of bismuth-213-HuM195 (anti-CD33) [abstract]. *Blood*. 1997;90:2245.
13. Geerlings MW, Kaspersen FM, Apostolidis C, van der Hout R. The feasibility of ^{225}Ac as a source of alpha-particles in radioimmunotherapy. *Nucl Med Commun*. 1993;14:121–125.
14. Zalutsky MR, Reardon DA, Akabani G, et al. Clinical experience with alpha-particle emitting ^{211}At : treatment of recurrent brain tumor patients with ^{211}At -labeled chimeric antineoplastic monoclonal antibody 81C6. *J Nucl Med*. 2008;49:30–38.
15. Nilsson S, Larsen RH, Fossa SD, et al. First clinical experience with alpha-emitting radium-223 in the treatment of skeletal metastases. *Clin Cancer Res*. 2005;11:4451–4459.
16. Hultborn R, Andersson H, Back T, et al. Pharmacokinetics and dosimetry of ^{211}At -MX35 F(AB')₂ in therapy of ovarian cancer: preliminary results from an ongoing phase I study [abstract]. *Cancer Biother Radiopharm*. 2006;21:395.
17. Kennel SJ, Mirzadeh S, Eckelman WC, et al. Vascular-targeted radioimmunotherapy with the alpha-particle emitter ^{211}At . *Radiat Res*. 2002;157:633–641.
18. Kennel SJ, Mirzadeh S. Vascular targeted radioimmunotherapy with ^{213}Bi : an alpha-particle emitter. *Nucl Med Biol*. 1998;25:241–246.
19. Akabani G, McLendon RE, Bigner DD, Zalutsky MR. Vascular targeted endoradiotherapy of tumors using alpha-particle-emitting compounds: theoretical analysis. *Int J Radiat Oncol Biol Phys*. 2002;54:1259–1275.
20. McDevitt MR, Ma D, Simon J, Frank RK, Scheinberg DA. Design and synthesis of ^{225}Ac radioimmunopharmaceuticals. *Appl Radiat Isot*. 2002;57:841–847.
21. Jurcic JG, McDevitt MR, Pandit-Taskar N, et al. Alpha-particle immunotherapy for acute myeloid leukemia (AML) with bismuth-213 and actinium-225 [abstract]. *Cancer Biother Radiopharm*. 2006;21:396.
22. Zirkle RE. Some effects of alpha radiation upon plant cells. *J Cell Comp Physiol*. 1932;2:251–274.
23. Brown A, Suit H. The centenary of the discovery of the Bragg peak. *Radiation Oncol*. 2004;73:265–268.
24. Barendsen GW, Koot CJ, van Kerson GR, Bewley DK, Field SB, Parnell CJ. The effect of oxygen on the impairment of the proliferative capacity of human cells in culture by ionizing radiations of different LET. *Int J Radiat Biol*. 1966;10:317–327.
25. Barendsen GW, Walter HMD. Effects of different ionizing radiations on human cells in tissue culture. IV. Modification of radiation damage. *Radiat Res*. 1964;21:314–329.
26. Barendsen GW. Modification of radiation damage by fractionation of dose anoxia + chemical protectors in relation to LET. *Ann N Y Acad Sci*. 1964;114(A1):96–114.
27. Barendsen GW. Impairment of the proliferative capacity of human cells in culture by alpha-particles with differing linear-energy transfer. *Int J Radiat Biol Relat Stud Phys Chem Med*. 1964;8:453–466.
28. Barendsen GW, Walter HMD, Bewley DK, Fowler JF. Effects of different ionizing radiations on human cells in tissue culture. III. Experiments with cyclotron-accelerated alpha-particles and deuterons. *Radiat Res*. 1963;18:106.
29. Barendsen GW. Dose-survival curves of human cells in tissue culture irradiated with alpha-, beta-, 20-kv x- and 200-kv x-radiation. *Nature*. 1962;193:1153.
30. Barendsen GW, Beusker TLJ. Effects of different ionizing radiations on human cells in tissue culture. I. Irradiation techniques and dosimetry. *Radiat Res*. 1960;13:832–840.
31. Barendsen GW, Beusker TLJ, Vergroesen AJ, Budke L. Effect of different ionizing radiations on human cells in tissue culture. II. Biological experiments. *Radiat Res*. 1960;13:841–849.
32. Barendsen GW, Vergroesen AJ. Irradiation of human cells in tissue culture with alpha-rays, beta-rays and x-rays [abstract]. *Int J Radiat Biol Relat Stud Phys Chem Med*. 1960;2:441.
33. Goodhead DT, Munson RJ, Thacker J, Cox R. Mutation and inactivation of cultured mammalian cells exposed to beams of accelerated heavy ions. IV. Biophysical interpretation. *Int J Radiat Biol Relat Stud Phys Chem Med*. 1980;37:135–167.
34. Munson RJ, Bance DA, Stretch A, Goodhead DT. Mutation and inactivation of cultured mammalian cells exposed to beams of accelerated heavy ions. I. Irradiation facilities and methods. *Int J Radiat Biol Relat Stud Phys Chem Med*. 1979;36:127–136.
35. Thacker J, Stretch A, Stephens MA. Mutation and inactivation of cultured mammalian cells exposed to beams of accelerated heavy ions. II. Chinese hamster V79 cells. *Int J Radiat Biol Relat Stud Phys Chem Med*. 1979;36:137–148.
36. Cox R, Masson WK. Mutation and inactivation of cultured mammalian cells exposed to beams of accelerated heavy ions. III. Human diploid fibroblasts. *Int J Radiat Biol Relat Stud Phys Chem Med*. 1979;36:149–160.
37. Fisher DR, Frazier ME, Andrews TK Jr. Energy distribution and the relative biological effects of internal alpha emitters. *Radiat Prot Dosimetry*. 1985;13:223–227.
38. Humm JL, Chin LM. A model of cell inactivation by alpha-particle internal emitters. *Radiat Res*. 1993;134:143–150.
39. Kvinnsland Y, Stokke T, Aurlien E. Radioimmunotherapy with alpha-particle emitters: microdosimetry of cells with a heterogeneous antigen expression and with various diameters of cells and nuclei. *Radiat Res*. 2001;155:288–296.
40. Netti PVS, Howell RW. Log normal distribution of cellular uptake of radioactivity: implications for biologic responses to radiopharmaceuticals. *J Nucl Med*. 2006;47:1049–1058.
41. Munro TR. Relative radiosensitivity of nucleus and cytoplasm of Chinese hamster fibroblasts. *Radiat Res*. 1970;42:451–470.
42. Lloyd EL, Gemmell MA, Henning CB, Gemmell DS, Zabransky BJ. Cell survival following multiple-track alpha particle irradiation. *Int J Radiat Biol Relat Stud Phys Chem Med*. 1979;35:23–31.
43. Raju MR, Eisen Y, Carpenter S, Inkret WC. Radiobiology of alpha particles. III. Cell inactivation by alpha particle traversals of the cell nucleus. *Radiat Res*. 1991;128:204–209.
44. Bird RP, Rohrig N, Colvett RD, Geard CR, Marino SA. Inactivation of synchronized Chinese hamster V79 cells with charged-particle track segments. *Radiat Res*. 1980;82:277–289.
45. Todd P, Wood JCS, Walker JT, Weiss SJ. Lethal, potentially lethal, and nonlethal damage induction by heavy-ions in cultured human-cells. *Radiat Res*. 1985;104(suppl):S5–S12.
46. Roberts CJ, Goodhead DT. The effect of ^{238}Pu alpha-particles on the mouse fibroblast cell line C3H 10T1/2: characterization of source and RBE for cell survival. *Int J Radiat Biol Relat Stud Phys Chem Med*. 1987;52:871–882.
47. Barendsen GW. LET dependence of linear and quadratic terms in dose-response relationships for cellular-damage: correlations with the dimensions and structures of biological targets. *Radiat Prot Dosimetry*. 1990;31:235–239.
48. Howell RW, Rao DV, Hou DY, Narra VR, Sastry KSR. The question of relative biological effectiveness and quality factor for auger emitters incorporated into proliferating mammalian cells. *Radiat Res*. 1991;128:282–292.
49. Macklis RM, Lin JY, Beresford B, Atcher RW, Hines JJ, Humm JL. Cellular kinetics, dosimetry, and radiobiology of alpha-particle radioimmunotherapy: induction of apoptosis. *Radiat Res*. 1992;130:220–226.
50. Charlton DE, Nikjoo H, Humm JL. Calculation of initial yields of single-strand and double-strand breaks in cell-nuclei from electrons, protons and alpha-particles. *Int J Radiat Biol*. 1989;56:1–19.

51. Charlton DE, Turner MS. Use of chord lengths through the nucleus to simulate the survival of mammalian cells exposed to high LET alpha-radiation. *Int J Radiat Biol.* 1996;69:213–217.
52. Crawford-Brown DJ, Hofmann W. A generalized state-vector model for radiation-induced cellular transformation. *Int J Radiat Biol.* 1990;57:407–423.
53. Crawford-Brown DJ, Hofmann W. Correlated hit probability and cell transformation in an effect-specific track length model applied to in vitro alpha irradiation. *Radiat Environ Biophys.* 2001;40:317–323.
54. Holthusen H. Articles on the biology of radiation effects: analysis on nematode eggs. *Pflugers Arch Gesamte Physiol Menschen Tiere.* 1921;187:1–24.
55. Thomlinson RH, Gray LH. The histological structure of some human lung cancers and the possible implications for radiotherapy. *Br J Cancer.* 1955;9:539–549.
56. Unruh A, Ressel A, Mohamed HG, et al. The hypoxia-inducible factor-1 alpha is a negative factor for tumor therapy. *Oncogene.* 2003;22:3213–3220.
57. Ewing D, Powers EL. Oxygen-dependent sensitization of irradiated cells. In: Meyn RE, Withers HR, eds. *Radiation Biology in Cancer Research.* New York, NY: Raven Press; 1979:143–168.
58. Hall EJ. *Radiobiology for the Radiologist.* Philadelphia, PA: JB Lippincott Co.; 1994:118.
59. Machinami R, Ishikawa Y, Boecker BB. The international workshop on health effects of Thorotrast, radium, radon and other alpha-emitters, 1999 [preface]. *Radiat Res.* 1999;152(suppl):S1–S2.
60. International Commission on Radiological Protection. *Relative Biological Effectiveness (RBE), Quality Factor (Q), and Radiation Weighting Factor (w_R).* Philadelphia, PA: Elsevier; 2004. ICRP publication 92.
61. Harrison JD, Muirhead CR. Quantitative comparisons of cancer induction in humans by internally deposited radionuclides and external radiation. *Int J Radiat Biol.* 2003;79:1–13.
62. Brown I, Mitchell JS. The development of a [At-211]-astatinated endoradiotherapeutic drug: Part IV—late radiation effects. *Int J Radiat Oncol Biol Phys.* 1998;40:1177–1183.
63. Durbin PW, Asling CW, Johnston ME, et al. The induction of tumors in the rat by astatine-211. *Radiat Res.* 1958;9:378–397.
64. Yokoro K, Kunii A, Furth J, Durbin PW. Tumor induction with astatine-211 in rats: characterization of pituitary tumors. *Cancer Res.* 1964;24:683–688.
65. Hall EJ, Brenner DJ. The radiobiology of radiosurgery: rationale for different treatment regimes for AVMs and malignancies. *Int J Radiat Oncol Biol Phys.* 1993;25:381–385.
66. Dale RG, Jones B. The assessment of RBE effects using the concept of biologically effective dose. *Int J Radiat Oncol Biol Phys.* 1999;43:639–645.
67. Takata M, Sasaki MS, Sonoda E, et al. Homologous recombination and non-homologous end-joining pathways of DNA double-strand break repair have overlapping roles in the maintenance of chromosomal integrity in vertebrate cells. *EMBO J.* 1998;17:5497–5508.
68. Oliveira NG, Castro M, Rodrigues AS, et al. Wortmannin enhances the induction of micronuclei by low and high LET radiation [erratum]. *Mutagenesis.* 2003;18:217.
69. Oliveira NG, Castro M, Rodrigues AS, et al. Wortmannin enhances the induction of micronuclei by low and high LET radiation. *Mutagenesis.* 2003;18:37–44.
70. Harapanhalli RS, Narra VR, Yaghamai V, et al. Vitamins as radioprotectors in vivo. II. Protection by vitamin A and soybean oil against radiation-damage caused by internal radionuclides. *Radiat Res.* 1994;139:115–122.
71. Narra VR, Harapanhalli RS, Goddu SM, Howell RW, Rao DV. Radioprotection against biological effects of internal radionuclides in vivo by S-(2-aminoethyl)isothiuronium bromide hydrobromide (AET). *J Nucl Med.* 1995;36:259–266.
72. Rao DV, Howell RW, Narra VR, Govelitz GF, Sastry KSR. In-vivo radiotoxicity of DNA-incorporated ¹²⁵I compared with that of densely ionizing alpha-particles. *Lancet.* 1989;2:650–653.
73. Rao DV, Narra VR, Howell RW, Lanka VK, Sastry KSR. Induction of sperm head abnormalities by incorporated radionuclides: dependence on subcellular distribution, type of radiation, dose rate, and presence of radioprotectors. *Radiat Res.* 1991;125:89–97.
74. Goddu SM, Narra VR, Harapanhalli RS, Howell RW, Rao DV. Radioprotection by DMSO against the biological effects of incorporated radionuclides in vivo: comparison with other radioprotectors and evidence for indirect action of Auger electrons. *Acta Oncol.* 1996;35:901–907.
75. Narra VR, Harapanhalli R, Howell RW, Sastry KSR, Rao DV. Vitamins as radioprotectors in vivo. I. Protection by vitamin C against internal radionuclides in mouse testes: implications to the mechanism of damage caused by the Auger effect. *Radiat Res.* 1994;137:394–399.
76. Wright HA, Magee JL, Hamm RN, Chatterjee A, Turner JE, Klots CE. Calculations of physical and chemical-reactions produced in irradiated water containing DNA. *Radiat Prot Dosimetry.* 1985;13:133–136.
77. International Commission on Radiological Protection. *RBE for Deterministic Effects.* Philadelphia, PA: Elsevier; 1990. ICRP publication 58.
78. Schwartz JL, Rotmensch J, Atcher RW, et al. Interlaboratory comparison of different alpha-particle and radon sources: cell survival and relative biological effectiveness. *Health Phys.* 1992;62:458–461.
79. Jostes RF, Hui TE, James AC, et al. In vitro exposure of mammalian cells to radon: dosimetric considerations. *Radiat Res.* 1991;127:211–219.
80. Charlton DE, Utteridge TD, Allen BJ. Theoretical treatment of human haemopoietic stem cell survival following irradiation by alpha particles. *Int J Radiat Biol.* 1998;74:111–118.
81. Howell RW, Goddu SM, Narra VR, Fisher DR, Schenter RE, Rao DV. Radiotoxicity of gadolinium-148 and radium-223 in mouse testes: relative biological effectiveness of alpha-particle emitters in vivo. *Radiat Res.* 1997;147:342–348.
82. Howell RW, Goddu SM, Rao DV. Design and performance characteristics of an experimental cesium-137 irradiator to simulate internal radionuclide dose rate patterns. *J Nucl Med.* 1997;38:727–731.
83. Goddu SM, Bishayee A, Bouchet LG, Bolch WE, Rao DV, Howell RW. Marrow toxicity of ³³P-versus ³²P-orthophosphate: implications for therapy of bone pain and bone metastases. *J Nucl Med.* 2000;41:941–951.
84. Feinendegen LE, McClure JJ. Meeting report: Alpha-emitters for medical therapy—Workshop of the United States Department of Energy, Denver, Colorado, May 30–31, 1996. *Radiat Res.* 1997;148:195–201.
85. 1990 recommendations of the International Commission on Radiological Protection. *Ann ICRP.* 1991;21:1–201.
86. Radiation protection in medicine: ICRP publication 105. *Ann ICRP.* 2007;37:1–63.
87. Neti PVSV, Howell RW. Biological response to nonuniform distributions of ²¹⁰Po in multicellular clusters. *Radiat Res.* 2007;168:332–340.
88. Goddu SM, Rao DV, Howell RW. Multicellular dosimetry for micrometastases: dependence of self-dose versus cross-dose to cell nuclei on type and energy of radiation and subcellular distribution of radionuclides. *J Nucl Med.* 1994;35:521–530.
89. Charlton DE. Radiation effects in spheroids of cells exposed to alpha emitters. *Int J Radiat Biol.* 2000;76:1555–1564.
90. Akabani G, Zalutsky MR. Microdosimetry of astatine-211 using histological images: application to bone marrow. *Radiat Res.* 1997;148:599–607.
91. Humm JL, Macklis RM, Bump K, Cobb LM, Chin LM. Internal dosimetry using data derived from autoradiographs. *J Nucl Med.* 1993;34:1811–1817.
92. Baxter LT, Jain RK. Transport of fluid and macromolecules in tumors. IV. A microscopic model of the perivascular distribution. *Microvasc Res.* 1991;41:252–272.
93. Jain RK, Baxter LT. Mechanisms of heterogeneous distribution of monoclonal antibodies and other macromolecules in tumors: significance of elevated interstitial pressure. *Cancer Res.* 1988;48:7022–7032.
94. Sgouros G. Plasmapheresis in radioimmunotherapy of micrometastases: a mathematical modeling and dosimetric analysis. *J Nucl Med.* 1992;33:2167–2179.
95. Goddu SM, Howell RL, Bouchet LG, Bolch WE, Rao DV. *MIRD Cellular S Values.* Reston VA: Society of Nuclear Medicine; 1997.
96. Goddu SM, Howell RW, Rao DV. Cellular dosimetry: absorbed fractions for monoenergetic electron and alpha particle sources and S-values for radionuclides uniformly distributed in different cell compartments. *J Nucl Med.* 1994;35:303–316.
97. Polig E. Localized alpha-dosimetry. In: Eberg M, Howard A, eds. *Current Topics in Radiation Research.* Vol 13. Amsterdam, The Netherlands: Elsevier; 1978:189–327.
98. Rossi HH. Microdosimetric energy distribution in irradiated matter. In: Atx FH, Roesch WC, eds. *Radiation Dosimetry.* Vol 1. New York, NY: Academic Press; 1968.
99. Roesch WC. Microdosimetry of internal sources. *Radiat Res.* 1977;70:494–510.
100. Fisher DR. The microdosimetry of monoclonal antibodies labeled with alpha emitters. In: Schlafke-Stelson AT, Watson EE, eds. *Fourth International Radiopharmaceutical Dosimetry Symposium.* Oak Ridge, TN: Oak Ridge Associated Universities; 1986:26–36.
101. Stinchcomb TG, Roeske JC. Analysis of survival of C-18 cells after irradiation in suspension with chelated and ionic bismuth-212 using microdosimetry. *Radiat Res.* 1994;140:48–54.
102. Stinchcomb TG, Roeske JC. Analytic microdosimetry for radioimmunotherapeutic alpha emitters. *Med Phys.* 1992;19:1385–1393.
103. Kellere AM. Analysis of patterns of energy deposition: a survey of theoretical relations in microdosimetry. In: Ebert HG, ed. *Proceedings of the Second*

- Symposium on Microdosimetry*. Brussels, Belgium: Commission of European Communities; 1970:107–134.
104. Olko P, Booz J. Energy deposition by protons and alpha-particles in spherical sites of nanometer to micrometer diameter. *Radiat Environ Biophys*. 1990;29:1–17.
 105. Ziegler JF, Biersack JP, Littmark U. *The Stopping and Range of Ions in Matter*. New York, NY: Pergamon Press; 1985.
 106. Ziegler JF. The stopping and range of ions in solids (*Stopping and Range of Ions in Matter*, Vol. 1). New York, NY: Pergamon; 1985.
 107. Bichsel H. *Stopping Powers of Fast Charged Particles in Heavy Elements*. Springfield, VA: U.S. National Technical Information Service; 1992. NIST report IR-4550.
 108. International Commission on Radiation Units and Measurements. *Stopping Powers and Ranges for Protons and Alpha Particles*. Bethesda, MD: ICRU; 1993. ICRU publication 49.
 109. Kellerer AM, Chmelevsky D. Criteria for applicability of LET. *Radiat Res*. 1975;63:226–234.
 110. Roeske JC, Stinchcomb TG. Dosimetric framework for therapeutic alpha-particle emitters. *J Nucl Med*. 1997;38:1923–1929.
 111. Loevinger R, Budinger TF, Watson EE. *MIRD Primer for Absorbed Dose Calculations*. Revised ed. New York, NY: Society of Nuclear Medicine; 1991.
 112. Stinchcomb TG, Roeske JC. Values of “S,” $\langle z1 \rangle$, and $\langle (z1)^2 \rangle$ for dosimetry using alpha-particle emitters. *Med Phys*. 1999;26:1960–1971.
 113. Fisher DR. Specific energy distributions for alpha emitters in the dog lung. *Ann Occup Hyg*. 1988;32(suppl 1):1095–1104.
 114. Humm JL. A microdosimetric model of astatine-211 labeled antibodies for radioimmunotherapy. *Int J Radiat Oncol Biol Phys*. 1987;13:1767–1773.
 115. Stinchcomb TG, Roeske JC. Survival of alpha particle irradiated cells as a function of the shape and size of the sensitive volume (nucleus). *Radiat Prot Dosimetry*. 1995;62:157–164.
 116. Aubineau-Laniece I, Pihet P, Winkler R, Hofmann W, Charlton DE. Monte Carlo code for microdosimetry of inhaled alpha emitters. *Radiat Prot Dosimetry*. 2002;99:463–467.
 117. Fakir H, Hofmann W, Aubineau-Laniece I. Modelling the effect of non-uniform radon progeny activities on transformation frequencies in human bronchial airways. *Radiat Prot Dosimetry*. 2006;121:221–235.
 118. Fakir H, Hofmann W, Aubineau-Laniece I. Microdosimetry of radon progeny alpha particles in bronchial airway bifurcations. *Radiat Prot Dosimetry*. 2005;117:382–394.
 119. Fakir H, Hofmann W, Caswell RS, Aubineau-Laniece I. Microdosimetry of inhomogeneous radon progeny distributions in bronchial airways. *Radiat Prot Dosimetry*. 2005;113:129–139.
 120. Palm S, Humm JL, Rundqvist R, Jacobsson L. Microdosimetry of astatine-211 single-cell irradiation: role of daughter polonium-211 diffusion. *Med Phys*. 2004;31:218–225.
 121. Iyer R, Lehnert BE. Alpha-particle-induced increases in the radioresistance of normal human bystander cells. *Radiat Res*. 2002;157:3–7.
 122. Azzam EI, de Toledo SM, Gooding T, Little JB. Intercellular communication is involved in the bystander regulation of gene expression in human cells exposed to very low fluences of alpha particles. *Radiat Res*. 1998;150:497–504.
 123. Utteridge TD, Charlton DE, Allen BJ. Monte Carlo modeling of the effects of injected short-, medium- and longer-range alpha-particle emitters on human marrow at various ages. *Radiat Res*. 2001;156:413–418.
 124. Hamacher KA, Sgouros G. A schema for estimating absorbed dose to organs following the administration of radionuclides with multiple unstable daughters: a matrix approach. *Med Phys*. 1999;26:2526–2528.
 125. Fisher DR, Sgouros G. Dosimetry of radium-223 and progeny. In: Stelton AT, Stabin MG, Sparks RB, eds. *Proceedings of the Sixth International Radiopharmaceutical Dosimetry Symposium*. Gatlinburg, TN: U.S. Department of Energy and Oak Ridge Associated Universities; 1999:375–391.
 126. Sgouros G. Long-lived alpha emitters in radioimmunotherapy: the mischievous progeny. *Cancer Biother Radiopharm*. 2000;15:219–221.
 127. Miederer M, McDevitt MR, Sgouros G, Kramer K, Cheung NK, Scheinberg DA. Pharmacokinetics, dosimetry, and toxicity of the targetable atomic generator, ^{225}Ac -HuM195, in nonhuman primates. *J Nucl Med*. 2004;45:129–137.
 128. Hamacher KA, Den RB, Den EI, Sgouros G. Cellular dose conversion factors for alpha-particle-emitting radionuclides of interest in radionuclide therapy. *J Nucl Med*. 2001;42:1216–1221.
 129. Muller WA. Studies on short-lived internal alpha-emitters in mice and rats. II. ^{227}Th . *Int J Radiat Biol Relat Stud Phys Chem Med*. 1971;20:233–243.
 130. Dahle J, Borrebaek J, Melhus KB, et al. Initial evaluation of ^{227}Th -p-benzyl-DOTA-rituximab for low-dose rate alpha-particle radioimmunotherapy. *Nucl Med Biol*. 2006;33:271–279.
 131. Dahle J, Borrebaek J, Jonasdottir TJ, et al. Targeted cancer therapy with a novel low dose rate alpha-emitting radioimmunoconjugate. *Blood*. 2007;110:2049–2056.
 132. Siegel JA, Thomas SR, Stubbs JB, et al. MIRD pamphlet no. 16: techniques for quantitative radiopharmaceutical biodistribution data acquisition and analysis for use in human radiation dose estimates. *J Nucl Med*. 1999;40(suppl):37S–61S.
 133. Sgouros G. Treatment planning for internal emitter therapy: methods, applications and clinical implications. In: Schafke-Stelson AT, Watson EE, eds. *Proceedings of the 6th International Radiopharmaceutical Dosimetry Symposium, May 7–10, 1996, Gatlinburg, TN*. Oak Ridge, TN: Oak Ridge Associated Universities; 1996:13–24.
 134. Sgouros G. Radioimmunotherapy of micrometastases. In: Riva P, ed. *Cancer Radioimmunotherapy: Present and Future*. Newark, NJ: Harwood Academic Publishers; 1998:191–207.
 135. Kirschner AS, Ice RD, Beierwaltes WH. Radiation dosimetry of ^{131}I -iodocholesterol: the pitfalls of using tissue concentration data [reply]. *J Nucl Med*. 1975;16:248–249.
 136. Sgouros G, Ballangrud AM, Jurcic JG, et al. Pharmacokinetics and dosimetry of an alpha-particle emitter labeled antibody: ^{213}Bi -HuM195 (anti-CD33) in patients with leukemia. *J Nucl Med*. 1999;40:1935–1946.
 137. Patton PW, Rajon DA, Shah AP, Jokisch DW, Inglis BA, Bolch WE. Site-specific variability in trabecular bone dosimetry: considerations of energy loss to cortical bone. *Med Phys*. 2002;29:6–14.
 138. Bolch WE, Patton PW, Rajon DA, Shah AP, Jokisch DW, Inglis BA. Considerations of marrow cellularity in 3-dimensional dosimetric models of the trabecular skeleton. *J Nucl Med*. 2002;43:97–108.
 139. Shah AP, Patton PW, Rajon DA, Bolch WE. Adipocyte spatial distributions in bone marrow: implications for skeletal dosimetry models. *J Nucl Med*. 2003;44:774–783.
 140. Shah AP, Rajon DA, Patton PW, Jokisch DW, Bolch WE. Accounting for beta-particle energy loss to cortical bone via paired-image radiation transport (PIRT). *Med Phys*. 2005;32:1354–1366.
 141. Watchman CJ, Jokisch DW, Patton PW, Rajon DA, Sgouros G, Bolch WE. Absorbed fractions for alpha-particles in tissues of trabecular bone: considerations of marrow cellularity within the ICRP reference male. *J Nucl Med*. 2005;46:1171–1185.
 142. Bolch WE, Eckerman KF, Sgouros G, Thomas SR. MIRD pamphlet no. 21: a generalized schema for radiopharmaceutical dosimetry—standardization of nomenclature. *J Nucl Med*. 2009;50:477–484.
 143. Eckerman KF, Endo A. *MIRD: Radionuclide Data and Decay Schemes*. Reston, VA: Society of Nuclear Medicine; 2007.
 144. Snyder WS, Fisher HL, Ford MR, Warner GG. Estimates of absorbed fractions for monoenergetic photon sources uniformly distributed in various organs of a heterogeneous phantom. *J Nucl Med*. 1969;10(suppl):7–52.
 145. Bouchet LG, Jokisch DW, Bolch WE. A three-dimensional transport model for determining absorbed fractions of energy for electrons within trabecular bone. *J Nucl Med*. 1999;40:1947–1966.
 146. Snyder WS, Ford MR, Warner GG. *MIRD Pamphlet No. 5, Revised: Estimates of Specific Absorbed Fractions for Photon Sources Uniformly Distributed in Various Organs of a Heterogeneous Phantom*. New York, NY: Society of Nuclear Medicine; 1978.
 147. Sgouros G, Howell RW, Bolch WE, Fisher DR. MIRD commentary: proposed name for a dosimetry unit applicable to deterministic biological effects—the Barendsen (Bd). *J Nucl Med*. 2009;50:485–487.
 148. Kneifel S, Cordier D, Good S, et al. Local targeting of malignant gliomas by the diffusible peptidic vector 1,4,7,10-tetraazacyclododecane-1-glutaric acid-4,7,10-triacetic acid-substance P. *Clin Cancer Res*. 2006;12:3843–3850.
 149. Heeger S, Moldenhauer G, Egerer G, et al. Alpha-radioimmunotherapy of B-lineage non-Hodgkin’s lymphoma using ^{213}Bi -labelled anti-CD19- and anti-CD20-CHX-A’-DTPA conjugates [abstract]. *Abstracts of Papers of the American Chemical Society*. 2003;225:U261.
 150. Allen BJ, Raja C, Rizvi S, et al. Intralesional targeted alpha therapy for metastatic melanoma. *Cancer Biol Ther*. 2005;4:1318–1324.
 151. Bruland OS, Nilsson S, Fisher DR, Larsen RH. High-linear energy transfer irradiation targeted to skeletal metastases by the alpha-emitter Ra-223: adjuvant or alternative to conventional modalities? *Clin Cancer Res*. 2006;12(suppl):6250S–6257S.
 152. Nilsson S, Franzen L, Parker C, et al. Bone-targeted radium-223 in symptomatic, hormone-refractory prostate cancer: a randomised, multicentre, placebo-controlled phase II study. *Lancet Oncol*. 2007;8:587–594.
 153. Goodhead DT. Talk 23, Alpha Emitters, from Session 6, Effects from Specific Sources of Internal Radiation. Presented at: CERRIE Workshop; July 21–23, 2003; Oxford, U.K.
 154. Powsner RA, Powsner ER. *Essentials of Nuclear Medicine Physics*. Malden MA: Blackwell Science, Inc.; 1998.
 155. Cole A, ed. *Theoretical and Experimental Biophysics*. New York, NY: Marcel Dekker, Inc.; 1967.



The Journal of
NUCLEAR MEDICINE

MIRD Pamphlet No. 22 (Abridged): Radiobiology and Dosimetry of α -Particle Emitters for Targeted Radionuclide Therapy

George Sgouros, John C. Roeske, Michael R. McDevitt, Stig Palm, Barry J. Allen, Darrell R. Fisher, A. Bertrand Brill, Hong Song, Roger W. Howell and Gamal Akabani

J Nucl Med. 2010;51:311-328.
Published online: January 15, 2010.
Doi: 10.2967/jnumed.108.058651

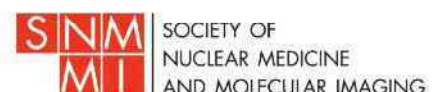
This article and updated information are available at:
<http://jnm.snmjournals.org/content/51/2/311>

Information about reproducing figures, tables, or other portions of this article can be found online at:
<http://jnm.snmjournals.org/site/misc/permission.xhtml>

Information about subscriptions to JNM can be found at:
<http://jnm.snmjournals.org/site/subscriptions/online.xhtml>

The Journal of Nuclear Medicine is published monthly.
SNMMI | Society of Nuclear Medicine and Molecular Imaging
1850 Samuel Morse Drive, Reston, VA 20190.
(Print ISSN: 0161-5505, Online ISSN: 2159-662X)

© Copyright 2010 SNMMI; all rights reserved.



Production of [^{211}At]-Astatinated Radiopharmaceuticals and Applications in Targeted α -Particle Therapy

François Guérard,¹ Jean-François Gestin,² and Martin W. Brechbiel¹

Abstract

^{211}At is a promising radionuclide for α -particle therapy of cancers. Its physical characteristics make this radionuclide particularly interesting to consider when bound to cancer-targeting biomolecules for the treatment of microscopic tumors. ^{211}At is produced by cyclotron irradiation of ^{209}Bi with α -particles accelerated at ~ 28 MeV and can be obtained in high radionuclidic purity after isolation from the target. Its chemistry resembles iodine, but there is also a tendency to behave as a metalloid. However, the chemical behavior of astatine has not yet been clearly established, primarily due to the lack of any stable isotopes of this element, which precludes the use of conventional analytical techniques for its characterization. There are also only a limited number of research centers that have been able to produce this element in sufficient amounts to carry out extensive investigations. Despite these difficulties, chemical reactions typically used with iodine can be performed, and a number of biomolecules of interest have been labeled with ^{211}At . However, most of these compounds exhibit unacceptable instability *in vivo* due to the weakness of the astatine–biomolecule bond. Nonetheless, several compounds have shown high potential for the treatment of cancers *in vitro* and in several animal models, thus providing a promising basis that has allowed initiation of the first two clinical studies.

Key words: α -immunotherapy, Astatine-211, radiolabeling

Introduction

WHILE β^- -EMITTERS HAVE PROVEN their usefulness in the therapy of localized macroscopic cancerous tumors, limited successes have been obtained in the case of microscopic and disseminated cancers. The disappointing results are explained by the relatively long path length of the β^- -particles in tissue (several millimeters), leading to the loss of most of the deposited energy in healthy tissues when the tumor being treated is too small. In contrast, α -particle emitters are promising radionuclides for the treatment of such small tumors. When such a radionuclide is conjugated to a suitable targeting agent, the short path length of the α -particles (~ 25 – $100\ \mu\text{m}$), in association with their high energy (~ 4 – 8.5 MeV), makes them highly efficient at eradicating small clusters or isolated cancerous cells with a reduced dose deposited to the

surrounding healthy tissues. Such radiopharmaceuticals are of high interest for the treatment of disseminated micrometastasis, diseases consisting of monocellular cancer cells such as lymphoma and leukemia, or in the case of residual disease after surgical debulking. Among the hundred α -particle emitters known, a limited number of radionuclides exhibit characteristics that have been considered as potentially suitable for therapeutic applications (^{225}Ac , ^{211}At , ^{212}Bi , ^{213}Bi , ^{223}Ra , ^{149}Tb , ^{227}Th , and ^{212}Pb as an *in vivo* generator of ^{212}Bi , see Table 1). All have been the object of increasing attention in recent years, and several have reached different stages of clinical evaluation while production and availability of the radionuclides and their labeling chemistry issues are being overcome with varying levels of success.¹

Among these radionuclides, ^{211}At exhibits particularly favorable characteristics, with a 7.2-hour half-life suitable to

¹Radioimmune and Inorganic Chemistry Section, Radiation Oncology Branch, NCI, NIH, Bethesda, Maryland.

²Centre de Recherche en Cancérologie Nantes-Angers (CRCNA), Université de Nantes, Inserm, UMR 892, Institut de Recherche Thérapeutique de l'Université de Nantes, Nantes Cedex 1, France.

Address correspondence to: Martin W. Brechbiel; Radioimmune and Inorganic Chemistry Section, Radiation Oncology Branch, NCI, NIH; 10 Center Drive, MSC-1002, Rm B3B69, Bethesda, MD 20892-1002
E-mail: martinwb@mail.nih.gov

TABLE 1. CHARACTERISTICS OF α -EMITTING RADIONUCLIDES OF POTENTIAL INTEREST FOR THE THERAPY OF CANCERS

Nuclide	Half-life	Decays	Energy α (MeV)	Production	Clinical trial status
^{225}Ac	10 days	4 α , 2 β^-	5.1–8.4	^{233}U decay/cyclotron	First phase I ongoing
^{211}At	7.2 hours	1 α , 1 EC	5.9 or 7.4	Cyclotron	Two phase I published
^{212}Bi	61 minutes	1 α , 1 β^-	6.1/7.8	^{228}Th decay/ ^{224}Ra generator	Preclinical
^{213}Bi	46 minutes	1 α , 2 β^-	6.0/8.4	^{225}Ac generator	Phase I/II
^{223}Ra	11.4 days	4 α , 2 β^-	5.7–7.5	^{227}Ac generator	Phase I/II/III
^{149}Tb	4.1 hours	1 α , EC	4.0	Accelerator	Preclinical
^{227}Th	18.7 days	5 α , 2 β^-	5.7–7.5	^{227}Ac generator	Preclinical
$^{212}\text{Pb}/^{212}\text{Bi}^a$	10.6 hours	1 α , 2 β^-	6.1/7.8	^{224}Ra generator	First phase I ongoing

^aAlthough ^{212}Pb is not an α -particle emitter, it is included in this table for its considerations in several studies as an *in vivo* generator of the α -particle emitter ^{212}Bi . See Yong and Brechbiel² for a definition of the concept.

the kinetics of full antibodies or other biomolecules that require several hours to reach an optimal tumor-to-blood dose ratio. Furthermore, with 100% of its decay leading to the production of an α -particle, high efficiency of the treatments and limited toxicity are expected at relatively low doses. However, the introduction of ^{211}At -based radiopharmaceuticals into clinics has been slowed by difficulties related to the production and availability of the radionuclide, the limited knowledge of the chemistry of elemental astatine, the lack of stability of the astatine–biomolecule bond, and concerns about the potential toxicity of α -radiation on humans.

In this review, the characteristics of ^{211}At and its methods of production and purification for radiolabeling purposes are presented. The different aspects of its chemistry as well as the strategies for the radiolabeling of biomolecules are also described. Finally, the latest advances in the use of ^{211}At -based radiopharmaceuticals in radiotherapy of cancers from the *in vitro* studies to the very first clinical trials that have been published recently are presented.

^{211}At : Characteristics and Production

The 85th element in the periodic table classification was first produced in 1940 when Corson irradiated ^{209}Bi with a beam of α -particles accelerated to 32 MeV.³ Expected by Mendeleiev to be below the element iodine (and named eka-iodine at that time), it is the only halogen without a stable isotope, which is why its discoverers named it astatine, from the Greek word *αστατος* (astatos=unstable).

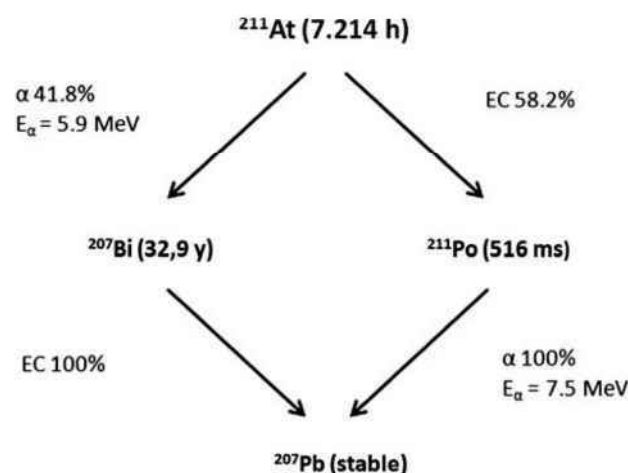
Astatine exists on the Earth in very small quantities (estimated to be a few milligrams in the whole Earth's crust) by some decay branches of ^{235}U , ^{238}U , and ^{232}Th , which actually makes it the rarest natural element.⁴ There are 32 astatine isotopes known: ^{191}At and all the rest from ^{193}At to ^{223}At . Their half-lives range from 125 nanoseconds for ^{213}At up to 8.1 hours for ^{210}At , and most of them are α -particle emitters. Among these isotopes, only ^{211}At exhibits physical characteristics that are reasonably adapted for targeted radiotherapy.

The most relevant characteristics of the radionuclide are summarized below, and the reader is referred to the Gmelin Handbook of Inorganic Chemistry on Astatine for an exhaustive review of the topic.⁵

Physical properties

The disintegration of ^{211}At follows a branched decay scheme with a 7.21 hours half-life (Fig. 1). One branch leads

to ^{207}Bi by emission of an α -particle. ^{207}Bi , with a 33.9 year half-life, decays to ^{207}Pb via electron capture. The other decay branch occurs via electron capture and leads to the 516 milliseconds half-life radionuclide ^{211}Po , which in turn decays to stable ^{207}Pb by emission of an α -particle. The result of these decay pathways is 100% α -particle emission during the decay of ^{211}At (5.87 and 7.45 MeV in 42% and 58% of the decays, respectively). Concerns have been raised regarding the fate of the ^{211}Po decay during targeted radiotherapy. Palm et al. investigated the influence of the diffusion of ^{211}Po on the dose absorbed by isolated cells in suspension.⁶ They estimated that the diffusion distance from the initial ^{211}At nucleus bound to the cell reduces the absorbed dose by a factor of 2 in this model. Part of the deposited dose may indeed be lost from the target in case of dispersed cells, but this phenomenon might be reduced in cell cluster environments, where the dose could be deposited toward a neighboring malignant cell. Also, as noted by the authors of the study, cellular localization may reduce the diffusion of ^{211}Po depending upon the viscosity of the tissue. Another concern is the fate of ^{207}Bi with its long half-life (32.9 years), and the potential issues due to its uptake in the bone, liver, and kidneys. However, 347 MBq of ^{211}At , which is the highest dose that has been administered to a human, leads to only 310 kBq of ^{207}Bi , making its potential toxicity negligible.

FIG. 1. Simplified decay scheme of ^{211}At .

Also, another interesting characteristic is the emission of X-rays during the decay to ^{211}Po . With energies between 77 and 92 keV, these X-rays can be easily monitored by γ -detectors classically used in laboratory or clinical centers. This combination of emission and instrumentation makes detection relatively easy and useful for *in vivo* monitoring by SPECT imaging.⁷

Production

^{211}At is produced by irradiation of natural bismuth (^{209}Bi) following the nuclear reaction: $^{209}\text{Bi}(\alpha, 2n)^{211}\text{At}$. Other production methods have been investigated, such as the production of a $^{211}\text{Rn}/^{211}\text{At}$ generator by irradiation of ^{209}Bi with ^7Li ,⁸ or by fusion of ^9Li with ^{208}Pb .⁹ However, these alternative methods remain anecdotal with respect to the production of medical research quantities of the radionuclide.

^{211}At production is possible for α -beam energies ranging from 21 to more than 40 MeV, with a maximum cross-section observed for 31 MeV (Fig. 2). However, at this level of energy, ^{210}At is also produced. This 8.1-hour half-life isotope exhibits characteristics that are not compatible with pharmaceutical applications because of its decay into the long half-life ^{210}Po (138.2 days), which is highly toxic, especially to the bone marrow.¹⁰ Production of ^{210}Po is also observed from 26.7 MeV beam energies. Nonetheless, the presence of this isotope after irradiation is generally irrelevant due to an efficient isolation of ^{211}At from the target and impurities during the purification process. For these reasons, the beam energy is generally controlled to 28–29 MeV to limit formation of ^{210}At while maintaining acceptable yields of ^{211}At . However, only a limited number of cyclotrons in the world are able to generate α -beam energies beyond 25 MeV, which strongly limits the availability of this radionuclide.¹¹

Another limitation to consider is the low melting point of the irradiated material (Bismuth mp=272°C) and its low thermal conductivity ($k=7.9\text{ W m}^{-1}\text{ K}^{-1}$). Together, with the relatively high volatility of astatine (337°C), this potentially leads to vaporization of the produced activity due to overheating of the target during the irradiation. Solutions have been developed to limit this overheating issue, such as

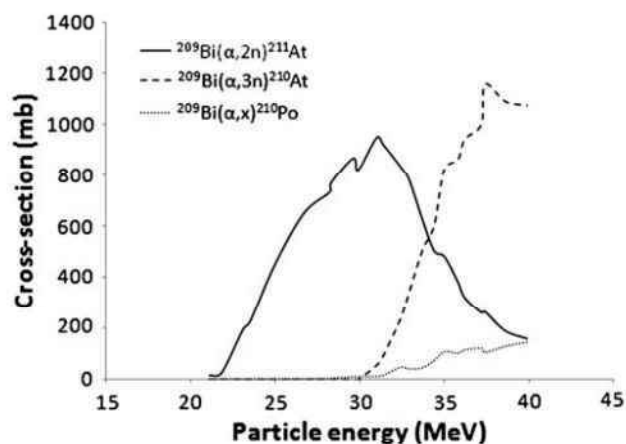


FIG. 2. Cross-section of the irradiation of ^{209}Bi as a function of the alpha particles energy. Plotted from the experimental data from Hermanne et al.¹²

cooling systems using cold gas and water during irradiation, or the use of an irradiation angle that spreads the beam over a larger impact surface on the bismuth. Furthermore, the bismuth is deposited as a thin layer on a material with a better thermal conductivity to enhance cooling. Aluminum has frequently been used as backing material ($k=250\text{ W m}^{-1}\text{ K}^{-1}$), although some reports make reference to the use of copper ($k=390\text{ W m}^{-1}\text{ K}^{-1}$).

Purification

After irradiation, the target contains the initial ^{209}Bi , traces of ^{210}Po , and the desired ^{211}At activity, which must be obtained in solution with the highest purity. Two methods are described to harvest ^{211}At : dry distillation that is probably the most widely used or liquid extraction that requires dissolution of the target in an acidic solution.

Dry distillation. In this method, the target is placed in a furnace and heated above the boiling point of astatine. The boiling points of bismuth and polonium being 1564°C and 962°C, respectively, the furnace temperature is generally set to 650°C–900°C. During the distillation, while the bismuth and the polonium melt and stay on the support, the volatile astatine is carried away by a stream of gas (generally nitrogen or argon) and trapped at the outlet. The astatine activity can be obtained by bubbling that stream of gas directly into the solvent of choice, or it can be captured in capillary tubing cooled in dry ice/ethanol placed at the outlet.¹³ In the latter case, the activity is subsequently dissolved in the solvent of choice (Fig. 3). With this kind of system, the astatine activity is collected in the trap in 20–30 minutes with recovery yields up to 80%.

Wet extraction. This alternative procedure consists of dissolution of the target in concentrated nitric acid. After evaporation of the nitric acid, the residue containing the bismuth and the astatine is dissolved in dilute nitric acid and extracted with di-isopropyl ether, which is the most efficient and practical solvent for this purpose.^{14,15} With this method, the astatine activity is obtained in high yields (~90%) in ~1 hour with high radionuclidic purity. The advantage of this

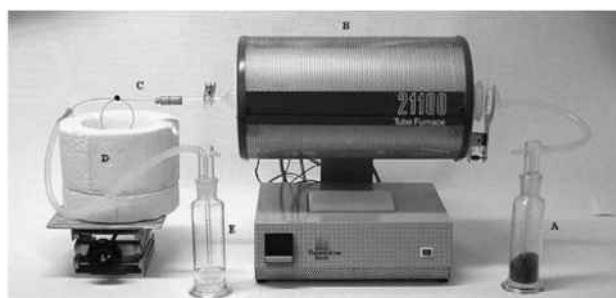


FIG. 3. Example of a typical furnace used for the distillation of ^{211}At . (A) Gas inlet with desiccant. (B) Furnace heated to 650°C–900°C. (C) Capillary trap cooled in (D) a dry ice/ethanol bath. It can be replaced by a cooled bubbler containing the solvent of interest. (E) Gas-wash bottle containing a reducing agent such as $\text{Na}_2\text{S}_2\text{O}_5$ to trap traces of astatine that would escape from the capillary. Reprinted by permission from Lindegren et al.¹³

technique over dry distillation is that it makes use of simple and cheap materials. Moreover, harvesting yields are obtained with an excellent reproducibility. However, the choice of extraction solvent is reduced to di-isopropyl ether or analogous solvents that can limit radiochemistry work. Furthermore, some nitric acid is extracted into the organic phase in concentrations that are not negligible, and that can cause side reactions during the radiolabeling chemistry. Nonetheless, it has been demonstrated that biomolecules can be radiolabeled efficiently using standard procedures with ^{211}At recovered with this method.¹⁶

Chemical Properties of Astatine

Despite more than 70 years of research on astatine, its chemistry is still not clearly established. The main reason is the fact that no stable isotope exists, the most stable isotope being ^{210}At with a half-life of only 8.1 hours. The highest reported activity produced is 6.59 GBq (which corresponds to 0.087 μg of ^{211}At).¹⁷ These amounts preclude the use of standard analysis techniques such as nuclear magnetic resonance, mass spectrometry (although some experiments have been reported¹⁸), UV, IR, or X-rays. Furthermore, with the astatine being obtained in highly dilute solutions, traces of unavoidable contaminants in solution can become competitive species and cause side reactions. Another impediment to the understanding of astatine chemistry is the lack of cyclotrons to produce this element leading to a reduced number of research laboratories able to run experiments.¹¹ Despite these obstacles, a relatively clear idea of some of the chemical properties of astatine has been established by analogy with its closest element in the periodic table of the elements, iodine. However, in its positive oxidation states, astatine exhibits many properties specific to metal ions. While almost identical to iodine in the $\text{At}(-\text{I})$ state, it is, in some respects, also comparable to silver in the $\text{At}(+\text{I})$ state, and close to polonium in its higher oxidation states.

In this section, the inorganic and organic chemistry of astatine is covered. Radiolabeling approaches for biomolecules of interest are also discussed as well as the issue of the limited *in vivo* stability of some ^{211}At -radiolabeled compounds.

Inorganic chemistry of astatine

Six oxidation states have been identified or hypothesized with varying degrees of certainty: $-\text{I}$, 0 , $+\text{I}$, $+\text{III}$, $+\text{V}$, and $+\text{VII}$. These forms of astatine were determined at low concentration with chemistry techniques that can be used at a tracer level such as co-precipitation, liquid extraction, or electromigration experiments, with the knowledge of iodine chemistry as a guide. Most of the descriptions of the oxidation states presented below rely on works by Johnson et al.,¹⁹ Appelman,²⁰ Visser and Diemer,^{21,22} and Dreyer et al.²³⁻²⁵ Also, more exhaustive information can be found in the DOE-Sponsored Nuclear Science Series monograph by Ruth et al.²⁶

$\text{At}(-\text{I})$. The $(-\text{I})$ oxidation state is probably the most clearly established form of astatine with a strong similarity with iodide. It is obtained in the presence of reducing agents such as SO_3^{2-} , Zn^0 , or cysteine, which form the astatide species (At^-). It is characterized by electromigration at the anode or by co-precipitation with AgI , TlI , or PbI_2 , and is

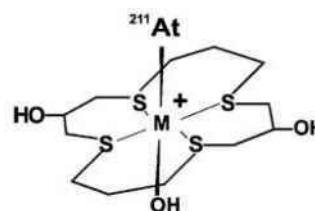


FIG. 4. ^{211}At -M(16-S4-diol) complex, with $\text{M} = \text{Rh}(\text{III})$ or $\text{Ir}(\text{III})$.

stable over a wide pH range. The astatide anion exhibits soft base characteristics, similar to iodide. It forms stable complexes with soft cations such as Hg^{2+} , Rh^{3+} , or Ir^{3+} . Pruszyński et al.²⁷ investigated the complexation of astatide in the presence of mercury nitrate in aqueous solution. Interestingly, the complex formed, assumed to be $\text{Hg}(\text{OH})\text{At}$, exhibited a higher stability than the iodinated analog.²⁷ Similarly, complexes have been prepared with rhodium (III) and iridium (III), and chelated in a macrocyclic agent bearing soft donors sulfur atoms (Fig. 4).²⁸ These compounds could lead to an interesting approach for the radiolabeling of biomolecules if they exhibit acceptable *in vivo* stability.

$\text{At}(0)$. This oxidation state of astatine, also denoted At^0 , remains unresolved, mainly because of its highly irreproducible behavior. It is hypothesized that astatine is obtained as At_2 in the gas phase (such as during the distillation process), but in solution, At_2 or the radical At^\cdot is highly unlikely at this level of dilution. Recombination with impurities or other species of the solvent is supposed to occur very rapidly. At^0 has often been referred to as the species that does not exhibit mobility in an electric field. It is supposed to be in the AtX form (with $\text{X} = \text{HSO}_4$, NO_3 , OAc , etc.) and extracted from an aqueous medium by organic solvents as AtXL_n (n depending on the solvent L used). Also, At^0 was observed to co-precipitate with elemental Ag or Tl .

$\text{At}(+\text{I})$. This oxidation state can be obtained under moderately oxidizing conditions (i.e., dilute HClO_4 or $\text{H}_2\text{Cr}_2\text{O}_7$) in the At^+ form in acidic medium, or AtO^- in alkaline medium. In the cationic form, it exhibits a relatively weak electrophilic behavior similarly to I^+ . Characteristics similar to metals are also observed, with a cationic form stable toward hydrolysis in acidic medium, unlike the other halogens. Denoted $\text{At}(\theta)^+$, this cationic form of astatine exhibits the characteristics of a soft acid with an affinity for soft-base ligands (I^- , CN^- , and SCN^-) similar to Ag^+ , as demonstrated by the stability of the interhalogen complexes according to the following sequence²⁹:



Several pseudohalogen ligands such as SCN^- , N_3^- or $\text{C}(\text{CN})_3^-$, with lower stability than AtI_2^- , have also been investigated.³⁰ Better results were obtained with selenoureas and thioureas with complexes assumed to be in the $\text{At}(\text{L}_2)$ form (Fig. 5).^{31,32} Soft-donor ligands containing phosphorus have also been considered. However, their use seems unlikely for medical applications because of the reductive properties of these ligands at $\text{pH} > 2$, leading to the reduction of At^+ to At^- (Fig. 5).³³

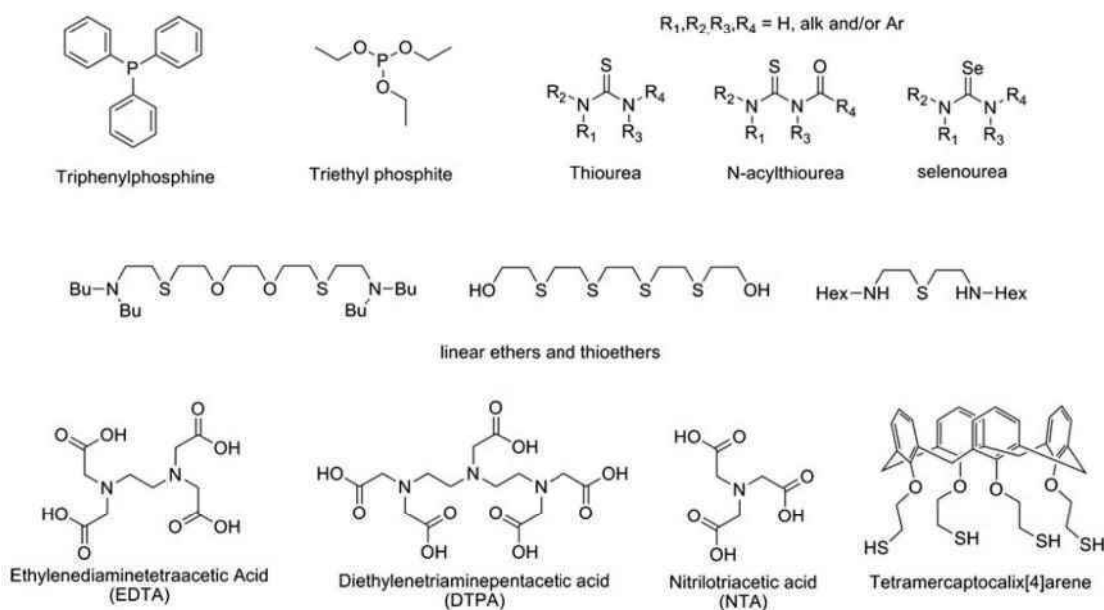


FIG. 5. Organic ligands investigated for the complexation of ^{211}At discussed in the text.

The metalloid-like behavior of astatine led Milesz et al. to study well-known chelating agents for the sequestration of metals such as EDTA,³⁴ DTPA,³⁵ or NTA³⁶ (Fig. 5). The feasibility of radiolabeling an antibody with ^{211}At complexed to DTPA has been demonstrated, but the *in vivo* stability was too low for biomedical applications.³⁷ While the proof of concept of astatine as a metal for radiolabeling an antibody has been demonstrated, polyaminocarboxylates do not appear to be appropriate for the soft-cation At^+ due to the presence of only hard-donor atoms in their structure (nitrogen and negatively charged oxygen). According to the cited studies, soft donors should be more appropriate for complexation of At^+ . This was confirmed by a comparative study of linear nitrogen-, oxygen-, and sulfur-containing ligands, with better results being obtained with the sulfur-containing compounds (Fig. 5).³⁸ However, no chelating agents stable enough for biomedical applications have been reported yet, the most recent example of the use of ^{211}At in the At^+ form being a sulfur-containing calixarene, which exhibited a weak *in vivo* stability (Fig. 5).³⁹

At(III). This oxidation state is obtained in the presence of stronger oxidizing agents such as $\text{S}_2\text{O}_8^{2-}$ or H_2O_2 . However, it is difficult to obtain in a pure form, and is often associated with At^+ in proportions dependent upon experimental conditions. It has been described as a component in anionic (AtOX_2^- and AtX_4^-), neutral [XAtO , $\text{At}(\text{OH})_3$, $\text{At}(\text{OH})\text{X}_2$, or AtX_3], and cationic forms (AtSO_4^+ and AtCrO_4^+). This form of astatine behaves similarly to At^+ , however, as a harder acid with higher affinity for harder bases such as Cl^- , NO_3^- , or SO_4^{2-} . Recent examples of the investigation of this species are limited to a comparative study of the complexation of the $\text{At}(\text{I})$ and the $\text{At}(\text{III})$ species with thiocyanate and calixarene ligands.⁴⁰

At(V). Obtained as AtO_3^- in strong oxidizing conditions (Ce^{IV} , NaBiO_3 , hot $\text{S}_2\text{O}_8^{2-}$, or IO_4^-), it is characterized by coprecipitation with AgIO_3 , $\text{Ba}(\text{IO}_3)_2$, or $\text{Pb}(\text{IO}_3)_2$. No com-

plexation chemistry has been reported yet, but a relatively hard acid behavior can be expected.

At(VII). Many studies have reported the inability to demonstrate the formation of this high oxidation state of astatine, even under the strongest oxidizing conditions. Although preparation of AtO_4^- by use of xenon fluoride in hot NaOH has been reported,⁴¹ its existence remains highly hypothetical.

In conclusion for this section, it must be kept in mind that none of the forms of astatine presented above have actually been definitely established, but rather that some of them seem to be in good agreement with the observed reactivity. Furthermore, extreme caution must be used in the experiments to obtain reproducible results. The purity of the solutions used is a primary factor influencing the results, but clearly, elapsed time also plays an important role in the behavior of astatine as demonstrated by studies by Pozzi and Zalutsky.⁴² Indeed, evolution of the oxidation state of astatine in solution has been observed over time. This evolution has been attributed to the high ionizing energy emitted by the α -particles in the medium. As a consequence, oxidizing species such as peroxides can be generated, leading to evolution of astatine to higher oxidation states. On the other hand, it was also hypothesized that solvents such as methanol could be radiolyzed into reducing species (such as hydrogen or formaldehyde) that can reduce At^+ into At^- . These phenomena can highly influence the results of the complexation chemistry of astatine as well as the organic chemistry discussed that follows below.

The organic chemistry of astatine

While the inorganic chemistry of astatine is difficult to comprehend, in part because of its dual behavior between halogen and metalloid, its organic chemistry appears to be

TABLE 2. PHENYL- AND ALKYL-HALOGEN BOND ENERGIES (KJ/MOL)

X	Phenyl-X	Alkyl-X
F	523	444
Cl	398	339
Br	335	285
I	268	222 ± 12
At	197 ± 20	163 ± 12

Data from Coenen et al.⁴⁴

closer to halogens, and reactions typically used with iodine are generally applicable to the formation of C-At bonds.⁴³ However, given the tendency of the carbon-halogen bond energy to decrease from the lighter to the heavier halogens, the bonding of At has been mostly limited to sp² carbons (preferentially aromatic carbons) rather than sp³ carbons, whose resulting bond energies are too weak to provide sufficient stability for biomedical applications (see Table 2).

The reactions employed are similar to the ones used for labeling with radioiodine. They are generally optimized to accelerated procedures required by the relatively short half-life of ²¹¹At. Synthetic approaches have been considered with nucleophilic At⁻ in halogen exchange or dediazonation processes, but also with electrophilic At⁺ in direct aromatic electrophilic substitution (EAS) or in demetallation reactions (Fig. 6). Alternatively, boron-astatine bonds in boron cages with improved stability have been the subject of several investigations recently.

In most cases, At⁻ is formed in the presence of sodium sulfite, while At⁺ is often obtained with hydrogen peroxide, peracetic acid, or *N*-chlorosuccinimide, the latter being the most commonly employed. Advantages and drawbacks of each synthetic approach are discussed in the following sections.

Halogen exchange. Because of the higher nucleofugal character of iodine over the lighter halogens, this reaction is generally performed on iodinated derivatives. Examples are described for substitution on alkyl carbons, but they are unusual because of the weakness of the C_{alkyl}-At bond and the resulting low interest in these compounds for biomedical applications. Aromatic nucleophilic substitution is generally preferred, and while iodinated compounds with which the reaction is facilitated are often the starting material, bromoaryls can be advantageously used to facilitate the chromatographic purification; thanks to the higher difference in polarity between them and the astatinated compounds.

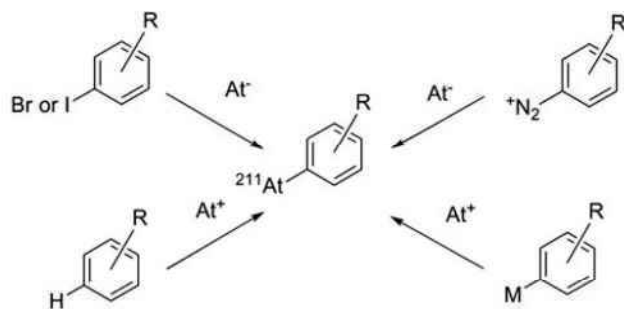
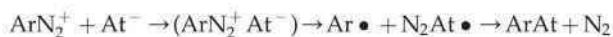


FIG. 6. Main reaction pathways used for the formation of a C-At bond.

The advantages of this approach are the rapidity of the reaction and good radiochemical yields that can be obtained. However, because of the high temperatures required, its use is restrained to substrates tolerant of relatively harsh conditions. Catalysts such as crown ethers or Cu(I) can be used to promote the reaction (see examples in Table 3). However, the effective specific activity that may be achieved through this route remains low.

Dediazonation. Diazonium salts are widely used in organic synthesis for the derivatization of aromatic rings, including halogenations. In standard organic synthesis, this reaction is performed with an excess of halogen to limit the competing reaction of water with the diazonium leading to the phenol derivative. Because of the high dilution of astatine involved, it seems unlikely to obtain a good radiochemical yield by this method. Indeed, reactions with radioiodine have been shown to work, but with low yields (max 15%). However, much better results have been obtained on identical compounds with ²¹¹At (up to 90%).⁴⁸ This difference in reactivity can be explained by looking at the dediazonation mechanisms. Indeed, two modes of cleavage of the C-N bond can occur: heterolytic cleavage leading to the formation of an aryl cation, or homolytic cleavage leading to an aryl radical (Fig. 7). As suggested by Meyer et al.,⁴⁹ the homolytic pathway seems more likely. Because of its higher polarizability, astatine has a higher propensity to form a stable complex with the diazonium than iodine. For the same reason, astatine also has a higher propensity to cede an electron to form a radical that is able to recombine with the aryl radical according to the following sequence:

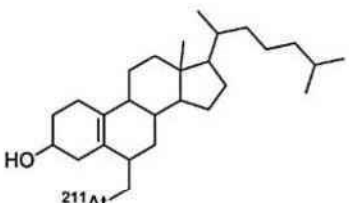
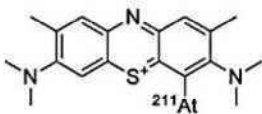
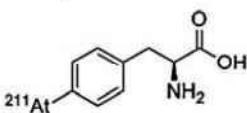


The use of this approach is marginal due to the harsh conditions required (oxidative and acidic media) for the preparation of the diazonium, thus limiting the method to less-sensitive substrates. Furthermore, a high proportion of side-products, often precipitated in the medium, makes purification and isolation of the product difficult. Examples of astatinated compounds obtained by this approach are uncommon (see Table 4).

Direct EAS. Hydrogen substitution on aromatic rings has been investigated by several research groups to understand the mechanisms of introduction of astatine on protein (which differ from iodine, see next section). Thus, it was demonstrated that the astatination of tyrosine requires conditions that are denaturing for proteins ($T=160^\circ\text{C}$ in the presence of an oxidizing agent),⁵¹ highlighting the fact that direct radiolabeling of antibodies on tyrosine residues as it is performed with radioiodine is unlikely with astatine.

Only a limited number of biomolecules were obtained using direct EAS because of the harsh conditions required for this chemistry. One of the most interesting examples of such procedure is the preparation of methylene blue astatide (which was shown to accumulate in melanoma). It was obtained in 15 minutes at 100°C in the presence of sodium persulfate as oxidizing agent, with a 68% radiolabeling yield.⁵² However, because of the high amounts of starting material required, the specific activity is very low, and purification is necessary.

TABLE 3. EXAMPLES OF ASTATINATED COMPOUNDS OBTAINED VIA A HALOGEN EXCHANGE REACTION

Compound	Reaction conditions	Yield	Ref.
 6-[²¹¹ At]-astatomethyl-19-norcholest-5(10)-en-3β-ol	Prepared from the iodinated derivative in 10 minutes at 70°C in the presence of a crown ether.	80%	45
 methylene blue astatide	Prepared from the iodinated derivative in 5 minutes at 80°C in the presence of a crown ether.	71% ± 16%	46
 4-[²¹¹ At]-astato-L-phenylalanine	Prepared from the iodinated derivative in 60 minutes at 120°C in the presence of Cu(I)	67%–80%	47

Demetallation. Electrophilic substitution of At^+ on an organometallic precursor is currently the most widely used reaction. It exhibits many advantages over direct EAS because of the high reactivity of the carbon–metal bond leading to high yields in mild conditions, thereby allowing its use on a wide variety of substrates. Furthermore, high specific activities can be obtained.

Organomercuric compounds were the first precursors to be studied that allowed the introduction of ^{211}At with high yields on various compounds.^{53,54} However, the presence of highly toxic traces of mercury in the final compound, even after purification, hampered their use for pharmaceutical purposes. Metals from group IV of the periodic table have been preferred, especially Boron, Silicon, and Tin. Organotin compounds are the most interesting because of the weakness of the carbon–metal bond, making the tin group an excellent leaving group (see Table 5). Furthermore, tin precursors are

easily introduced on a large variety of compounds by well-established synthetic approaches.

Even with toxicity, several orders of magnitude lower than mercury compounds, organotin compounds remain highly toxic molecules that must be separated efficiently from the desired astatinated compound. While high-performance liquid chromatography can be used to remove the tin precursor with a relatively high efficiency, other methods have been developed that achieve a very low level of tin in the final compounds, such as the use of a precursor grafted on a polymer support. This method simplifies the purification process and highly limits the amount of liberated tin. For example, *meta*-[²¹¹At]astatobenzylguanidine (MABG), a molecule with potential clinical applications in the treatment of neuroblastoma, was synthesized via a solid-supported tin precursor with good yields and low levels of tin in the final product ($[\text{Sn}] < 1 \text{ ppm}$) (Fig. 8).⁵⁵

Organotin precursors have become the most widely used method for the introduction of ^{211}At on biomolecules. Many examples describe the radiolabeling of proteins with *N*-succinimidyl astatobenzoate (SAB), a prosthetic group prepared from the tin precursor, as well as a variety of small molecules (see Table 6). Because of its lower toxicity, the tributyltin derivatives seem more appropriate for pharmaceutical applications than the trimethyltin, especially since no significant differences in the reactivity are detectable.⁵⁶

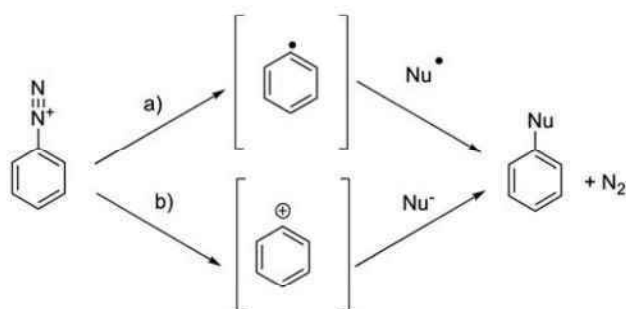
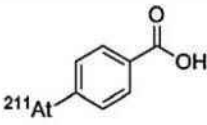
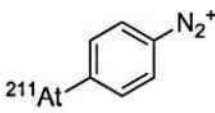


FIG. 7. Two possible dediazonium pathways: (a) homolytic cleavage and (b) heterolytic cleavage.

The B–At bond in boron clusters. Because of the higher dissociation energy of the B–I bond compared to C–I ($381 \pm 21 \text{ kJ/mol}$ and $222 \pm 12 \text{ kJ/mol}$, respectively), the use of boron clusters such as decaborate, dodecaborate and carborane has been considered recently to improve the stability of antibodies labeled with ^{211}At . Carboranes, containing both

TABLE 4. EXAMPLES OF ASTATINATED COMPOUNDS OBTAINED VIA DEDIAZONIATION

Compound	Reaction conditions	Yield	Ref.
 4-[²¹¹ At]-astatobenzoic acid	Obtained by heating at 50°C until end of nitrogen evolution	70%–85%	48
 4-[²¹¹ At]-astatobenzenediazonium	²¹¹ At reacted with the bisdiazonium in the presence of a protein for 1 hour at 20°C. The second diazonium reacts with tyrosines on the protein.	50%–55% of activity on the protein	50

boron and carbon atoms, are particularly interesting for the functionalization of biomolecules because of their orthogonal reactivity. While the CHs are weak acids (pKa ranging from 22 to 27, depending on position) that can be deprotonated to generate a nucleophile, the borons are reactants toward electrophiles, and many reactions characteristic to aromatic carbons can be considered.⁶⁰ These characteristics were used to prepare various structures radiolabeled with ²¹¹At with excellent radiolabeling efficiency (yields up to 90% in <10 minutes, see Fig. 9).⁶¹ Their advantages and drawbacks for the radiolabeling of proteins are discussed in the next section.

Astatination and stability of biomolecules of interest

Since the first studies of astatinated biomolecules, concerns about the lack of *in vivo* stability of the At–biomolecule bond have been raised.⁶² Release of free astatine *in vivo* (assumed to be in the form of At[−]) leading to irradiation of nontargeted tissues can occur dramatically depending on the nature of the molecules considered and on the radiolabeling method employed. As defined in several animal studies, astatide has a similar behavior to iodide with a high uptake in the thyroid and stomach. However, unlike iodide, significant uptake is also observed in the spleen and lungs (Fig. 10). This phenomenon could be attributed to the *in vivo* oxidation of At[−] into At⁺, as it was observed that preinjection of thiocyanide (known to form complexes with At⁺) decreased astatine uptake in these organs, and that preinjection of periodate, known to oxidize At[−] to At⁺, increased the uptake in the lung and spleen.⁶³

Several animal studies have highlighted the toxicity of free ²¹¹At[−], with damage observed to various organs, especially

the thyroid and the ovaries, and development of cancerous tumors due to the ionizing radiation, and to the disturbance of the endocrine system.^{64,65} In a long-term study by McLendon et al.,⁶⁶ the LD₁₀ of [²¹¹At]-astatide was found to be 0.56 MBq (15.1 μCi) in B6C3F₁ mice with 37.8% weight difference versus saline control and 0.28 MBq (7.7 μCi) in BALB/c (nu/nu) mice with 9.44% weight difference versus controls at the 0.37 MBq (10 μCi) dose 1 year after injection. Histological analyses revealed that damage to the bone marrow, testes, heart, spleen, and stomach increased with the injected dose.⁶⁶

To avoid toxicity issues, a highly stable radiolabeled compound must be achieved. Studies with promising astatinated compounds have been hampered because of their insufficient stability *in vivo*. Depending on the class of biomolecule considered, different levels of stability are observed. There is a tendency for the smaller molecules, which are more rapidly metabolized, to release free astatine more extensively.

Protein-based carriers. Thanks to the increasing number of successful applications of radioimmunotherapy (RIT) in the treatment of cancers over the last 30 years; antibodies and their derivatives have quickly become the vectors of choice for ²¹¹At.⁶⁷ The half-life of ²¹¹At seems reasonably long enough to fit the kinetics of antibodies or their fragments. The first astatination studies using well-known methods for radioiodination of proteins were disappointing. In 1975, Aaij et al. demonstrated that it was possible to directly astatinate by using electrophilic ²¹¹At (using chloramine-T or H₂O₂ as oxidizing agent), without denaturation of the protein.⁶⁸ The products of this direct labeling procedure were later

TABLE 5. CARBON–METAL BOND CHARACTERISTICS (HYDROGEN INCLUDED FOR COMPARISON)

Element M	Electronegativity	Covalent radius (Å)	Energy of the C–M bond (kJ/mol)	% Ionicity of the C–M bond
H	2.20	0.37	418.8	2
B	2.01	0.79	372.7	6
Si	1.74	1.18	301.5	16
Sn	1.72	1.40	226.1	16
Hg	2.00	1.50	113.1	6

Data from Coenen et al.⁴⁴

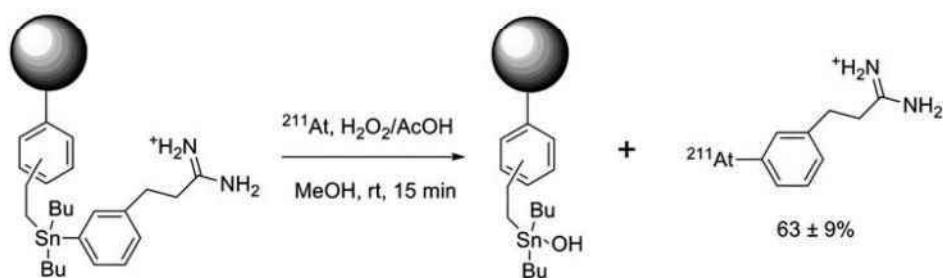


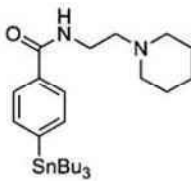
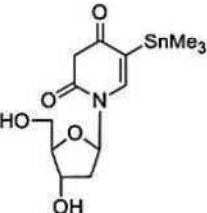
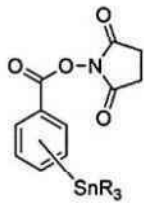
FIG. 8. Synthesis of *meta*-[²¹¹At]astatobenzylguanidine (MABG) via a supported tin precursor.⁵⁵

demonstrated to be unstable *in vivo*, as free ²¹¹At was released.⁶⁹ This instability was first attributed to the weakness of the At–C bond, with astatination assumed to occur on the same sites as for the radioiodination, that is, tyrosine and histidine residues (this kind of bonding having shown to be unstable in previous studies⁷⁰), but later, Visser et al. demonstrated in a series of reports that the conditions employed did not allow the introduction of ²¹¹At on tyrosine and histidine.^{53,71} Based on their observations, they hypothesized that astatine reacted with the cysteine residues of the proteins when using the direct radiolabeling approach.⁷² Consequently, the weak At–S bond formed is easily hydrolyzed *in vivo*, resulting in release of free astatide. These early investigations led to the conclusion that unlike iodine, astatine could not be used in direct radiolabeling procedures of proteins, and that development of prosthetic groups for indirect radiolabeling analogous to those developed for radioiodination would be necessary.

The first stably astatinated proteins were obtained via three-step procedures by production of astatobenzoic acid in a first step, followed by activation of the carboxyl moiety to a mixed anhydride. This activated astatinated compound was then conjugated to the protein in the last step. Animal studies of bovine serum albumin labeled with this method indicated a low uptake of ²¹¹At in the stomach, thyroid, spleen, and intestine compared to free ²¹¹At in mice.⁷³ This methodology was improved and simplified by Zalutsky and Narula⁷⁴ with the development of an aromatic organotin precursor bearing an activated ester as the conjugation moiety. With a precursor activated for conjugation, this time-saving and more efficient procedure became a standard for radiolabeling proteins with radiolabeling of various antibodies in ~2 hours in sufficient yields to support production of clinical trial doses (Fig. 11).

While initially performed in chloroform in the presence of *N*-chlorosuccinimide with good radiochemical yields (up to 90%),

TABLE 6. EXAMPLES OF TIN PRECURSORS USED FOR THE RADIOLABELING WITH ²¹¹At

Tin precursor	Radiolabeling conditions	Yield	Ref.
 4-tributylstannyl- <i>N</i> -piperidinoethylbenzamide	25 minutes at rt in the presence of chloramine T in EtOH/CHCl ₃ /AcOH	74%	57
 5-(trimethylstannyl)-2'-deoxyuridine	Ultrasounds 15–20 seconds in the presence of H ₂ O ₂ in CHCl ₃ /AcOH	85%–90%	58
 <i>N</i> -succinimidyl trialkylstannylbenzoate	Radiolabeling in chloroform or methanol in the presence of a variety of oxidizers. Most of the astatinated proteins were labeled via this prosthetic group.	Up to 90% depending on the conditions used	59

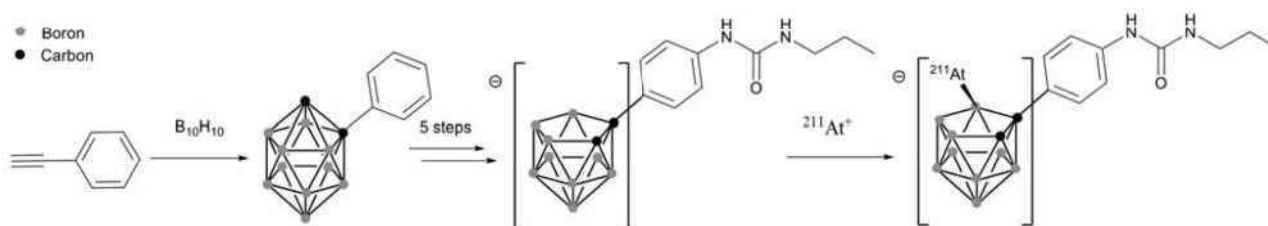


FIG. 9. Preparation of a *nido*-carborane precursor and its radiolabeling with $^{211}\text{At}^+$.⁶¹

radiolabeling the organotin precursor exhibited decreasing yields at higher activities. In a study by Pozzi and Zalutsky,⁷⁵ this phenomenon was attributed to radiolysis of the chloroform when exposed to high radiation doses of ^{211}At , leading to free-radical chlorination reaction capable of competing with astatine during the electrophilic substitution. A comparison study of different solvents determined methanol as the optimal solvent among chloroform, benzene, and methanol for the production of SAB at high levels of activity.⁷⁵

With the improved stability provided by SAB, clinical translation became feasible as demonstrated by the first clinical study with astatinated ch81C6 antitenascin antibody for the treatment of glioma published recently by Zalutsky et al.⁷⁶ Despite the notable *in vivo* stability using of SAB for most of the full antibodies studied, several reports have highlighted the lack of stability for more rapidly metabolized proteins. This phenomenon is observed with rapidly internalized antibodies that are exposed to accelerated metabolism due to additional catabolic processes occurring in the

cells, such as the lysosomal proteolysis. To resolve this issue, positively charged prosthetic groups such as pyridine carboxylate or guanidinomethylbenzoate derivatives were developed with the purpose of retaining the positively charged astatinated catabolites inside the tumor cell.^{77,78} The conjugation of *N*-succinimidyl 3- ^{211}At -4-astato-guanidinomethyl benzoate to monoclonal antibody L8A4 known to be internalized in cells expressing the anti-epidermal growth factor (EGF) receptor variant III interestingly resulted with uptake in the spleen, lungs, and thyroid similar to the radioiodinated counterpart.

The main concerns have been for antibody fragments such as Fab or F(ab')_2 , which are extensively deastatinated *in vivo* when radiolabeled with SAB, as demonstrated by the significant uptake of activity in the thyroid, stomach, spleen, and lung compared to their radioiodinated counterparts (Fig. 12).^{79,80} Several approaches, mostly based on structural modifications of the SAB, have been considered to improve the stability. They have consisted either of increasing the electronic density of the aromatic ring of the prosthetic group to strengthen the C-At bond (e.g., addition of electron donor groups and suppression of electron withdrawing group^{56,81,82}), or by the addition of hindering groups such as a methyl in the vicinity of the ^{211}At atom, which was proposed to sterically hinder dehalogenation mechanisms⁸³ (see examples in Fig. 13). However, limited successes were obtained, except in the case of methyl-SAPS, which appears to improve the *in vivo* characteristics of the antibodies investigated. However, none of these compounds seems to be a real final solution to the stability issue with antibody fragments.

Alternatives to astataryl derivatives, boron cages, were proposed more recently by Wilbur et al.⁶¹ with promising results (see structure in Fig. 9—previous section). In a series of reports, it was first demonstrated with small molecules that *nido*-carboranyles are much more stable than aryls toward deastatination.⁶¹ These interesting results led the authors to investigate the radiolabeling of a Fab' antibody fragment with selected *nido*-carboranes and *closo*-decaborate derivatives and to compare them to the classic radiolabeling results obtained from using SAB.⁸⁴ It was demonstrated that the first advantage of the boron derivatives over the SAB was the possibility of direct astatination of the antibody fragment. With a modification of the Fab' by conjugation to the boron clusters before radiolabeling, it was possible to reach astatination yields up to 75% in only one step, in 10 minutes. Then, biodistribution studies in mice indicated the superiority of the radiolabeling via the boron cages with a significantly lower uptake of ^{211}At in the thyroid, stomach, spleen, and lungs. The best results were obtained with the *closo*-decaborate derivatives, but significant uptake in the liver and

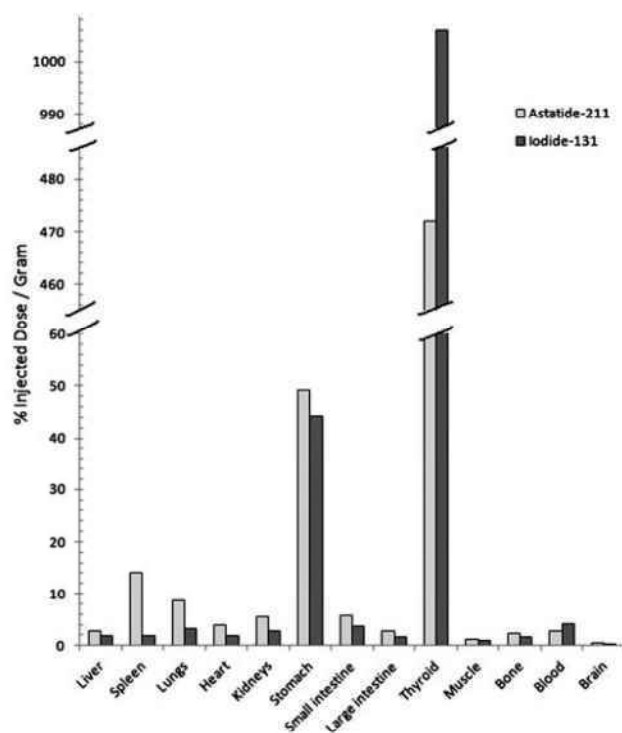


FIG. 10. Uptake of ^{211}At and ^{131}I in normal mice 1 hour post-injection of ^{211}At astatide and ^{131}I iodide. Chart plotted with data from Larsen et al.⁶³

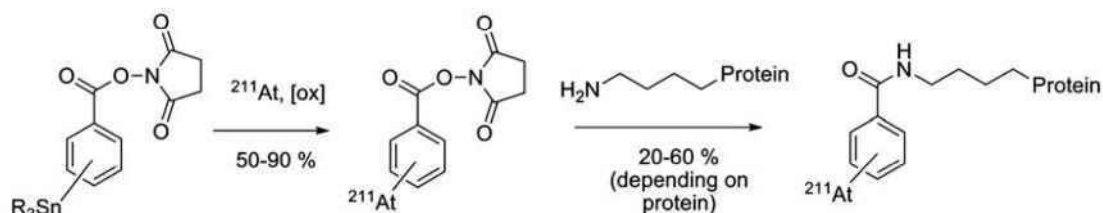


FIG. 11. Standard indirect labeling procedure for the astatination of proteins via the preparation of succinimidyl astatobenzoate (SAB).

kidneys were observed, suggesting that modifications to the boron cage or to the linkers are necessary. Studies by this research group are ongoing to solve this issue, such as the investigation of cleavable linkers to increase the clearance rate from these organs.^{85,86}

Peptide/biotin carriers. Because of the relatively short half-life of ²¹¹At, smaller biomolecules have been considered as

better carriers for targets that are not quickly accessible to full antibodies. This includes peptides that exhibit fast kinetics, or biotin derivatives for pretargeting strategies. Octreotide has been a peptide of interest investigated by Vaidyanathan et al.⁸⁷ for targeting somatostatin receptors. In an initial article, they demonstrated that it was possible to radiolabel octreotide via a two-step procedure by conjugation to SAB. Further studies were performed with an octreotide premodified with

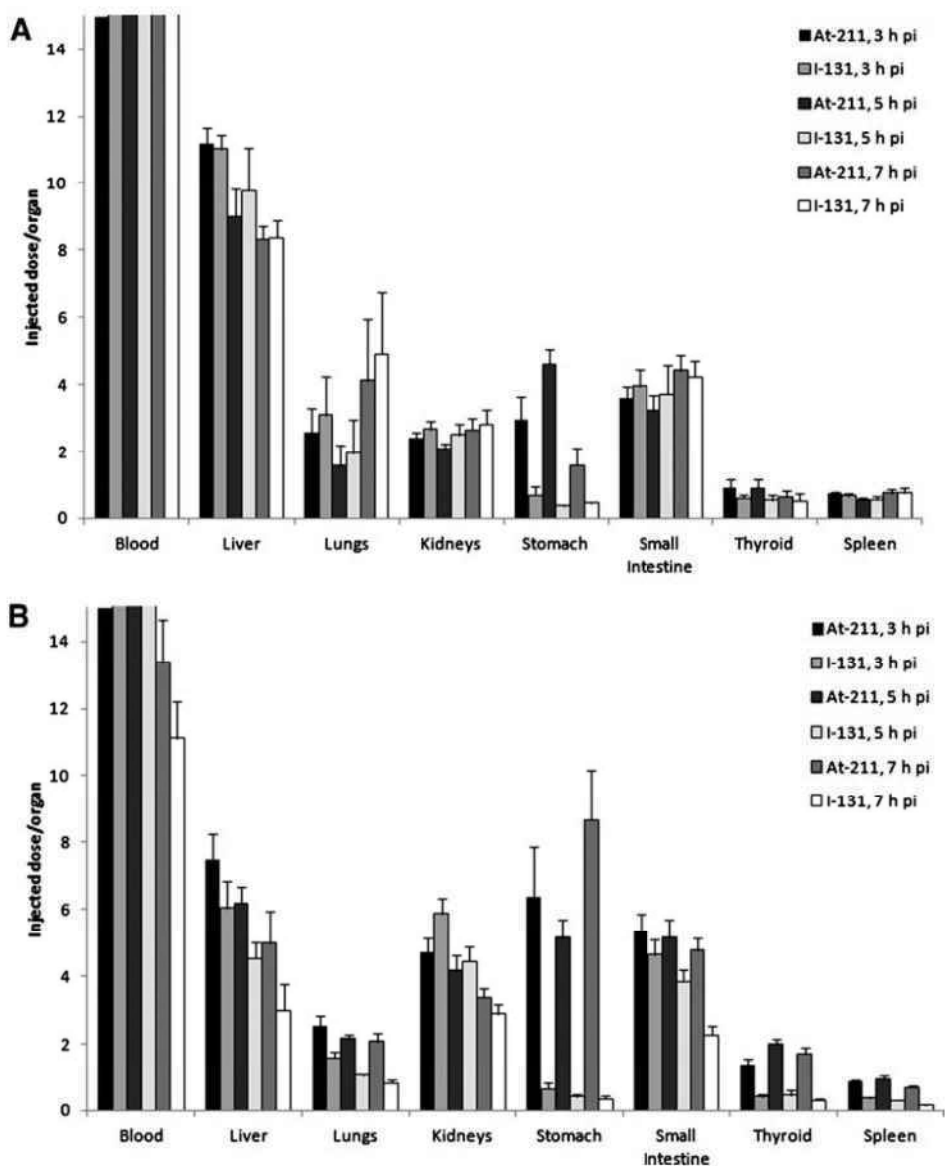
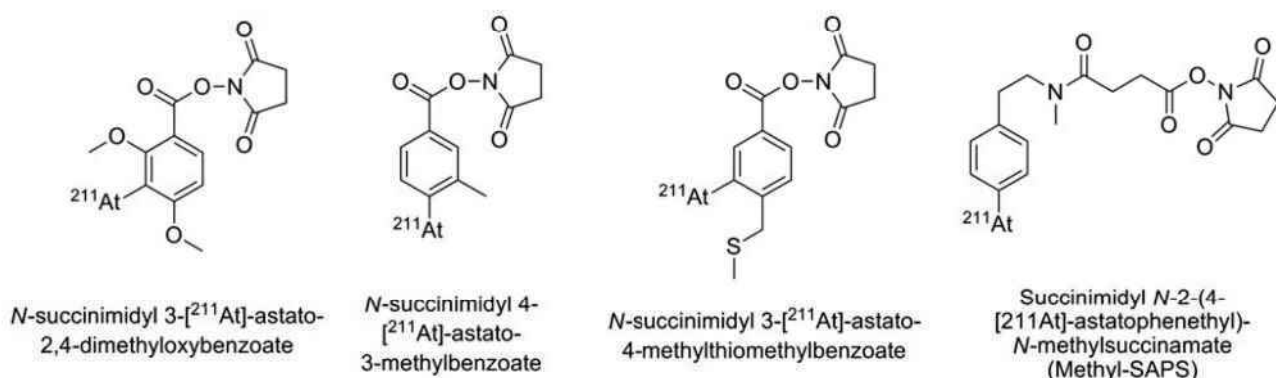
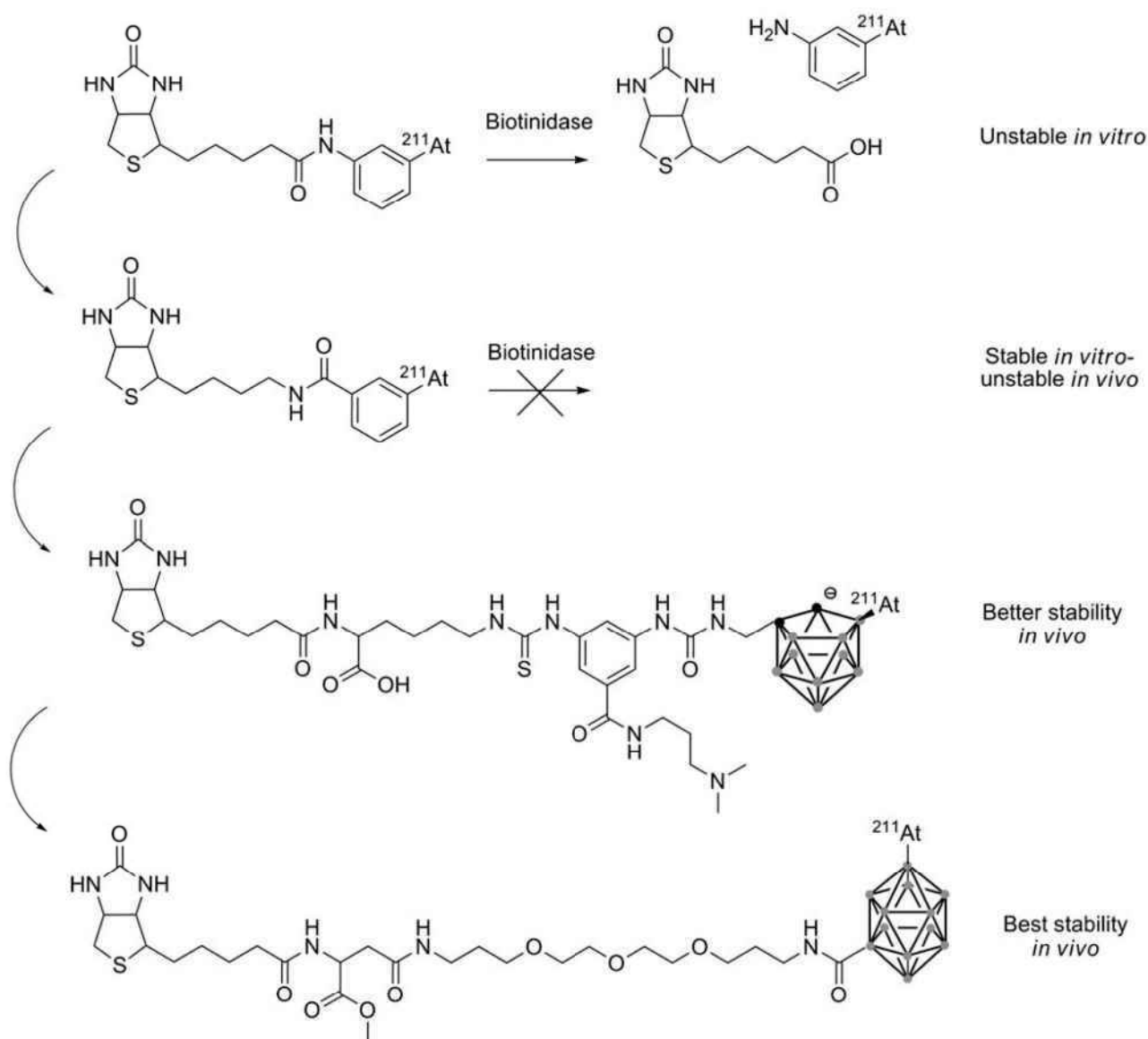


FIG. 12. Comparative biodistribution of ²¹¹At-astatinated and [¹³¹I]-iodinated full antibody C110 IgG (A) with its F(ab')₂ fragment (B) in mice. Charts plotted from data by Garg et al.⁸⁰


 FIG. 13. Modified prosthetic groups based on the SAB structure.^{56,81-83}

 FIG. 14. Successive improvements to the biotin to increase the astatination stability.⁹¹⁻⁹⁴

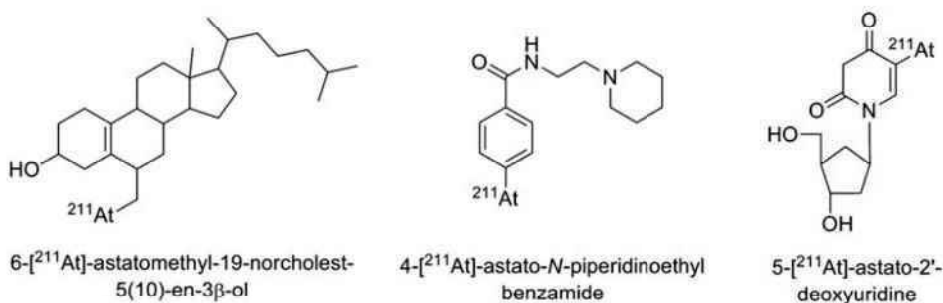


FIG. 15. Examples of small astatinated molecules unstable *in vivo*.^{45,57,58}

guadininomethyl trimethylstannylbenzoate for direct radiohalogenation of the peptide. Assays indicated an excellent binding to the somatostatin receptor *in vitro*. No biodistribution study was performed with the astatinated octreotide, but the results obtained with the radioiodinated counterpart, although good in tumor-binding properties, unfortunately demonstrated an elevated uptake of the peptide in the liver and in the kidneys. These results precluded the use of this compound for i.v. administration, although its use in locoregional administration for targeting of medulloblastoma was suggested.⁸⁸ Later improvements were attempted by glycosylation of the octreotide that met with limited success on improving binding properties and pharmacokinetics.⁸⁹ Nevertheless, while astatination of the octreotide derivatives cited above was demonstrated, no data on the *in vivo* stability are available, and instability of the SAB-like compound would be expected for this kind of rapidly internalized compound.

Several reports relate the use of astatinated biotin for pretargeting (for general details on pretargeting, see Lesch et al.⁹⁰). Initial studies by Foulon et al.⁹¹ described direct astatination of biotin preconjugated to a trialkylstannylamine moiety. However, the resulting astatinated compound was unstable when incubated in murine serum.⁹¹ The same instability was observed with the radioiodinated counterpart, and analysis of the catabolites led the authors to conclude that cleavage of the amide bond occurred *in vitro* due to a biotinidase enzyme. This issue was resolved by reversing the position of the nitrogen and the carbonyl of the amide bond to avoid the action of the biotinidase (see Fig. 14), and provided high stability of the astatinated compound in murine serum.⁹² Unfortunately, biodistribution studies indicated release of the astatine with significant uptake in the lungs, stomach, and thyroid. Thereafter, modifications using the promising boron cages developed by Wilbur et al.⁹³ provided a higher *in vivo* stability with a *nido*-carborane compared to the aryl compounds. While biodistribution studies indicated that deastatination was still occurring (but at a lower level than with aryl derivatives), latest results

suggest that *closo*-decaborate(2-) is the most promising group for a strong stabilization of the astatination of biotin derivatives (see Fig. 14).⁹⁴

Alternatively, Lindegren's group investigated biotinylated polylysines conjugated to SAB in a pretargeting strategy. In the first study, the poly-L-lysines had molecular weights of 13, 38, and 363 kDa with excellent avidin binding *in vitro*. As expected, biodistribution studies indicated that the smaller compound was rapidly excreted through the kidneys while the larger compounds had an increased liver excretion pathway. Uptake in the thyroid, stomach, lungs, and spleen indicated that release of astatine also increased with the size of the polymer.⁹⁵ In a second study, both L- and D-isomers of the polylysine were compared for their biodistribution properties. Interestingly, the poly-D-lysine, probably more resistant to metabolism, exhibited a significantly lower release of astatine as indicated by a decreased uptake in the lungs, spleen, stomach, and thyroid. However, because of an elevated uptake in kidneys for this isomer, the poly-L-lysine was preferred.⁹⁶ Recently, this astatinated biotinylated poly-L-lysine was investigated for use with mAb MX35 conjugated to avidin and administered intraperitoneally to tumor-free mice. High uptake of astatine was observed in the lungs, spleen, stomach, and throat, which could be reduced in a second experiment by preadministration of sodium perchlorate as a blocking agent.⁹⁷ However, while more studies are necessary to assess the efficiency of this poly-L-lysine derivative for the treatment of tumors, it remains equally clear that improvement of the astatine stability is required.

Other small molecules. Several other small astatinated molecules have been investigated for their propensity to be incorporated quickly to some tumor cells. However, because of their small size, many of these compounds have a natural tendency to be rapidly metabolized, resulting in marked deastatination being observed *in vivo*. This is the case of the majority of such investigated compounds, for example, 6-[²¹¹At]-astatomethyl-19-norcholest-5(10)-en-3β-ol, which targets the adrenal gland,⁴⁵ 4-[²¹¹At]-astato-N-piperidinoethyl benzamide considered for the treatment of melanoma and glioma,⁵⁷ or 5-[²¹¹At]-astato-2'-deoxyuridine for DNA-targeting strategy⁵⁸ (structures in Fig. 15).

Other examples, however, show that small molecules can be very stable with minimal release of ²¹¹At. This is the case of two ²¹¹At-arylbisphosphonates studied for applications in bone metastasis pain palliation⁹⁸ and 1-(3-[²¹¹At]-astatobenzyl)guanidine ([²¹¹At]MABG) with potential applications in the treatment of glioma⁹⁹ (see structures in Fig. 16). These compounds could be interesting to consider as

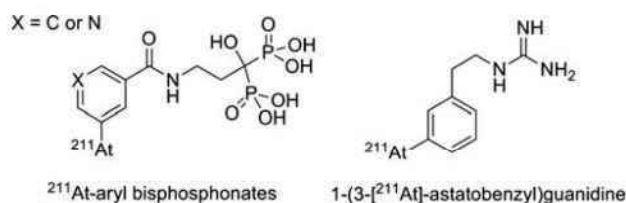


FIG. 16. Small molecules stable *in vivo*.^{98,99}

prosthetic groups for radiolabeling substrates that have demonstrated instabilities cited above, although it is not clear if the stability comes from the molecular structures themselves or from biodistribution pathways circumventing deastatination mechanisms.

Nanoparticles and microspheres. Although devoid of active targeting properties, nanoparticles and larger particles have been investigated with potential applications for locoregional administration. Larsen et al.¹⁰⁰ prepared ²¹¹At-microspheres by conjugation of aminated polymer particles to SAB. The resulting particles with a size of 1.8 μm were stable in various media *in vitro*.¹⁰⁰ They were compared to free ²¹¹At⁻ and astatinated antibodies by i.p. administration to mice inoculated with the K13 hybridoma cell line.¹⁰¹ Biodistribution studies indicated that free ²¹¹At⁻ spread rapidly in the whole body, whereas the microsphere and the antibodies were mostly retained in the peritoneal cavity, highlighting a good stability. However, the authors concluded that the efficiency of the astatinated antibodies was superior to the microspheres due to a better diffusion in the peritoneal area.

Another approach developed by Kucka et al.¹⁰² is the preparation of astatinated silver nanoparticles coated with poly(ethylene oxide) (PEO). The authors suggested that the high affinity of silver for astatine could result in a stable radiolabeling. They incubated ²¹¹At with nanoparticles made of a silver proteinate core coated with PEO (size of 2000 and 5000 g/mol) in the presence of a reducing agent (NaBH₄). Quantitative yields were obtained, and *in vitro* measurements indicated a good stability, even in the presence of high concentration of chloride ions as a competitive agent. However, no data on *in vivo* behavior are available.

More recently, use of carbon nanotubes was proposed by Hartman et al.¹⁰³ The free carbon nanotubes, with a length in the 20–50 nm range, were incubated with [²¹¹At]-astatide. The astatine trapped inside the nanotubes was then oxidized into the AtCl form in the presence of chloramine-T or *N*-chlorosuccinimide. The stability of the labeling was assessed by successive washing with water or with human serum. Even though moderate, a loss of activity was observed in both cases. This phenomenon was attributed to either a release of the AtCl portion close to the ends of the nanotubes, or by leakage through damage in the walls of the nanotubes caused by the high-energy α -particles from ²¹¹At decay.

Alpha-Therapy of Cancers with ²¹¹At-Labeled Targeting Agents

In vitro studies

A number of *in vitro* studies on astatinated bioconjugates have focused on the determination of the cytotoxicity and microdosimetric data with various carriers (mostly antibodies) and cell lines. Cell conditions have varied from suspended isolated cells to monolayers to spheroid cell clusters, thereby modeling different possible configurations occurring *in vivo*, but then also making difficult any actual direct comparison between the studies. While it is not intended to make an exhaustive description of all *in vitro* studies, a selection of reports covering different aspects of ²¹¹At effects on *in vitro* cells is described below.

Larsen et al. investigated the cytotoxicity of astatinated mAb 81C6 (targeting tenascin in the extracellular matrix of the

cell), mAb Me1-14 (targeting proteoglycan chondroitin sulfate on the cell membrane), and TPS3.2 (nonspecific) on microcolonies of D-247 MG glioma cells and SK-MEL-28 melanoma cells.¹⁰⁴ After 1-hour incubation with 18 kBq/mL activity concentration, results indicated two-to-five times more activity bound to the cells of the specific antibodies compared to the nonspecific mAb. A survival fraction of 0.37 (D_0) was obtained with one to two α -decays hitting the cell nucleus with only little differences between both specific mAbs and both cell lines. In another study, the cytotoxicity of ²¹¹At-trastuzumab was investigated against three breast carcinoma cell lines expressing the HER2 receptor (SKBr-3, BT-474, and MCF7/HER2-18).¹⁰⁵ Cell survival studies indicated a relative biological effectiveness (RBE) of ²¹¹At-trastuzumab 10-fold higher than external irradiation. At the low amount of antibody used, the toxicity was attributed exclusively to the α -decay of ²¹¹At, with no contribution from trastuzumab. To estimate absorbed dose and toxicity *in vivo* on nonspecific tissues, the anti-CD20 mAb, rituximab, labeled with ²¹¹At was investigated on cultured RAEL lymphoma cells and bone marrow cells.¹⁰⁶ The absorbed dose when using a 10 kBq/mL activity concentration was 0.645 and 0.021 Gy for lymphoma cells and bone marrow cells, respectively, after 1-hour exposure. However, a higher radiosensitivity to α -particles was observed for bone marrow ($D_0=0.34$ Gy) compared to lymphoma cells ($D_0=0.55$ Gy), whereas reversed sensitivity was observed from exposure to ⁶⁰Co γ -irradiation ($D_0=1.21$ and 0.72 Gy for bone marrow and lymphoma, respectively). Despite these observations, the high specificity of RAEL cell binding of ²¹¹At-rituximab over bone marrow cells made these results interesting in the perspective of the treatment of non-Hodgkin's lymphoma. Recently, Petrich et al. investigated ²¹¹At-anti-CD33 antibodies to overcome the cellular resistance observed in a number of patients to gemtuzumab ozogamicin (GO), the recently withdrawn toxin-mAb conjugate Mylotarg, used in the treatment of acute myeloid lymphoma.¹⁰⁷ The better results observed for ²¹¹At-anti-CD33 over GO were promising in the perspective of treatment of GO-resistant cases of acute myeloid lymphoma.

Within the realm of preclinical studies, cetuximab was investigated in combination with astatinated cMab U36 on cultured squamous cell carcinomas. The results indicated a higher growth inhibition for the combination therapy compared to RIT alone or cetuximab alone. However, a radioprotective effect was observed in the presence of cetuximab, as well as a decrease of the internalization of cMab U36.¹⁰⁸ Although these phenomena have not been explained yet, the results suggest that RIT after treatment with cetuximab would be more efficient than combination of both treatments at the same time to avoid this radioprotective effect.

Alternatively, a limited number of nonantibody carriers have also been studied *in vitro*, including ²¹¹At-EGF, a small protein (MW \approx 6 kDa) targeting the EGF receptor, which is overexpressed in a number of cancerous tumors. Internalization of ²¹¹At-EGF in A-431 carcinoma cells was compared to the [¹²⁵I]iodinated counterpart. Interestingly, a longer retention for the astatinated compound was observed, resulting in an increased biological half-life from 1.5 hours for ¹²⁵I-EGF to 3.5 hours for ²¹¹At-EGF.¹⁰⁹ These results suggested that ²¹¹At conjugated to EGF would be a radionuclide of choice due to its favorable biological and physical characteristics. In another study, 5-[²¹¹At]-astato-2'-deoxyuridine (²¹¹AtdU) was

investigated for its DNA incorporation properties in Chinese hamster V79 lung fibroblasts. It was shown that <1% of free $^{211}\text{At}^-$ was incorporated compared to $^{211}\text{AtdU}$. The survival study indicated a D_0 of 1.3 decays/cell, and that unlabeled cells were killed by neighboring labeled cells. Furthermore, DNA double-strand break (DSB) levels were 10-fold higher with $^{211}\text{AtdU}$ compared to the [^{125}I]iodinated counterpart.⁵⁸

A limited number of studies have specifically focused on the radiobiology of ^{211}At and the biological consequences of the α -decay to the cell material. The most recent reports were published by Claesson et al.,¹¹⁰ who investigated the RBE for induction of DSB for ^{211}At on human fibroblasts compared to ^{60}Co γ -irradiation and X-rays. In a first article, it was observed that two to three times more DSB occurred with ^{211}At compared to ^{60}Co γ -rays and X-rays. Furthermore, the study of the size of the DNA fragments induced by ^{211}At revealed a nonrandom distribution compared to γ -rays and X-rays, which resulted in a random distribution.¹¹⁰ In a second study, the RBE of DSB for ^{211}At and X-rays was investigated at different cell cycle phases (V79-379A fibroblasts synchronized with mimosine in G1, early, mid-, and late S phase). As expected, ^{211}At exhibited a higher efficiency in generating DSB, with DSB varying in the cell cycle phases according to the following sequence: G1 < S early < S late < S mid < mitosis. It was however observed that X-rays were more efficient in inducing clustered damage than ^{211}At .¹¹¹

Preclinical therapy studies

A number of preclinical therapy animal studies have been performed to assess the targeting properties of the astatinated biomolecules and their efficacy and toxicity, sometimes in comparison with other radionuclides of interest. Therapy studies were conducted mostly with antibodies or their fragments as delivery vectors as described below. Interestingly, models involving locoregional administration of the radiopharmaceutical have been more frequently investigated over systemic injection. Indeed, the biological and physical half-lives of the astatinated proteins seem particularly appropriate to localized compartmental tumors such as in i.p. implanted ovarian tumor models. Furthermore, concerns on the deastatination of the proteins as a result of accelerated metabolism when administered intravenously may have been a limiting factor with some carriers.

Nonetheless, the feasibility of therapy using i.v. injected astatinated antibodies has been demonstrated in several studies, and promising results have been obtained for the treatment of disseminated cancers. The astatinated anti-CD25 antibody 7G7/B6 was evaluated in a murine model of leukemia. Therapy with i.v. injection of 0.55 MBq (15 μCi) ^{211}At -7G7/B6 in karpas299 leukemia-bearing mice resulted in 70% survival at 46 days and 33% survival after 5 months, whereas untreated mice and mice treated with nonspecific antibody (^{211}At -11F11) all died after 46 days.¹¹² These promising results led the authors to investigate ^{211}At -7G7/B6 in combination with mAb daclizumab for therapy in mice inoculated with MET-1 human T-cell leukemia. Excellent results were obtained with improved survival for combination therapy (91% survival at 94 days) compared to RIT with 0.44 MBq (12 μCi) ^{211}At -7G7/B6 (32% survival at 94 days) or daclizumab treatment alone (47% at 94 days) while all mice died after 70 days when treated with nonspecific ^{211}At -

11F11.¹¹³ The same authors also investigated the anti-CD30 antibody ^{211}At -HeFi-1 in a model of karpas299 leukemia-bearing mice. Again, the combination of RIT with cold HeFi-1 significantly prolonged the survival of the animals (33% and 84% survival at 120 days for RIT alone and combination therapy, respectively).¹¹⁴ In another study, Cheng et al.¹¹⁵ evaluated the astatinated mAb U36 for the treatment of head and neck squamous cell carcinoma (HNSCC). Intravenous injection of 200 kBq radiolabeled antibody in mice inoculated with HNSCC resulted in the reduction or the stabilization of the tumor volume, while control group (treated with non-labeled U36) had its tumor volume steadily increasing after treatment.¹¹⁵ Alternatively to full antibodies, Robinson et al.¹¹⁶ investigated the smaller C6.5 diabody (targeting HER2 receptors) that exhibits faster targeting properties compared to antibodies. Mice bearing HER2/neu-positive MDA-MB-361/DYT2 tumors were treated by i.v. injection of 0.74 MBq (20 μCi) to 1.67 MBq (45 μCi) ^{211}At -C6.5. Compared to the control group, the tumor volume doubling time was delayed by 30 days for the 20 μCi group and by 57 days with 60% of the mice being tumor free after 1 year for the 45 μCi group.¹¹⁶ Unfortunately, no biodistribution data were reported for the ^{211}At -C6.5 diabody. The *in vivo* stability of the ^{211}At -diabody bond of this engineered antibody fragment, which can be expected to be rapidly metabolized, would be interesting to study.

In the case of locoregional injections, the most documented astatinated compound is probably MX35 in its $\text{F}(\text{ab}')_2$ form. MX35 targets an antigen (Le^y) expressed in 90% of human epithelial ovarian cancers. It has been extensively studied for α -RIT in a murine model of ovarian NIH:OVCAR-3 cancer cells inoculated intraperitoneally at the Sahlgrenska academy at Göteborg University. Early investigations on ^{211}At -MX35 $\text{F}(\text{ab}')_2$ allowed for the determination of the minimum required dose by i.p. administration of doses ranging from 25 to 200 kBq 4 weeks after inoculation of NIH:OVCAR-3 cells in mice. With an increase from 22% to 50% of animals presenting no sign of tumor with doses of 50 and 100 kBq, respectively, it was concluded that 100 kBq of ^{211}At -MX35 $\text{F}(\text{ab}')_2$ was the minimal required dose to give clear evidence of the therapeutic efficacy of this treatment.¹¹⁷ The authors also investigated the efficacy of the treatment against different tumor sizes. In this study, groups of mice were treated with 400 kBq ^{211}At -MX35 $\text{F}(\text{ab}')_2$ at different times (1, 3, 4, 5, or 7 weeks) after inoculation of the NIH:OVCAR-3 cells. Eight weeks after treatment, the mice were sacrificed, and the proportions of tumor-free mice were found to be 95%, 68%, 58%, 47%, and 26% for 1–7 weeks post-treatment, respectively, thus confirming the suitability of α -radiation for the treatment of smaller tumors.¹¹⁸ Fractionated administration of the treatment was also compared to single injection. Four weeks after inoculation of the NIH:OVCAR-3 cells, groups of mice received a total of 800, 400, or 50 kBq ^{211}At -MX35 $\text{F}(\text{ab}')_2$ in a single injection or in three equal injections separated by 4 days. However, no advantages were found in fractionated treatment with the best results being obtained for the 800 kBq single-injection group (56% tumor-free animals 8 weeks post-treatment compared to 41% for the corresponding fractionated-injection group).¹¹⁹ However, a subsequent investigation showed that weekly repeated injections of a 400 kBq dose of ^{211}At -MX35 $\text{F}(\text{ab}')_2$ (from one to six injections) led to a significantly

higher therapeutic efficacy after three or more injection with 17% free tumor animals after one injection, 39% after three injection, and up to 67% after six injections. Furthermore, no ascites were detected in the group receiving five or six injections, while 15 out of 18 animals exhibited ascites when receiving one injection.¹²⁰ Recently, the ²¹¹At-MX35 F(ab')₂ efficacy was compared to its ²¹³Bi counterpart. Groups of mice were treated with either 2.7 MBq of ²¹³Bi-MX35 F(ab')₂ or 440 kBq of ²¹¹At-MX35 F(ab')₂ 2 or 4 weeks after inoculation of NIH:OVCAR-3 cells. No significant superiority of either radionuclide was observed.¹²¹ Finally, with the promising results obtained for ²¹¹At-MX35 F(ab')₂ in pre-clinical studies and the absence of significant toxicity of these treatments at the doses employed, one of the first clinical trial with a ²¹¹At radiopharmaceutical was recently initiated with this antibody (see next section).

Another antibody that deserves attention is ch81C6, as it was used in the first phase I ²¹¹At-mAb clinical trial (see next section). It was initially used in the murine form for the treatment of neoplastic meningitis in preclinical studies. In a rat model, animals were inoculated with TE-671 human rhabdomyosarcoma cells by intrathecal injection into the subarachnoid space. In a series of experiments, dose escalation was first performed by intrathecal administration of 0.15–0.48 MBq (4–13 μ Ci) of ²¹¹At-81C6 mAb to determine the dose inducing a therapeutic effect. Increases in median survival of 30%, 29%, and 51% were observed with 4, 7, and 13 μ Ci, respectively, compared to control (saline) with 20% of the animals still alive after 190 days in the 13 μ Ci group. In a second experiment, animals were treated with 0.44 MBq (12 μ Ci) or 0.67 MBq (18 μ Ci) of ²¹¹At-81C6 and compared with nonspecific ²¹¹At-45.6 mAb and saline. No significant increase in the median survival was observed for the non-specific mAb compared to saline while 113% and 357% survival prolongation was observed for the 12 μ Ci and the 18 μ Ci ²¹¹At-81C6 groups, respectively.¹²² To reduce the potential immunogenicity of the treatment from the perspective of the clinical use of the 81C6 mAb, the human/mouse chimeric version of the antibody (ch81C6) was assessed. Biodistribution, dosimetry, and toxicity studies were performed and confirmed the superior characteristics of the ch81C6 mAb over its murine form.¹²³

Trastuzumab, an anti-HER2, labeled with ²¹¹At is another antibody that has shown promising results in recent studies. In a radioresistant SKOV-3 ovarian tumor model implanted in mice intraperitoneally, ²¹¹At-trastuzumab was investigated in a series of experiments. First, a dose-escalation study from 0 to 800 kBq of the radiolabeled antibody injected i.p. was performed. A dose-dependent reduction of the tumor size was observed from 0 to 400 kBq without better results at 800 kBq compared to the 400 kBq dose. In a second experiment, the mice were treated with 400 kBq ²¹¹At-trastuzumab in combination with increasing doses of cold trastuzumab (5–500 μ g). Increased efficacy was observed while increasing the dose of cold trastuzumab with the best result obtained at 500 μ g cold trastuzumab with a total eradication of the tumors. Finally, fractionated administration at various doses of ²¹¹At-trastuzumab combined with various doses of cold trastuzumab did not exhibit any advantages.¹²⁴ In another study, ²¹¹At-trastuzumab was also investigated for the treatment of breast carcinomatous meningitis by intrathecal injection

with significantly improved survival compared to the control groups (saline or nonspecific astatinated mAb).¹²⁵

Clinical studies

To date, only two phase-I clinical trials have been reported. The first one was published in 2008 by the Zalutsky group at the Duke University. Astatinated ch81C6 was used for the treatment of residual disease after surgical removal of the glioma tumor in the brain. The classical treatment for this pathology is surgery followed by external radiotherapy and chemotherapy. In this study, 18 patients with glioblastoma multiforme or anaplastic oligodendroglioma were enrolled and received an injection of ²¹¹At-ch81C6 (71–347 MBq) in the cavity resulting from the surgery. The biodistribution was monitored directly by a γ -camera and demonstrated that 96.7% \pm 3.6% of the ²¹¹At decays occurred within the cavity. Blood counts indicated minimal leakage from the cavity with <0.05% of injected dose measured. These data highlighted the low catabolism of the antibody when injected into the cavity. Final results were promising with a median survival time that increased from 31 weeks with the classical treatment of GMB to 54 weeks with additional ²¹¹At-RIT without dose-limiting toxicity being observed.⁷⁶

The second clinical trial was reported in 2009 for the treatment of ovarian cancer with ²¹¹At-MX35 F(ab')₂. The classical treatment for ovarian carcinoma is surgery in combination with chemotherapy, but in many cases, relapse occurs with a low chance of survival. The purpose of this study was to demonstrate the potential of α -RIT after a clinical trial has failed as a phase-III study with a β^- -emitter (HMFG1 mAb radiolabeled with ⁹⁰Y). The disappointing results obtained with ⁹⁰Y-HMFG1 were attributed to the nature of the radionuclide and its associated β^- -particles being unsuitable for the treatment of microscopic tumors. Nine female patients in total remission after chemotherapy were enrolled in the study. After laparoscopy to check the absence of macroscopic tumor, the patients received 20–100 MBq ²¹¹At-MX35 via a catheter. The biodistribution was monitored with a γ -camera and indicated that most of the radioactivity was retained in the abdomen. A noticeable uptake in the thyroid was observed for the patients who did not receive a blocking agent before the treatment. No significant uptake was observed in the other organs. Analyses of the dosimetric data indicated that this treatment allowed for the deposition of the necessary dose for the destruction of micrometastases without noticeable toxicity to the bone marrow and to the other healthy organs.¹²⁶ No conclusions on the therapeutic efficacy of this treatment are available as yet, but further investigations and reports can be expected in the near future.

Conclusions

Shortly after the discovery of ²¹¹At in 1940, the therapeutic potential of this radionuclide was investigated, with applications considered for the treatment of thyroid disorders.¹²⁷ However, because of the high toxicity of α -radiation to healthy tissue, it appeared obvious that ²¹¹At could not be used alone, and needed to be conjugated to an appropriate targeting carrier, especially for potential applications in the treatment of cancers.

With the exploration of the chemical properties of astatine, methodologies for the radiolabeling of various molecules of interest have been proposed. However, it is still difficult today to work with this radionuclide because of the unpredictable aspects of its reactivity and its halogen/metalloid duality. Fortunately, simple, fast, and reproducible radiolabeling methods applicable to a number of molecules of interest have been developed. Particularly, antibodies and their engineered fragments promising for RIT of cancers can now be astatinated efficiently using as-tatobenzoyl-based prosthetic groups. The high potential of ^{211}At for the treatment of residual disease has been recently highlighted by the first clinical trials realized with a chimeric antibody (ch81C6) and a F(ab')_2 fragment (MX35) using such radiolabeling methods. Promising results were obtained with a real therapeutic gain and/or limited toxicity observed.

However, many compounds of interest labeled with ^{211}At have been eliminated from the process of development of new radiopharmaceuticals because of the lack of stability on radiolabeling with astatine. From the review of the recent literature, it is clear that an effort in the understanding of the chemistry of astatine for the development of new radiolabeling approaches is required to provide new astatinated radiopharmaceuticals. Recent reports show that several research groups are working on alternative chemistries to reach that goal.^{40,128,129} Furthermore, implementation of new high-energy cyclotrons capable of producing ^{211}At should improve the availability of this radionuclide in the near future and accelerate the development of new astatinated radiopharmaceuticals.^{11,130}

Acknowledgment

This work was supported by the Intramural Research Program of the NIH, National Cancer Institute, Center for Cancer Research.

Disclosure Statement

No competing financial interests exist.

References

- Kim Y-S, Brechbiel MW. An overview of targeted alpha therapy. *Tumor Biol* 2012;33:573.
- Yong K, Brechbiel MW. Towards translation of ^{212}Pb as a clinical therapeutic; getting the lead in! *Dalton Trans* 2011;40:6068.
- Corson DR, MacKenzie KR, Segrè E. Possible production of radioactive isotopes of element 85. *Phys Rev* 1940; 57:1087.
- Hyde EK. The present status of elements 85 and 87. *J Phys Chem* 1954;58:21.
- Gmelin L, Berei K, Kugler HK, et al. *Gmelin Handbook of Inorganic Chemistry: At, Astatine*. Berlin, New York: Springer-Verlag, 1985.
- Palm S, Humm JL, Rundqvist R, et al. Microdosimetry of astatine-211 single-cell irradiation: Role of daughter polonium-211 diffusion. *Med Phys* 2004;31:218.
- Turkington TG, Zalutsky MR, Jaszczak RJ, et al. Measuring astatine-211 distributions with SPECT. *Phys Med Biol* 1993;38:1121.
- Meyer GJ, Lambrecht RM. Excitation function for the $209\text{-Bi}(7\text{-Li},5n)211\text{-Rn}$ nuclear reaction as a route to the $211\text{-Rn}-211\text{-At}$ generator. *J Label Compd Radiopharm* 1981; 28:233.
- Vinodkumar AM, Loveland W, Sprunger PH, et al. Fusion of ^9Li with ^{208}Pb . *Phys Rev C* 2009;80:054609.
- Harrison J, Leggett R, Lloyd D, et al. Polonium-210 as a poison. *J Radiol Prot* 2007;27:17.
- Zalutsky MR, Pruszyński M. Astatine-211: Production and availability. *Current Radiopharm* 2011;4:177.
- Hermanne A, Tárkányi F, Takács S, et al. Experimental study of the cross-sections of [alpha]-particle induced reactions on ^{209}Bi . *Appl Radiat Isot* 2005;63:1.
- Lindgren S, Bäck T, Jensen HJ. Dry-distillation of astatine-211 from irradiated bismuth targets: A time-saving procedure with high recovery yields. *Appl Radiat Isot* 2001; 55:157.
- Yordanov A, Pozzi O, Carlin S, et al. Wet harvesting of no-carrier-added ^{211}At from an irradiated ^{209}Bi target for radiopharmaceutical applications. *J Radioanal Nucl Chem* 2005;262:593.
- Alliot C, Chérel M, Barbet J, et al. Extraction of astatine-211 in diisopropylether (DIPE). *Radiochim Acta* 2009;97:161.
- Bourgeois M, Guérard F, Alliot C, et al. Feasibility of the radioastatination of a monoclonal antibody with astatine-211 purified by wet extraction. *J Label Compd Radiopharm* 2008;51:379.
- Zalutsky MR, Zhao XG, Alston KL, et al. High-level production of alpha-particle-emitting (^{211}At) and preparation of (^{211}At) labeled antibodies for clinical use. *J Nucl Med* 2001;42:1508.
- Appelman EH, Sloth EN, Studier MH. Observation of astatine compounds by time-of-flight mass spectrometry. *Inorg Chem* 1966;5:766.
- Johnson GL, Leininger RF, Segrè E. Chemical properties of astatine. I. *J Chem Phys* 1949;17:1.
- Appelman EH. The oxidation states of astatine in aqueous solution. *J Am Chem Soc* 1961;83:805.
- Visser GWM, Diemer EL. Inorganic astatine chemistry: Formation of complexes of astatine. *Radiochim Acta* 1983; 33:145.
- Visser GWM. Inorganic astatine chemistry part II: The chameleon behaviour and electrophilicity of At-species. *Radiochim Acta* 1989;47:97.
- Dreyer I, Dreyer R, Chalkin VA. Investigation of the movement of astatine in an electric field. *Radiochem Radioanal Lett* 1978;35:257.
- Dreyer I, Dreyer R, Chalkin VA. Cations of astatine in water: illustration and properties. *Radiochem Radioanal Lett* 1978;36:389.
- Dreyer R, Dreyer I, Rosch F, et al. Studies of polyhalogenide ions of astatine. *Radiochem Radioanal Lett* 1982;54:165.
- Ruth TJ, D'Auria JM, Dombosky M, et al. The Radiochemistry of Astatine. DOE sponsored Nuclear Science Series monogram (NAS-NS-3064; DE88015386) 1988. Available at www.ntis.gov/search/product.aspx?ABBR=DE88015386 Accessed on July 16, 2012.
- Pruszyński M, Bilewicz A, Was B, et al. Formation and stability of astatide-mercury complexes. *J Radioanal Nucl Chem* 2006;268:91.
- Pruszyński M, Bilewicz A, Zalutsky MR. Preparation of $\text{Rh}[16\text{aneS4-diol}]^{211}\text{At}$ and $\text{Ir}[16\text{aneS4-diol}]^{211}\text{At}$ complexes as potential precursors for astatine radiopharmaceuticals. Part I: Synthesis. *Bioconjug Chem* 2008;19:958.

29. Appelman EH. Solvent extraction studies of interhalogen compounds of astatine. *J Phys Chem* 1961;65:325.
30. Fischer S, Dreyer R, Albrecht S. Pseudohalogen compounds of astatine: Synthesis and characterization of At(I/-tricyanomethanide-and At(I/-azide-compounds. *J Radioanal Nucl Chem* 1987;117:275.
31. Dreyer R, Dreyer I, Fischer S, et al. Synthesis and characterization of cationic astatine compounds with sulphur-containing ligands stable in aqueous solutions. *J Radioanal Nucl Chem* 1985;96:333.
32. Fischer S, Dreyer R, Hussein H, et al. Synthesis and first characterization of cationic At(I/-compounds with selenium-containing neutral ligands. *J Radioanal Nucl Chem* 1987;119:181.
33. Ludwig R, Dreyer R, Fisher S. First investigation of complex formation of At(I) with phosphorous organic compounds. *Radiochim Acta* 1989;47:129.
34. Milesz S, Jovchev M, Schumann D, et al. The EDTA complexes of astatine. *J Radioanal Nucl Chem* 1988; 127:193.
35. Milesz S, Norseev YV, Szücs Z, et al. Characterization of DTPA complexes and conjugated antibodies of astatine. *J Radioanal Nucl Chem* 1989;137:365.
36. Schumann D, Milesz S, Jovchev M, et al. Nitrilotriacetate complex of univalent astatine. *Radiochim Acta* 1992; 56:173.
37. Ning L, Jiannan J, Shangwu M, et al. Preparation and preliminary evaluation of astatine-211 labeled IgG via DTPA anhydride. *J Radioanal Nucl Chem* 1998;227:187.
38. Ludwig R, Fischer S, Dreyer R, et al. Complex formation equilibria between astatine(I) and sulphur-containing chelating ligands. *Polyhedron* 1991;10:11.
39. Yordanov AT, Deal K, Garmestani K, et al. Synthesis and biodistribution study of a new 211-At-calix[4]arene complex. *J Label Compd Radiopharm* 2000;43:1219.
40. Champion J, Alliot C, Huclier S, et al. Determination of stability constants between complexing agents and At(I) and At(III) species present at ultra-trace concentrations. *Inorg Chim Acta* 2009;362:2654.
41. Greenwood N, Earnshaw A. Chapter 17: The halogens: Fluorine, Chlorine, Bromine, Iodine and Astatine. In: *Chemistry of the Elements*. 2nd edition, Elsevier, Oxford, UK: Butterworth-Heinemann, 1997;789.
42. Pozzi OR, Zalutsky MR. Radiopharmaceutical chemistry of targeted radiotherapeutics, part 3: Alpha-particle-induced radiolytic effects on the chemical behavior of (211)At. *J Nucl Med* 2007;48:1190.
43. Berei K, Vasáros L. Recent Advances in the Organic Chemistry of Astatine. In: *PATAI'S Chemistry of Functional Groups*. John Wiley and Sons, Ltd; 2009. Available at <http://onlinelibrary.wiley.com/doi/10.1002/9780470682531.pat0014/abstract> Accessed on July 16, 2012.
44. Coenen HH, Moerlein SM, Stöcklin G. No-carrier added radiohalogenation methods with heavy halogens. *Radiochim Acta* 1983;34:47.
45. Liu BL, Jin YT, Liu ZH, et al. Halogen exchanges using crown ethers: Synthesis and preliminary biodistribution of 6-[²¹¹At]astatomethyl-19-norcholest-5(10)-en-3 beta-ol. *Int J Appl Radiat Isot* 1985;36:561.
46. Brown I, Carpenter RN, Link E, et al. Potential diagnostic and therapeutic agents for malignant melanoma: Synthesis of heavy radiohalogenated derivatives of methylene blue by electrophilic and nucleophilic methods. *J Radioanal Nucl Chem Lett* 1986;107:337.
47. Meyer GJ, Walte A, Sriyapureddy SR, et al. Synthesis and analysis of 2-[²¹¹At]-l-phenylalanine and 4-[²¹¹At]-l-phenylalanine and their uptake in human glioma cell cultures *in-vitro*. *Appl Radiat Isot* 2010;68:1060.
48. Visser GWM, Diemer EL. The reaction of astatine with aromatic diazonium compounds. *Radiochem Radioanal Lett* 1982;51:135.
49. Meyer GJ, Rössler K, Stöcklin G. Reaction of aromatic diazonium salts with carrier-free radioiodine and astatine. Evidence for complex formation. *J Am Chem Soc* 1979;101:3121.
50. Wunderlich G, Fischer S, Dreyer R, et al. A simple method for labelling proteins with ²¹¹At via diazotized aromatic diamine. *J Radioanal Nucl Chem Lett* 1987;117:197.
51. Norseev YV, Nhan DD, Khalkin VA, et al. The preparation of astatine labelled tyrosine using an electrophilic reaction. *J Radioanal Nucl Chem* 1985;94:185.
52. Norseev YV. Synthesis of astatine-tagged methylene blue, a compound for fighting micrometastases and individual cells of melanoma. *J Radioanal Nucl Chem* 1998;237:155.
53. Visser GWM, Diemer EL, Kaspersen FM. The preparation and stability of astatotyrosine and astatiodotyrosine. *Int J Appl Radiat Isot* 1979;30:749.
54. Visser GWM, Diemer E, Kaspersen FM. The preparation of aromatic astatine compounds through aromatic mercury compounds part II: Astatination of pyrimidines and steroids. *J Label Compd Radiopharm* 1981;18:799.
55. Vaidyanathan G, Affleck DJ, Alston KL, et al. A kit method for the high level synthesis of [²¹¹At]MABG. *Bioorg Med Chem* 2007;15:3430.
56. Vaidyanathan G, Affleck DJ, Zalutsky MR. Monoclonal antibody F(ab')₂ fragment labeled with *N*-succinimidyl 2,4-dimethoxy-3-halobenzoates: *In vivo* comparison of iodinated and astatinated fragments. *Nucl Med Biol* 1994; 21:105.
57. Garg PK, John CS, Zalutsky MR. Preparation and preliminary evaluation of 4-[²¹¹At]astato-*N*-piperidinoethyl benzamide. *Nucl Med Biol* 1995;22:467.
58. Vaidyanathan G, Larsen RH, Zalutsky MR. 5-[²¹¹At]astato-2'-deoxyuridine, an [alpha]-particle-emitting endoradiotherapeutic agent undergoing DNA incorporation. *Cancer Res* 1996;56:1204.
59. Narula AS, Zalutsky MR. No-carrier added astatination of *N*-succinimidyl-3-(tri-*n*-butylstannyl) benzoate (ATE) via electrophilic destannylation. *Radiochim Acta* 1989;47:131.
60. Valliant JF, Guenther KJ, King AS, et al. The medicinal chemistry of carboranes. *Coord Chem Rev* 2002;232:173.
61. Wilbur DS, Zalutsky MR, Wedge TJ, et al. Reagents for astatination of biomolecules: Comparison of the *in vivo* distribution and stability of some radioiodinated/astatinated benzamidyl and nido-carboranyl compounds. *Bioconjug Chem* 2004;15:203.
62. Wilbur DS. [²¹¹At]Astatine-labeled compound stability: Issues with released [²¹¹At]astatide and development of labeling reagents to increase stability. *Current Radiopharm* 2008;1:144.
63. Larsen RH, Slade S, Zalutsky MR. Blocking [²¹¹At]astatide accumulation in normal tissues: Preliminary evaluation of seven potential compounds. *Nucl Med Biol* 1998;25:351.
64. Hamilton JG, Asling CW, Garrison WM, et al. Destructive action of astatine 211 (element 85) on the thyroid gland of the rat. *Proc Soc Exp Biol Med* 1950;73:51.
65. Durbin PW, Asling CW, Johnston ME, et al. The induction of tumors in the rat by astatine-211. *Radiat Res* 1958; 9:378.

66. McLendon RE, Archer GE, Garg PK, et al. Radiotoxicity of systemically administered [^{211}At]astatide in B6C3F1 and BALB/c (nu/nu) mice: A long-term survival study with histologic analysis. *Int J Radiat Oncol Biol Phys* 1996; 35:69.
67. Zalutsky MR, Reardon DA, Pozzi OR, et al. Targeted alpha-particle radiotherapy with ^{211}At -labeled monoclonal antibodies. *Nucl Med Biol* 2007;34:779.
68. Aaij C, Tschroots WRJM, Lindner L, et al. The preparation of astatine labelled proteins. *Int J Appl Radiat Isot* 1975;26:25.
69. Vaughan AT, Fremlin JH. The preparation of astatine labelled proteins using an electrophilic reaction. *Int J Nucl Med Biol* 1978;5:229.
70. Vaughan AT, Fremlin JH. The preparation of astatotyrosine. *Int J Appl Radiat Isot* 1977;28:595.
71. Visser GWM, Diemer EL, Kaspersen FM. The preparation and stability of ^{211}At -astato-imidazoles. *Int J Appl Radiat Isot* 1980;31:275.
72. Visser GWM, Diemer EL, Kaspersen FM. The nature of the astatine-protein bond. *Int J Appl Radiat Isot* 1981;32:905.
73. Friedman AM, Zalutsky MR, Fitch FW, et al. Preparation of a biologically stable and immunogenically competent astatinated protein. *Int J Nucl Med Biol* 1977;4:219.
74. Zalutsky MR, Narula AS. Astatination of proteins using an *N*-succinimidyl tri-*n*-butylstannyl benzoate intermediate. *Int J Rad Appl Instrum A* 1988;39:227.
75. Pozzi OR, Zalutsky MR. Radiopharmaceutical chemistry of targeted radiotherapeutics, part 1: Effects of solvent on the degradation of radiohalogenation precursors by ^{211}At alpha-particles. *J Nucl Med* 2005;46:700.
76. Zalutsky MR, Reardon DA, Akabani G, et al. Clinical experience with alpha-particle emitting ^{211}At : Treatment of recurrent brain tumor patients with ^{211}At -labeled chimeric antitenascin monoclonal antibody 81C6. *J Nucl Med* 2008;49:30.
77. Reist CJ, Foulon CF, Alston K, et al. Astatine-211 labeling of internalizing anti-EGFRvIII monoclonal antibody using *N*-succinimidyl 5- ^{211}At [astato-3-pyridinecarboxylate. *Nucl Med Biol* 1999;26:405.
78. Vaidyanathan G, Affleck DJ, Bigner DD, et al. *N*-succinimidyl 3- ^{211}At [astato-4-guanidinomethylbenzoate: An acylation agent for labeling internalizing antibodies with alpha-particle emitting ^{211}At . *Nucl Med Biol* 2003;30:351.
79. Hadley SW, Wilbur DS, Gray MA, et al. Astatine-211 labeling of an antimelanoma antibody and its Fab fragment using *N*-succinimidyl *p*-astatobenzoate: Comparisons *in vivo* with the *p*- ^{125}I iodobenzoyl conjugate. *Bioconjug Chem* 1991;2:171.
80. Garg PK, Harrison CL, Zalutsky MR. Comparative tissue distribution in mice of the alpha-emitter ^{211}At and ^{131}I as labels of a monoclonal antibody and F(ab')₂ fragment. *Cancer Res* 1990;50:3514.
81. Talanov VS, Yordanov AT, Garmestani K, et al. Preparation and *in vivo* evaluation of novel linkers for ^{211}At labeling of proteins. *Nucl Med Biol* 2004;31:1061.
82. Talanov VS, Garmestani K, Regino CAS, et al. Preparation and *in vivo* evaluation of a novel stabilized linker for ^{211}At labeling of protein. *Nucl Med Biol* 2006;33:469.
83. Yordanov AT, Garmestani K, Zhang M, et al. Preparation and *in vivo* evaluation of linkers for ^{211}At labeling of humanized anti-Tac. *Nucl Med Biol* 2001;28:845.
84. Wilbur DS, Chyan M-K, Hamlin DK, et al. Reagents for astatination of biomolecules. 2. Conjugation of anionic boron cage pendant groups to a protein provides a method for direct labeling that is stable to *in vivo* deastatination. *Bioconjug Chem* 2007;18:1226.
85. Wilbur DS, Chyan M-K, Hamlin DK, et al. Preparation and *in vivo* evaluation of radioiodinated *closo*-decaborate(2-) derivatives to identify structural components that provide low retention in tissues. *Nucl Med Biol* 2010;37:167.
86. Wilbur DS, Chyan M-K, Hamlin DK, et al. Reagents for astatination of biomolecules. 5. Evaluation of hydrazine linkers in ^{211}At - and ^{125}I -labeled *closo*-decaborate(2-) conjugates of fab' as a means of decreasing kidney retention. *Bioconjug Chem* 2011;22:1089.
87. Vaidyanathan G, Affleck D, Welsh P, et al. Radioiodination and astatination of octreotide by conjugation labeling. *Nucl Med Biol* 2000;27:329.
88. Vaidyanathan G, Boskovitz A, Shankar S, et al. Radioiodine and ^{211}At -labeled guanidinomethyl halobenzoyl octreotate conjugates: Potential peptide radiotherapeutics for somatostatin receptor-positive cancers. *Peptides* 2004; 25:2087.
89. Vaidyanathan G, Affleck DJ, Schottelius M, et al. Synthesis and evaluation of glycosylated octreotate analogues labeled with radioiodine and ^{211}At via a tin precursor. *Bioconjug Chem* 2006;17:195.
90. Lesch HP, Kaikkonen MU, Pikkarainen JT, et al. Avidin-biotin technology in targeted therapy. *Expert Opin Drug Deliv* 2010;7:551.
91. Foulon CF, Schoultz BW, Zalutsky MR. Preparation and biological evaluation of an astatine-211 labeled biotin conjugate: Biotinyl-3- ^{211}At [astatoanilide. *Nucl Med Biol* 1997;24:135.
92. Foulon CF, Alston KL, Zalutsky MR. Astatine-211-labeled biotin conjugates resistant to biotinidase for use in pre-targeted radioimmunotherapy. *Nucl Med Biol* 1998;25:81.
93. Wilbur DS, Hamlin DK, Chyan M-K, et al. Biotin reagents in antibody pretargeting. 6. Synthesis and *in vivo* evaluation of astatinated and radioiodinated aryl- and *nido*-carboranyl-biotin derivatives. *Bioconjug Chem* 2004; 15:601.
94. Wilbur DS, Chyan M-K, Hamlin DK, et al. Reagents for astatination of biomolecules. 3. Comparison of *closo*-decaborate(2-) and *closo*-dodecaborate(2-) moieties as reactive groups for labeling with astatine-211. *Bioconjug Chem* 2009;20:591.
95. Lindegren S, Andersson H, Jacobsson L, et al. Synthesis and biodistribution of ^{211}At -labeled, biotinylated, and charge-modified poly-L-lysine: Evaluation for use as an effector molecule in pretargeted intraperitoneal tumor therapy. *Bioconjug Chem* 2002;13:502.
96. Lindegren S, Karlsson B, Jacobsson L, et al. (^{211}At)-labeled and biotinylated effector molecules for pretargeted radioimmunotherapy using poly-L- and poly-D-lysine as multicarriers. *Clin Cancer Res* 2003;9:3873S.
97. Frost SHL, Bäck T, Chouin N, et al. *In vivo* distribution of avidin-conjugated MX35 and ^{211}At -labeled, biotinylated poly-L-lysine for pretargeted intraperitoneal α -radioimmunotherapy. *Cancer Biother Radiopharm* 2011;26:727.
98. Larsen RH, Murud KM, Akabani G, et al. ^{211}At - and ^{131}I -labeled bisphosphonates with high *in vivo* stability and bone accumulation. *J Nucl Med* 1999;40:1197.
99. Vaidyanathan G, Zalutsky MR. 1-(*m*- ^{211}At [astato-benzyl]guanidine: Synthesis via astato demetalation and preliminary *in vitro* and *in vivo* evaluation. *Bioconjug Chem* 1992;3:499.

100. Larsen RH, Hassfjell SP, Hoff P, et al. 211-At-labelling of polymer particles for radiotherapy: Synthesis, purification and stability. *J Label Compd Radiopharm* 1993;33:977.
101. Larsen RH, Hoff P, Vergote IB, et al. Alpha-particle radiotherapy with ²¹¹At-labeled monodisperse polymer particles, ²¹¹At-labeled IgG proteins, and free ²¹¹At in a murine intraperitoneal tumor model. *Gynecol Oncol* 1995;57:9.
102. Kucka J, Hrubý M, Konák C, et al. Astatination of nanoparticles containing silver as possible carriers of ²¹¹At. *Appl Radiat Isot* 2006;64:201.
103. Hartman KB, Hamlin DK, Wilbur DS, et al. ²¹¹AtCl@US-tube nanocapsules: A new concept in radiotherapeutic agent design. *Small* 2007;3:1496.
104. Larsen RH, Akabani G, Welsh P, et al. The cytotoxicity and microdosimetry of astatine-211-labeled chimeric monoclonal antibodies in human glioma and melanoma cells *in vitro*. *Radiat Res* 1998;149:155.
105. Akabani G, Carlin S, Welsh P, et al. *In vitro* cytotoxicity of ²¹¹At-labeled trastuzumab in human breast cancer cell lines: Effect of specific activity and HER2 receptor heterogeneity on survival fraction. *Nucl Med Biol* 2006;33:333.
106. Aurlien E, Kvinnsland Y, Larsen RH, et al. Radiation doses to non-Hodgkin's lymphoma cells and normal bone marrow exposed *in vitro*. Comparison of an alpha-emitting radioimmunoconjugate and external gamma-irradiation. *Int J Radiat Biol* 2002;78:133.
107. Petrich T, Korkmaz Z, Krull D, et al. *In vitro* experimental ²¹¹At-anti-CD33 antibody therapy of leukaemia cells overcomes cellular resistance seen *in vivo* against gemtuzumab ozogamicin. *Eur J Nucl Med Mol Imaging* 2010;37:851.
108. Nestor M, Sundström M, Anniko M, et al. Effect of cetuximab in combination with alpha-radioimmunotherapy in cultured squamous cell carcinomas. *Nucl Med Biol* 2011;38:103.
109. Orlova A, Sjöström A, Lebeda O, et al. Targeting against epidermal growth factor receptors. Cellular processing of astatinated EGF after binding to cultured carcinoma cells. *Anticancer Res* 2004;24:4035.
110. Claesson AK, Stenerlöv B, Jacobsson L, et al. Relative biological effectiveness of the alpha-particle emitter (²¹¹At) for double-strand break induction in human fibroblasts. *Radiat Res* 2007;167:312.
111. Claesson K, Magnander K, Kahu H, et al. RBE of α -particles from ²¹¹At for complex DNA damage and cell survival in relation to cell cycle position. *Int J Rad Biol* 2011;87:372.
112. Zhang M, Yao Z, Zhang Z, et al. The anti-CD25 monoclonal antibody 7G7/B6, armed with the α -emitter ²¹¹At, provides effective radioimmunotherapy for a murine model of leukemia. *Cancer Res* 2006;66:8227.
113. Zhang Z, Zhang M, Garmestani K, et al. Effective treatment of a murine model of adult T-cell leukemia using ²¹¹At-7G7/B6 and its combination with unmodified anti-Tac (daclizumab) directed toward CD25. *Blood* 2006;108:1007.
114. Zhang M, Yao Z, Patel H, et al. Effective therapy of murine models of human leukemia and lymphoma with radiolabeled anti-CD30 antibody, HeFi-1. *Proc Natl Acad Sci U S A* 2007;104:8444.
115. Cheng J, Ekberg T, Engström M, et al. Radioimmunotherapy with astatine-211 using chimeric monoclonal antibody U36 in head and neck squamous cell carcinoma. *Laryngoscope* 2007;117:1013.
116. Robinson MK, Shaller C, Garmestani K, et al. Effective treatment of established human breast tumor xenografts in immunodeficient mice with a single dose of the α -emitting radioisotope astatine-211 conjugated to anti-HER2/neu diabodies. *Clin Cancer Res* 2008;14:875.
117. Elgqvist J, Andersson H, Bernhardt P, et al. Administered activity and metastatic cure probability during radioimmunotherapy of ovarian cancer in nude mice with ²¹¹At-MX35 F(ab')₂. *Int J Radiat Oncol Biol Phys* 2006;66:1228.
118. Elgqvist J, Andersson H, Bäck T, et al. [alpha]-radioimmunotherapy of intraperitoneally growing OVCAR-3 tumors of variable dimensions: Outcome related to measured tumor size and mean absorbed dose. *J Nucl Med* 2006;47:1342.
119. Elgqvist J, Andersson H, Bäck T, et al. Fractionated radioimmunotherapy of intraperitoneally growing ovarian cancer in nude mice with ²¹¹At-MX35 F(ab')₂: Therapeutic efficacy and myelotoxicity. *Nucl Med Biol* 2006;33:1065.
120. Elgqvist J, Andersson H, Jensen H, et al. Repeated intraperitoneal α -radioimmunotherapy of ovarian cancer in mice. *J Oncol* 2010;2010:1.
121. Gustafsson AME, Bäck T, Elgqvist J, et al. Comparison of therapeutic efficacy and biodistribution of ²¹³Bi- and ²¹¹At-labeled monoclonal antibody MX35 in an ovarian cancer model. *Nucl Med Biol* 2012;39:15.
122. Zalutsky MR, McLendon RE, Garg PK, et al. Radioimmunotherapy of neoplastic meningitis in rats using an alpha-particle-emitting immunoconjugate. *Cancer Res* 1994;54:4719.
123. Zalutsky MR, Stabin MG, Larsen RH, et al. Tissue distribution and radiation dosimetry of astatine-211-labeled chimeric 81C6, an α -particle-emitting immunoconjugate. *Nucl Med Biol* 1997;24:255.
124. Palm S, Bäck T, Claesson I, et al. Therapeutic efficacy of astatine-211-labeled trastuzumab on radioresistant SKOV-3 tumors in nude mice. *Int J Radiat Oncol Biol Phys* 2007;69:572.
125. Boskovitz A, McLendon RE, Okamura T, et al. Treatment of HER2-positive breast carcinomatous meningitis with intrathecal administration of [alpha]-particle-emitting ²¹¹At-labeled trastuzumab. *Nucl Med Biol* 2009;36:659.
126. Andersson H, Cederkrantz E, Bäck T, et al. Intraperitoneal [alpha]-particle radioimmunotherapy of ovarian cancer patients: Pharmacokinetics and dosimetry of ²¹¹At-MX35 F(ab')₂-a phase I study. *J Nucl Med* 2009;50:1153.
127. Hamilton JG, Soley MH. A comparison of the metabolism of iodine and of element 85 (eka-iodine). *Proc Natl Acad Sci U S A* 1940;26:483.
128. Wilbur DS, Thakar MS, Hamlin DK, et al. Reagents for astatination of biomolecules. 4. Comparison of maleimido-*cis*-decaborate(2-) and meta-[²¹¹At]astatobenzoate conjugates for labeling anti-CD45 antibodies with [²¹¹At]astatine. *Bioconjug Chem* 2009;20:1983.
129. Guerard F, Rajerison H, Faivre-Chauvet A, et al. Radiolabelling of proteins with stabilised hypervalent astatine-211: Feasibility and stability. *J Nucl Med* 2011;52:1486.
130. Haddad F, Barbet J, Chatal JF. The ARRONAX project. *Current Radiopharm* 2011;4:186.

1

Radioactive waste

Radioactive waste is the term used to describe radioactive substances for which no further use is planned or considered.

A radioactive substance is one that contains naturally occurring or man-made radionuclides, the radioactive level or concentration of which calls for radiation protection control.

According to the French Environmental Code (Art. L 542.1-1), final radioactive waste means radioactive waste for which no further treatment is possible under existing technical and economic conditions. Treatment particularly entails extracting any part of the waste that can be recycled or reducing any pollutants or hazardous substances it contains.

The radionuclides contained in radioactive waste may be man-made, such as caesium-137, or found in nature, such as radium-226.

The radioactive properties of this waste are:

- the type of radionuclides contained and the radiation emitted (alpha, beta, gamma), the activity (number of atomic nuclei which spontaneously disintegrate per unit time - expressed in becquerels);
- the radioactive half-life (the time it takes for a radioactive sample to lose half of its activity).



Containers for vitrified waste (left) and compacted waste (right).



Most radioactive waste comes from the nuclear industry. The remainder comes from the use of radioactive elements in hospitals, universities, and some

non-nuclear industries and defence-related activities.

□ Definitions and classification

Radioactive waste is classified according to its activity level and the radioactive half-life of the radionuclides it contains. The activity level determines the degree of protection to be provided. Waste is therefore divided into categories, namely very low-, low-, intermediate-

and high-level waste. Radioactive waste is said to be "short-lived" if it merely only contains radionuclides with a half-life of less than 31 years.

It is said to be "long-lived" if it contains a significant quantity of radionuclides with a half-life of over 31 years.

Radionuclide	Half-life
Cobalt-60	5.2 years
Tritium	12.2 years
Strontium-90	28.1 years
Caesium-137	30 years
Americium-241	432 years
Radium-226	1,600 years
Carbon-14	5,730 years
Plutonium-239	24,110 years
Neptunium-237	2,140,000 years
Iodine-129	15,700,000 years
Uranium-238	4,470,000,000 years

Waste categories are as follows:

- **very short-lived waste (VSLW)** much of which comes from medical applications of radioactivity (diagnoses and therapy), containing radioactive elements with a half-life of less than 100 days;
- **very low-level waste (VLLW)** which comes from the nuclear industry, in particular from facility decommissioning operations. It consists of very slightly contaminated dismantled equipment parts and rubble;
- **low- and intermediate-level short-lived waste (LILW-SL)** which mainly comes from the nuclear industry, as well as a few research laboratories;
- **low-level long-lived waste (LLW-LL)** which for the major part consists either of waste contaminated by radium (known as radium-bearing waste), resulting mainly from naturally radioactive raw materials used in industry, the retrieval of radium-bearing objects and the cleanup of polluted sites, or graphite waste, which comes from the decommissioning of old French gas-cooled reactors (GCRs);
- **intermediate-level long-lived waste (ILW-LL)** most of which is the result of spent fuel reprocessing (spent fuel claddings, reprocessing sludge, etc.) and nuclear facility maintenance work;
- **high-level and long-lived waste (HLW-LL)** consisting of products resulting from spent fuel reprocessing that cannot be recycled.



Decommissioning operations (VLLW).



Graphite sleeve.



Solid waste in cemented drums before being embedded in cement.



Embedding in cement.

□ Management solutions

Radioactive waste is extremely varied in terms of physical and chemical form, radioactivity and the half-life of the radioactive elements it contains, as well as volume. In France, a specific process is adopted for each category of waste, including a series of operations such as sorting, treatment, conditioning, storage and disposal.

Sorting: this consists in separating waste according to its different properties, in particular the half-lives of the radionuclides it contains. It also involves separating waste that can be compacted, incinerated or melted down to reduce the volume.

Treatment and conditioning: different types of waste undergo different types of treatment (incineration, calcination, melting, compacting, cementation, vitrification, etc.). It is then sealed in a container. The result is a radioactive waste package.

Storage and disposal: storage facilities are designed to accommodate waste packages for a limited period of time. Disposal is the final stage of the waste management process and implies that the packages have reached their final destination or, at least, that there is no intention of retrieving them. That means, of course,



VLLW comprises rubble, scrap metal and piping, primarily from decommissioned nuclear facilities.

that the steps taken must protect people and the environment both in the short and very long term.

Very short-lived waste (VSLW), the radioactivity level of which disappears almost entirely in a few weeks to a few hundred days, is stored long enough to decay before disposal, in particular via hospital waste systems.

Very low-level waste (VLLW) is sent to a disposal facility in Morvilliers (Aube) operated by Andra, the French National Radioactive Waste Management Agency. Once all nuclear power plants have been decommissioned, this waste should represent an estimated volume of one to two million m³.

Low- and intermediate-level short-lived waste (LILW-SL, also called LLW-ILW or "A" waste) is incinerated, melted, embedded or compacted. Most of it is cemented in metal or concrete containers. It is disposed of at two surface facilities: the CSM disposal facility (Manche), which

was closed in 1994, having reached its design capacity of 527,000 m³, and the CSA disposal facility (Aube), opened in 1992 and operated by Andra since.

Low-level long-lived waste (LLW-LL) is stored by the organisations that generated it pending a disposal solution.

Intermediate-level long-lived waste (ILW-LL, also called "B" waste) is compacted or cemented to make packages that are stored where the waste was generated.

High-level and long-lived waste (HLW-LL, also called "C" waste) is vitrified. This involves incorporating highly radioactive waste in molten glass.

The waste, which is in a liquid form, is mixed with molten glass and poured into stainless steel containers, then hermetically sealed by a welded lid. Once the glass has cooled down, the radioactivity is trapped inside the matrix. These waste



VLLW comprises rubble, scrap metal and piping, primarily from decommissioned nuclear facilities.

packages are currently stored by the organisations that generated the waste (CEA, Areva, their past

(Marcoule, Gard) or present (La Hague, Manche) production sites.

Uranium mill tailings are also considered as waste. Areva is responsible for the tailings, which are disposed of on twenty or so mining sites. They represent about 52 million tonnes of material. All uranium mines in France are now closed.

Spent fuel, which contains uranium and plutonium and is stored in spent fuel pools at Areva's La Hague plant, is not considered as waste as the French Government implements a recycling policy.



Different types of waste package.

Management solutions developed as part of the PNGMDR* for various waste categories

Half-life	Very short-lived (less than 100 days)	Short-lived (less than 31 years)	Long-lived (more than 31 years)
Very low-level waste	Managed by radioactive decay	Dedicated surface disposal Recycling solutions (activity < 100 Bq/g)	
Low-level waste		Surface disposal (CSA disposal facility - Aube)	Dedicated subsurface disposal (under consideration)
Intermediate-level waste			
High-level waste		Solutions under consideration under Article 3 of the Programme Act of 28 June 2006 on the sustainable management of radioactive materials and waste	

* French national radioactive materials and waste management programme.



Every three years, Andra, the French National Radioactive Waste Management Agency, prepares and publishes an inventory of radioactive materials and waste in France

<i>(Equivalent conditioned m³)</i>	Waste existing at the end of 2010	Forecasts for the end of 2020	Forecasts for the end of 2030
HLW	2,700	4,000	5,300
ILW-LL	40,000	45,000	49,000
LLW-LL	87,000	89,000	133,000
LILW-SL	830,000	1,000,000	1,200,000
VLLW	360,000	762,000	1,300,000
Management solution to be defined	3,600		
Total	approx. 1,320,000	approx. 1,900,000	approx. 2,700,000

Volumes at the end of 2010 and forecasts for the end of 2020 and 2030 for each radioactive waste category (National Inventory 2012 - source Andra).



At Andra's CSA disposal facility (Aube), waste packages are placed in concrete cells or "disposal structures". When they are full, the cells are covered with a concrete slab and polyurethane membrane.